KfK 3657
März 1984

FEBA — Flooding Experiments with Blocked Arrays Evaluation Report

P. Ihle, K. Rust
Institut für Reaktorbauelemente
Projekt Nukleare Sicherheit

Kernforschungszentrum Karlsruhe

KERNFORSCHUNGSZENTRUM KARLSRUHE
Institut für Reaktorbauelemente
Projekt Nukleare Sicherheit

KfK 3657

FEBA - Flooding Experiments with Blocked Arrays
Evaluation Report

P. Ihle, K. Rust

Kernforschungszentrum Karlsruhe GmbH, Karlsruhe

Kernforschungszentrum Karlsruhe GmbH
ISSN 0303-4003

ABSTRACT

Flooding Experiments with Blocked Arrays (FEBA) were conducted to study the effectiveness of the emergency core cooling of pressurized water reactors (PWR) with deformed claddings of some fuel rod clusters. Full length bundles of 1x5 as well as 5x5 electrically heated rods of PWR dimensions were used for a number of separate effect test series with various blockage geometries simulating ballooned fuel rod claddings.

The results of the eigth test series performed with the 5x5 rod bundle using full decay heat show the effects of grid spacers and coplanar coolant channel blockages with and without bypass on reflood heat transfer. The cooling enhancement downstream of grid spacers as well as within and downstream of blockages of 62 % blockage ratio mainly occurs during the early portion of reflood. For the 90 % blockage ratio only maximum cladding temperatures downstream of the blockage were slightly higher (max. 50 K) than in the bypass area.

The purpose of the investigations was to obtain an insight into the most important heat transfer mechnisms to broaden the data base for the development and assessment of improved thermal-hydraulic models.

FEBA - Flutexperimente mit blockierten Anordnungen
Auswertebericht

KURZFASSUNG

Experimente wurden durchgeführt zur Untersuchung der Wirksamkeit der Kernnotkühlung von Druckwasserreaktoren (DWR) bei deformierten Hüllrohren einiger Brennstäbe. Die 1x5 und 5x5 Bündel aus elektrisch beheizten Stäben voller Länge mit DWR-Abmessungen wurden für eine Reihe von Testserien mit verschiedenen Blockadegeometrien eingesetzt. Die Blockaden simulierten aufgeblähte Brennstabhüllrohre. Die Testserien dienten zur Untersuchung der Einzeleffekte.

Die mit dem 5x5 Stabbündel und voller Nachwärmeleistung erzielten Ergebnisse zeigen die Effekte von Abstandshaltern und koplanaren Kühlkanalblockaden mit und ohne Bypass auf den Wärmeübergang beim Fluten. Die Kühlungsverbesserung

sowohl nach Abstandshaltern als auch in und nach Blockaden mit einem Blockadegrad von 62 % trat hauptsächlich im frühen Teil der Flutphase auf. Beim Blockadegrad von 90 % waren die maximalen Hüllrohrtemperaturen nur nach der Blockade geringfügig höher (max. 50 K) als im Bypassbereich.

Absicht der Untersuchungen war, ein verbessertes Verständnis der wichtigsten Wärmeübergangsmechanismen zu gewinnen und die Basis experimenteller Daten zu erweitern für Entwicklung und Überprüfung verbesserter thermohydraulischer Rechenmodelle.

TABLE OF CONTENTS

		Page
1.	Introduction	1
1.1	Simulation of Thermohydraulics in a Core During LOCA of a PWR	1
1.2	FEBA Reflood Program	3
2.	Test Facility Design	5
2.1	Test Loop	5
2.2	Test Section	6
3.	Heater Rod Design	7
4.	Blockage Design	8
5.	Instrumentation	10
6.	Data Acquisition System	12
7.	Program Test Parameters	13
8.	Operational Procedure	13
9.	Results and Discussions	15
9.1	Qualitative Influence of Blockage Size and Shape (1 x 5 Rod Row)	15
9.2	Effects of Blockages with and without Bypass (5 x 5 Rod Bundle)	17
9.2.1	Base-Line Tests and Grid Spacer Effects, Series I and II	18
9.2.1.1	Measurements	18
9.2.1.2	Discussion of the Grid Spacer Effects	19
9.2.2	Separate Effects of Blockages with Bypass, Series III and IV	20
9.2.2.1	Measurements, Series III	20
9.2.2.2	Discussion, Series III	21

		Page
9.2.2.3	Measurements, Series IV	22
9.2.2.4	Discussion, Series IV	22
9.2.3	Combined Effects of Blockages with Bypass and Grid Spacers, Series V and VI	23
9.2.3.1	Measurements, Series V and VI	24
9.2.3.2	Discussion, Series V and VI	24
9.2.4	Effects of Blockages without Bypass, Cooling Enhancement for Known Mass Flux, Series VII and VIII	25
9.2.4.1	Measurements, Series VII and VIII	26
9.2.4.2	Discussion, Series VII and VIII	26
10.	Comparison of All Arrays with Each Other	26
11.	Analyses	29
11.1	Grid Spacer Effects on Two-Phase Flow Heat Transfer	30
11.1.1	Enhancement of Mist Cooling	31
11.1.2	Characteristic Time Scale for Mist Flow	32
11.1.3	Mist Cooling Enhancement Downstream of Grid Spacer	33
11.2	Blockage Effects on Two-Phase Flow Heat Transfer	37
12.	Summary of the Results	39
13.	Conclusions	41
14.	References	42

PREAMBLE

This report is an overall summary of an experimental investigation which is a part of the German LWR safety program. Within the framework of this program the Kernforschungszentrum Karlsruhe (KfK) started the Project Nuclear Safety (PNS) in 1973 for investigations on LWR fuel behavior under loss-of-coolant accident (LOCA) conditions /1/. Subjects of special importance were: The extent of core damage during a LOCA, the consequences of fuel rod failures on core coolability and fission product release, and the quantification of safety margins.

One of the experimental programs of the PNS was entitled

"Investigation of the Influence of the Size and the Shape of Coolant Channel Blockages upon Emergency Core Cooling (ECC) in the Reflood Phase of a LOCA".

It was defined mainly by Mr. A. Fiege (PNS) and Mr. G. Hofmann (IRB) who initiated the investigation in the Institut für Reaktorbauelemente (IRB) of the KfK.

The program evolved to the FEBA program (Flooding Experiments with Blocked Arrays) in 1977. The publication of this report as well as two complementing data reports marks the completion of this program.

Although many individuals have contributed to this program, we wish particularly to acknowledge the following:

Mr. H. Kreuzinger Mr. H. Schneider	Design of the test facility, test section assemblies, fuel rod simulators, instrumentation, rig operations.
Mr. S. Barth Mr. H. Weber Mr. W. Hame	Data acquisition systems, instrumentation, data processing.

Mr. A. Megerle — Electric power control,
Mr. K. Hitzig — electric power supply,
Mr. G. Huy — instrumentation,
Mr. H. Lechner — safety control system.

Mr. W. Götzmann — Data collecting,
Mr. S. Malang — processing and display.
Mr. M. Politzky

The main workshop VBW/HW of the KfK and the Hermann Kneißler KG at D-7230 Schramberg for heater rod instrumentation.

We greatly acknowledge the incentives and contributions of Dr. R.S.L. Lee, Professor of the State University of New York at Stony Brook. He spent many weeks with us evaluating FEBA results with respect to droplet cooling effects in mist flow (see References) and he drafted with us and reviewed this report.

SUMMARY

The influence of size and shape of coolant channel blockages on the effectiveness of the emergency core cooling of pressurized water reactors (PWR) has been investigated. The flooding experiments with blocked arrays (FEBA) were conducted to study separate effects in forced feed tests. Full length bundles of 1x5 as well as 5x5 electrically heated rods were used for a number of test series with various blockage geometries simulating ballooned fuel rod claddings. Eight consecutive test series were performed utilizing the 5x5 rod bundle of 3.9 m heated length with full decay heat rod power of chopped cosine axial distribution.

This report presents some typical data and a limited analysis of the reflood behavior to assist the development and assessment of computational models for predicting the effects of grid spacers and blockages on reflood heat transfer. The test series conducted are briefly described as follows:

Series I: Base-line tests with undisturbed bundle geometry, seven grid spacers,

Series II: Investigation of the effects of a grid spacer, without grid spacer at the bundle midplane,

Series III: Investigation of the effects of a 90 % flow blockage with bypass,
blockage at the bundle midplane of 3x3 rods placed in the corner of the 5x5 rod bundle, without grid spacer at the bundle midplane,

Series IV: Investigation of the effects of a 62 % flow blockage with bypass,
blockage at the bundle midplane of 3x3 rods placed in the corner of the 5x5 rod bundle, without grid spacer at the bundle midplane,

Series V: Investigation of the effects of a 90 % flow blockage with bypass combined with grid spacer effects, blockage immediately

upstream of the bundle midplane at 3x3 rods placed in the corner of the 5x5 rod bundle, grid spacer at the bundle midplane,

Series VI: Investigation of the effects of 90 % and 62 % flow blockages with bypass, combined with grid spacer effects, 90 % blockage immediately upstream of the bundle midplane, 62 % blockage immediately downstream of the bundle midplane, both blockages at the same 3x3 rods placed in the corner of the 5x5 rod bundle, grid spacer at the bundle midplane,

Series VII: Investigation of the effects of a 62 % flow blockage without bypass,
blockage at the bundle midplane of all rods of the 5x5 rod bundle,

Series VIII: Investigation of the effect of a 90 % flow blockage without bypass,
blockage at the bundle midplane of all rods of the 5x5 rod bundle.

For the reflood tests system pressures and flooding velocities of 2 through 6 bar and 2.2 through 5.8 cm/s, respectively, were applied for most of the test series.

The results show that for these reflood and blockage conditions the coolability of severely deformed fuel rod clusters seems not to be a serious problem.

The comparison of the results of the different test series with each other brings out the most important effects of coolant channel constrictions on two-phase flow heat transfer in rod bundles. The early portion of the reflood phase is characterized by mist flow regime for all flooding conditions investigated. Water droplets are entrained by highly superheated steam. Flow obstacles such as grid spacers and blockages increase local turbulence as well as droplet evaporation leading to significant increase of local heat transfer. This effect compensates to a large extent local coolant mass flux reduction due to blockages with bypass.

Typical transients measured and evaluated from the different test series, i.e. cladding and fluid temperatures, heat transfer coefficients, pressure differences and water carry over, are presented and discussed.

Short analyses of grid spacer and blockage effects conclude this report which is accompanied by two data reports /2,3/.

1. INTRODUCTION

1.1 SIMULATION OF THERMOHYDRAULICS IN A CORE DURING LOCA OF A PWR

The thermohydraulics in the core during a LOCA of a PWR depends mainly on the location and the size of the break in the primary coolant system. However, the conditions of the plant at initiation of a LOCA as well as the design and the operation of the emergency core cooling system influence time dependent core cooling conditions as well.

During a large break in the cold leg, the water within the primary coolant circuit rapidly depressurizes leading to a flow reversal in the core. The flow direction from top to bottom of the core prevails at least towards the end of the blowdown phase, i.e. when the system pressure corresponds to the pressure in the containment. The upper part of Fig. 1 shows a simplified scheme of a 4-loop steam generator system of a PWR. The lower part of Fig. 1 shows the reactor pressure vessel and the installations.

During blowdown emergency core cooling systems are initiated following the transient of the system pressure. However, it is assumed that the reactor pressure vessel is empty at the end of the blowdown phase. The low pressure emergency core cooling system already operating is assumed to need some time to fill up the pressure vessel until the lower end of the core is beginning to be submerged in the rising water column (refill phase). At that moment the main flow direction through the core again is reversed to from bottom to top, e.g. "the beginning of reflood". Ballooning of fuel rod claddings may occur at the end of the refill phase since the fuel and the claddings are heated up, and the system pressure is low. The deformation may be continued during the early portion of reflood. Figure 2 shows the fuel rod cladding loading in a 2F-cold leg break LOCA. The question to be answered is: "How and to what extent do coolant channel blockages (due to ballooned fuel rod claddings) influence the effectiveness of the reflood core cooling?"

For a reactor core characterized by axial and radial power distribution of roughly cosine shape it is expected that if any ballooning occurs it will be found in some fuel rod clusters of the core. Since a PWR core consists of a large number of parallel channels which are connected with each other in the radial direction, the rising reflood flow may bypass the blocked fuel rod

cluster partly including the wake of the blockage as well as a limited zone upstream of the blockage (see Fig. 3). In the investigation of the different geometries and flow conditions, it is important to include in the final results the real flow conditions due to, for example, additional hot leg injection.

The investigation of the complex flow conditions requires the simulation of a sufficiently large section of a PWR core including at least parts of the primary coolant circuit. However, to assess primarily the influence of deformed fuel rods on the effectiveness of reflood core cooling, an experimental facility was chosen which allows easy exchange of various blockages for the performance of a large number of tests for various reflood conditions. This has led to a separate effect test rig with a relatively small bundle size. However, small bundle cross sections do not allow an adequate simulation of flow pattern in the upper and lower plena of a reactor.

A number of bundle tests were conducted in order to generate heat transfer and fluid flow data needed for the safety analysis of reactors. In the majority of these tests the cooling conditions were investigated in undisturbed bundle and rod geometries /4,5/. Integral experiments with partly blocked coolant channels, e.g. some FLECHT-tests, indicated that the cooling effectiveness is enhanced in certain areas downstream of a blockage. This improved heat transfer is caused by the increased flow turbulence produced by the blockage /6/. These tests, however, were limited to only a few types of blockages and it was not clear whether this finding would generally be valid for all types of blockages. Model experiments on unheated bundles with partially blocked channels showed the phenomena occuring for single-phase flow conditions /7,8/. Experimental studies under simulated reactor decay heat power conditions were performed to study the effect of partial flow blockages on the capability of emergency core cooling. The tests conducted with both plate and sleeve blockages did not indicate any significant difference. These tests were performed in a 3x3 rod bundle, 762 mm heated length, with substantial bypass effects, at a flooding rate of 5 cm/s /9/.

To obtain a better understanding of the flow conditions and to provide an expanded data base for an adequate analytical description of the complex heat transfer processes taking place in a bundle of ballooned rods during the reflood phase, separate effect tests under forced reflood conditions

were performed. The primary goal of the tests was to study the influence of the shape and the size of cooling channel blockages on the thermal-hydraulic behavior that occurs during the reflood phase. The FEBA program (Flooding Experiments with Blocked Arrays) was carried out in consecutive test series, using a 1x5 array of electric heater rods for the preliminary tests and a 5x5 rod array as the main arrangement for all of the tests.

Similar experiments have been performed with the FLECHT-SEASET 21 rod bundle test configuration /10/ and in the THETIS rig using a 7x7 rod cluster /11/. In the FLECHT-SEASET tests, two blockage sleeve shapes have been utilized: a long non-concentric sleeve and a short concentric sleeve. Both coplanar and non-coplanar blockage arrays have been investigated under forced and gravity reflood conditions.

The THETIS cluster has contained a severe partial blockage formed by attaching sleeves to 4x4 rods. The experiments have been performed under single-phase cooling conditions as well as forced reflooding. The FEBA, FLECHT-SEASET and THETIS flow blockage programs provide complementary data. A comparison of the data shows a consistancy in trends and a general agreement in magnitude /12/. The final objective of these three flow blockage programs is the development of thermal-hydraulic models to predict the grid spacer and flow blockage effects on reflood heat transfer.

1.2 FEBA REFLOOD PROGRAM

The specific objectives of the separate effect tests under forced reflood conditions were:

- To measure and to evaluate thermal-hydraulic data for unblocked rod bundle geometries,
- To measure and to evaluate the effects of grid spacers upon the thermal-hydraulic behavior,
- To measure and to evaluate thermal-hydraulic data for blocked bundle geometries with and without bypass.

An initial set of tests with no channel blockages served as a comparison basis which would allow the evaluation of the effects of grid spacers and blockages. The second set of tests examined the perturbation effects of grid

spacers by the removal of the midplane grid spacer. The succeeding sets of test series served for variation of blockage geometries. A 5x5 rod bundle was used for all these sets of tests and a supplementary 1x5 rod row was also used as a flexible test vehicle for examining blockage shapes and sizes.

The 1x5 rod row was chosen mainly to investigate the influence of the shape of blockages on the cooling conditions. From the existing literature, for two-phase flow conditions only the results of plate blockage devices were known and this was the reason for starting the blockage tests using plate blockages characterized by sudden reduction and expansion of the flow path. The latter tests using solid as well as hollow sleves showed the influence of the shape and the size of blockages by comparison with tests using plate blockages /13/ through /16 / and /25/ through /28/. The variation of the blockage geometry is shown in Fig. 4.

The FEBA 5x5 rod bundle program consisted of eight test series with different grid spacer and sleeve blockage arrays within the bundle (see Fig. 5). The main purposes of the individual test series are:

Series I: Base-line tests with undisturbed bundle geometry containing all grid spacers for comparison with the subsequent series,

Series II: Investigation of the grid spacer effects on the axial temperature profile at bundle midplane,

Series III: 90 % blockage at the bundle midplane of 3x3 rods placed in a corner of the 5x5 rod bundle with bypass for localization of the worst cooling conditions in the blockage region, grid spacer effects near the blockage excluded,

Series IV: Same as Series III, however, for 62 % blockage at identical 3x3 rod cluster,

Series V: Similar as Series III, however, including grid spacer effects: 90 % blockage 100 mm upstream and grid spacer at bundle midplane. Investigation of a possibly hot region between blockage top end and subsequent grid spacer,

Series VI: Similar as Series V, however, including a second blockage region of 62 % blockage ratio placed downstream of the 90 % blockage at the same rod cluster. Investigation of a possibly hot region between the two blockages as well as downstream of both blockages,

Series VII: 62 % blockage ratio for all subchannels at the midplane of the bundle. Investigation of cooling enhancement downstream of blockages for a given mass flux in the blocked subchannel (mass flux in the blocked subchannel unknown for blockages with by-pass),

Series VIII: Same as Series VII, however, for 90 % blockage ratio.

The evolution of the FEBA program including the facility design as well as interim results are described successively in the semiannual and the annual reports of the Project Nuclear Safety (PNS) /13, 14, 17/.

2. TEST FACILITY DESIGN

The test facility is designed for a separate effect test program involving a constant flooding rate and a constant back pressure to allow investigation of the influence of coolant channel blockages independently of system effects.

2.1 TEST LOOP

Figure 6 shows schematically the test loop. It is a forced-flow reflood facility with a back pressure control system. Coolant water is stored in a tank (3). During operation, coolant is pumped (4) through a throttle valve (7) and a turbine meter (8) into the lower plenum region (10) of the test section (11). The coolant flow may be directed either upwards through the test assembly, or through the lower plenum (10) and water level regulation valve (9) back into the water supply. When reflood is initiated, coolant water rises in the test assembly and two-phase flow results when water reaches the hot zone of the heater rods. Entrained water droplets are transported upwards by the rising steam and may impinge on the steam water separator (13) placed above the test assembly. Figure 7 shows the design of the

upper plenum and water separator in detail. The liquid then drains into a collecting tank (17), where the water content is continuously measured. This tank had a volume of 10 dm^3 for Series I through III and a volume of 32 dm^3 for the following Series IV through VIII. Steam passes around the droplet deflector and is then flowing through a buffer tank (19) to the atmosphere. The buffer tank has an automatic pressure regulator (20) which maintains a constant exit or back pressure for the test assembly. A large external steam supply is connected to the buffer to heat up the total system and the buffer contents, and to maintain system pressure. The test rod instrumentation (15) exits from the lower end of the test assembly, as do the electric power connections (14) for the heater rods. Figure 8 shows the lower plenum, rod penetration, power supply and instrumentation exists. However, the instrumentation of the sleeve blockage is led to the top end of the housing such that it does not influence the two-phase mixture rising from the bottom. The housing is insulated to reduce heat loss to the outside air environment. Figure 9 shows a cross sectional view of the test section including the housing insulation as well as the instrumentation exits for the measurement of fluid and housing temperatures and differential pressures.

2.2 TEST SECTION

The 1x5 rod array as well as the 5x5 rod array are placed in full length housings which have a wall thickness of 6.5 mm of stainless steel (DIN 4571). The reasons for the use of this thick-wall housing are to simulate surrounding heat generating hot rods by having sufficient heat storage in the wall prior to the individual tests (see Section 8), to facilitate assembling of the test rig, and to allow easy penetration of the wall for instrumentation of the bundle with fluid thermocouples (see Section 5).

The dimensions of the housing inner cross section have been so chosen that the 5x5 rod bundle array and an infinite bundle are to have the same subchannel hydraulic diameter d_H:

$$d_H = \frac{4\ A}{C} = 13.47 \text{ mm}$$

where

A Flow area

C Wetted perimeter

The heater rod pitch is 14.3 mm. Original KWU-PWR grid spacers are located at the test midplane, and every 545 mm above and below that level. The grid spacers are attached to the rods by friction. They are sliding in the bundle housing in axial direction when relative motion between bundle and housing occurs.

The heater rods are bolted to the top flange of the test section (see Fig. 7), and the lower ends of the rods penetrate through the test assembly pressure barrier. The penetration is accomplished using O-ring sealings, and allows axial movement of the heater rods relative to the housing. Weights are hung from the bottom end of the rods to prevent them from bowing due to friction in the sealing during temperature changes (see Fig. 8).

3. HEATER ROD DESIGN

Indirect electrically heated rods are used to simulate the nuclear fuel rods. Figures 10 and 11 show the axial dimensions and the cross section of the heater rod which has PWR dimensions. A spiral wound heating element is embedded in the electrical insulator, and then encapsulated in the clad, which has a wall thickness of one millimeter. The cosine power profile of the fuel rods is approximated by 7 steps of different specific power. The left-hand side sketch of Fig. 12 shows the axial power distribution of the heater rod with a heated length of 3900 mm for the 5x5 rod bundle tests. For the 1x5 rod row tests a heated length of 2900 mm was used. The average step power level is shown together with the length of each power step. The axial power profile is flat. The peak to average ratio amounts to 1.19. The right-hand side sketch of Fig. 12 shows the axial positions of the seven grid spacers. In design, contruction and fabrication, the heater rods used in the tests are identical to the fuel rod simulators used in the PKL test facility of KWU /5/. In contrast to a nuclear fuel rod with a Zircaloy cladding and a gas filled gap, this heater rod is a "solid type" usually used for thermal-hydraulic tests without a gas filled gap between the NiCr cladding and the electrical insulation.

4. BLOCKAGE DESIGN

In the 1x5 rod array, both plate and sleeve blockages were used to simulate rod ballooning effects on the reflooding thermohydraulics. The plate blockage shown in Fig. 13 has a height of 23 mm. This figure shows also the sleeve blockage device of 80 mm length used in the 1x5 rod array. Both devices provided a 62 % flow blockage. The sleeves were located in the 1x5 rod array midplane. The plate blockage was fitted just above the midplane to have the upper end of the blockage set at the same axial position as the upper end of the sleeve blockage in the comparable tests /6, 7, 9/.

For the 5x5 rod bundle tests, sleeves of 180 mm length were used. Figures 14 and 15 show the shape of hollow sleeves used to simulate the smooth geometry expected from ballooned rods with blockages of 90 % and 62 %, respectively, of the subchannel flow area. In addition, side plate devices were placed between the sleeves and the test housing walls. The gap between the side plate devices and the housing provided sufficient insulation for reduction of radial heat loss to the housing of slightly lower temperature than the rods in the bundle.

The influence of blockage size and shape on two-phase flow and heat transfer was investigated in previous tests /13/ through /16/ and /25/ through /28/. No bypass flow existed during most of those investigations of the effect of droplet atomization at given mass flow rates. For all geometries, improved cooling was found downstream of such uniform blockages compared with baseline tests without blockages conducted under the same flooding conditions. The degree of improvement and the length of the region influenced depend on the geometrical shape of the blockage and the water content in the two-phase flow. Sleeves with slim conical ends cause the smallest improvement of cooling. This axial shape was chosen for the 25 rod bundle tests to be conservative with respect to cooling improvement.

Since an array of 5x5 rods is very small compared with the number of rods and parallel channels in a PWR core, a sufficient bypass cross section must be provided in a small bundle to suppress the unintended cooling improvement in the bypass region. A blockage cross section was chosen, thus blocking 90 % of the individual subchannel flow areas in a 3x3 rod cluster (see Fig. 16). This cross section was obtained with the minimum bending radius of

Zircaloy cladding producing no cracking of the cladding. The length of the fully reduced cross section was 65 mm. Including the conical part at both ends of the sleeves, the total length of the blockage placed symmetrically to the midplane of the rod bundle was 180 mm. For this array the grid spacer located at this level in previous tests with nominal geometry was removed.

For the test series performed with 62 % blockages, similar sleeves were used which blocked 62 % of the subchannel flow areas within the 3x3 cluster previously mentioned. The length of the fully reduced area was 125 mm. The sleeves were cylindrical and touching each other in the cluster. The total length of the sleeves including the conical ends were 180 mm, the same as that for the 90 % blockage (see Fig. 17).

To approximate the conditions of larger bundles with larger clusters of "ballooned" rods, the 3x3 cluster with sleeves was placed in a corner of the square bundle housing. The subchannels between sleeve blockages and housing were blocked by side plate devices causing the same blockage ratio for these subchannels. This geometry provides maximum path length for cross flow and may approximate one quarter of a 10x10 bundle with a blocked 6x6 cluster in the center. But, since especially the cross flow downstream of the blocked section will differ in these two situations, restrictions must be made for an extrapolation of the results from the 5x5 rod bundle geometry to a 10x10 rod bundle. However, for the conditions in the bypass region, upstream of the blockage and within the blockage, the two cases are not expected to differ very much from each other.

The amount of stored heat and the thermal inertia of the fuel rod simulators are different from those of fuel rods with lifted clads which are ballooned to the same outer shape. The thermal behavior of different sleeve designs was precalculated using the heat conduction program HETRAP /18/ and the material properties programmed in the PEW code /19/. Experimental investigations are reported in References /14, 17/. The design chosen for the 5x5 rod bundle tests is a compromise with the following properties: The gap of 0.8 mm width between heater rod surface and inner surface of the sleeve filled with stagnant steam leads to gap coefficients which are assumed to be of the same order of magnitude as those of ballooned fuel rods (0.02 W/cm^2 K) /36/. For flooding velocities of more than 4 cm/s, the 1 mm thick sleeve wall does not produce significantly different temperature transients compared with the

ballooned cladding of a fuel rod. At lower flooding velocities both the rate of temperature decrease after the beginning of reflood and the rate of the subsequent temperature increase are slightly diminished as shown in Fig. 18. Both effects are due to the higher heat capacity of the sleeves. A minimum sleeve wall thickness of 1 mm was maintained to allow instrumentation by embedded thermocouples. With respect to the quench time within the blockage, the 1 mm thick wall leads to rather conservative results.

5. INSTRUMENTATION

The flooding of heated rod bundles in a simulation of the reflood phase of a LOCA of a LWR core presents many complex two-phase flow phenomena. One of the most important results to be obtained from such experiments is the time dependent value of the local heat transfer coefficient at various axial and radial locations. Heat transfer coefficients are generally calculated using the saturation temperature at the system pressure as the coolant temperature. However, detailed investigation of the local phenomena, i.e. at grid spacers and other flow obstructions such as local blockages simulating ballooned fuel rods, calls for information about steam superheat, and the presence and distribution of water which mark a significant deviation from the situation of saturation. The cooling effectiveness of the dispersed flow depends mainly on these parameters.

Most part of the instrumentation consisted of thermocouples (Chromel-Alumel) since cladding, sleeve, local channel and housing temperatures are to be measured at various locations. Cladding and sleeve temperatures are measured with 0.5 mm sheath diameter thermocouples having insulated junctions. These thermocouples are embedded in grooves which are milled into the outer surface of the rod claddings and sleeves. The grooves are closed by brazing over the total length to avoid any disturbance of the coolant flow. Details of the heater rod instrumentation are shown in Fig. 19.

Fig. 20 shows photographs of both noninstrumented and instrumented flow blockage devices used in 1x5 rod row and 5x5 rod bundle, respectively.

Fig. 21 shows a photograph of the FEBA test rig.

Figures 22 through 30 show the axial and radial rod bundle instrumentation of the 5x5 rod array. Pressures and pressure differences were measured with pressure transducers. In addition to the inlet and outlet pressure, the pressure differences along the midplane as well as along both the lower and upper portion of the bundle were measured. The flooding rate was measured with a turbine flow meter. The amount of the water carry over was measured continuously by a pressure transducer on the water collecting tank. All data were digitally recorded with a scan frequency of 10 cycles per second.

Fluid temperatures were measured with 0.25 mm as well as with 0.50 mm diameter thermocouples with the junction protruding into the flow channel. Thermocouples both with and without radiation and/or droplet shields were used at different axial levels. High frequency 0.6 mm diameter probes were also used which could deliver signals from droplets, providing information about the two separate phases of the flow /20/.

Figure 31 shows temperature transients measured with the fluid thermocouples indicated on the figure and temperatures of the surrounding housing and rod claddings of a 1x5 rod bundle test. The signals of all three fluid thermocouples indicated roughly same temperatures during most part of reflood. Radiation effect for the unshielded thermocouple was not detectable. However, the shieldings led to earlier quenching of the shielded thermocouples while the unshielded TC showed the prevailance of steam superheat for a longer time span.

For Series I through III a small number of shielded fluid thermocouples were used at selected axial levels /2/. However, most of the fluid temperature measurement devices used in these series were unshielded thermocouples of 0.25 mm outer sheath diameter and for Series IV trough VIII no other devices were used.

For detection of the water level rising from the lower plenum at the ontset of the reflood phase water level detectors were used. These detectors consisted of two thermocouples (Chromel-Alumel) placed together with MgO insulation in a stainless steel sheath. One of the thermocouple junctions was heated by DC to dry out and heat up the tip of the detector protruding into a subchannel of the bundle at the axial levels indicated in Fig. 22. When the water level was passing the detector the heating of the tip was not

sufficient to keep the detector dry. The temperature drop measured with the second junction indicated clearly the passing of the water level as shown in Fig. 32.

High-frequency probes were used in a few tests to detect the presence of water in the flow channels. The method was developed to investigate the steady-state two-phase flow in phase equilibrium. The measuring principle is based on the different reflections of a high-frequency electric wave at the open end of the probe. The different terminating impedances there are caused by the different electric losses in the two separate phases. The measuring effect is a yes-or-no statement /21/ through /23/. The probe development and the signal analysis are extended to application in transient two-phase flow /20/. For this purpose, probes with the following features were needed:
- resistant to temperatures up to 800 ^{o}C,
- resistant to thermal shocks,
- signal quasi-independent of temperature changes.

For signal evaluation, integration methods were used. Several integration time steps had to be adapted to the different aims of the analysis of the flow conditions during reflood.

6. DATA ACQUISITION SYSTEM

For data acquisition of the different tests, two different systems were used during the investigation of the program. From Series I through VI, a 130-channel Digizet B system (Siemens) served for amplification, assembling and digitalization of the individual signals, which had been previously recorded on tapes by a central TR 44 computer (Telefunken). The measuring time for all 130 channels was about 10 ms, the scan frequency 10 cycles/s. For noise reduction, 15 Hz filters were placed at the entrance of the amplifiers. Fast transients as signals from fluid thermocouples, water detection probes and pressure transducers were simultaneously recorded on analog tape to investigate the loss of information due to the 15 Hz filters as well as to digitalization. The scan frequency of 10 cycles/s delivered sufficient information from the fluid thermocouple and pressure transducer signals. Therefore, the analog signal recording was maintained only for signals from the water detection probes used in some selected tests. For Series VII and VIII, the Digizet B and the TR 44 were replaced by NEFF amplifiers, a PDP-11 mini

computer and fast data recording by disks. Measuring time and scan frequency remained unchanged. The evaluation of the data recorded on tapes or disks was done using the central KfK computer (IBM 3033, Siemens 7890).

For the data transfer, data management, heat transfer analysis and data comparison and representation, a detailed computer code was written /24/ using the physical properties of the specific materials programmed in the PEW code /19/.

7. PROGRAM TEST PARAMETERS

The main test parameters which were varied included:
- system pressure,
- flooding rate given as flooding velocity, i.e. the velocity of the rising water level in the cold bundle,
- geometry of the blockages.

Figure 33 gives an overlook over the values chosen.
The tests performed are listed in Tables 1 through 8.

8. OPERATIONAL PROCEDURE

The investigation of separate effects of core reflood during a PWR LOCA requires well defined system parameters for each test. The quality of the comparison among the tests depends mainly on the repeatability of the individual tests. Therefore, with respect to the real sequence of events during a LOCA, the following modification of the heat up period during refill of a reactor vessel has been made:

For about two hours prior to reflood, the fuel rod simulators were heated in stagnant steam to the desired initial cladding temperature, using a low rod power. In the mean time the test housing was being heated up passively to the desired initial temperature by radiation from the rods. This led to a wall (6.5 mm thick) heat content of approximately the same as that of half a row of heater rods including the heat input during a test (rod power). For reflood tests of long duration, i.e. small flooding velocity and /or low pressure, the initial housing temperature had to be at a higher level than for test of short duration. This was achievable using the previously described, modified heat up period. The aim of choosing the "active wall" was

to prevent premature quenching of the wall relative to the bundle quench front progression. The hot steam film at the surface of the wall acts somewhat like a layer of insulation for the two-phase flow in the bundle subchannels. The "passive wall" design using a thin wall of low heat capacity is an alternative method. Such a wall has to be placed at symmetry lines of the bundle subchannels. However, this design needs a surrounding pressure tube which complicates the problems of instrumentation and assembling. Furthermore, premature quenching may occur during mist flow regime. Droplets entrained by steam flow may be caught by a wet wall leading to a certain additional dry out of the two-phase flow, possibly a significant effect for small bundle arrays. Due to this uncertainty, the "active wall" design was eventually chosen.

During the heat up period of the housing by radiation from the rods, the flow pattern shown in Fig. 34 was maintained. Water was flowing to the lower bundle plenum cooling the O-ring sealing of the rods which penetrated the bottom of the lower plenum. This water flow, depending on the parameters of the following test, was drained back to the water tank by a valve which controlled the water level in the lower plenum. The steam filled ducts and components of the test rig were heated up to temperatures slightly above the saturation temperature by a separate steam supply. Condensing water was drained to the water tank. The surplus steam left the system from the upper buffer to the atmosphere through a relieve valve for control of the system pressure. The supplied steam was fed into the upper buffer as well as into the lower bundle plenum. The rate of feeding of steam into the lower plenum had to compensate for the condensation at the water surface. When the rate was too low, steam flew from the upper bundle plenum to the cold surface of the lower plenum. In this way, the steam was heated up within the hot bundle, and the axial temperature profile in the bundle was deformed showing its maximum below the bundle midplane. When the rate into the lower plenum was too high, the maximum temperature within the bundle was shifted above the bundle midplane. This was a controlling method to vary as well as to correct the initial conditions for the individual tests. During the heat up period, the data acquisition system was used for control and check as well.

Reflood was initiated by closing the water exit and the steam inlet valve at the lower bundle plenum and the drain valve of the water collecting tank (see Fig. 34). The bundle power was stepped up to the controlled decay heat

transient, i.e. 120 % ANS-Standard 40 s after shut down of a reactor for most of the tests. About 30 s prior to reflood the data recording system was started. Figure 35 shows the operational procedure schematically. After the completion of a test the data recorded were checked to see whether the test including the data were correct or should be repeated.

For most of the tests the behavior of the housing was as expected. Quenching at the different axial levels occured roughly at the same time for both the housing and the bundle.

9. RESULTS AND DISCUSSIONS

The program consisted of two major steps to investigate separate effects of reflood cooling in a PWR core geometry with coolant channel deformations. In the first step, a 1x5 rod array (see Fig. 4) was used with a heated length of 2.90 m simulating the core height of a small PWR (Biblis A). The readily available fuel rod simulators were used for the qualitative investigation of the influence of size and shape of coolant channel blockages on reflood core cooling. The results, to be described in Section 9.1, were also used in the design of adequate simulation of ballooned fuel rods (sleeve design) including a severe and a hypothetical blockage ratio as well as in optimization of bundle instrumentation for the measurement of the blockage effects. In the second step, a 5x5 rod bundle (see Fig. 5) was used with a heated length of 3.90 m simulating the core height of a 1300 MW standard PWR (Biblis B). The results are presented in Sections 9.2 through 9.5 and Sections 10 and 11.

9.1 QUALITATIVE INFLUENCE OF BLOCKAGE SIZE AND SHAPE (1x5 ROD ROW)

From shakedown tests it was learned that small and local coolant channel constrictions did not affect the reflood cooling significantly. Therefore two relatively severe blockage ratios were chosen to obtain measurable effects of simulated clad ballooning:

- 62 % blockage which corresponds to symmetrical ballooning of rods until the ballooned claddings touch each other.

- 90 % blockage which corresponds roughly to continued ballooning leading to

square cross sections of the balloons with rounded edges. It is assumed that for a certain minimum bending radius of the cladding at the corners of the square balloons the cladding bursts, terminating the ballooning.

From ballooning tests, it has been learned that the ballooned fuel rod claddings are approximately cosine in axial shape with conical ends of various lengths. However, for previous thermal-hydraulic tests including flow blockages, mainly short plate blockages have been used. The plate blockages have sharp edges, presenting abrupt flow area changes. As a consequence, the plates produce more flow turbulence than do sleeves with conical ends for comparable blockage ratios and pressure drop.

Therefore the main aim of the 1x5 rod tests was the investigation of the different effects of plate and sleeve blockages. The plate blockages induced the flow path constriction in the center of the subchannels depriving cooling improvement at the rod surface over the constricted region of the bundle.

The sketches of Fig. 36 show respectively some of the plate and sleeve blockage arrangements investigated in the 1x5 rod row. Figure 37 presents cladding temperatures as a function of time after start of reflood for unblocked, 62 % sleeve blockage and 62 % plate blockage, respectively. Four measuring positions are shown, i.e. 50 mm upstream of the midplane as well as 85, 135 and 335 mm downstream of the midplane. The flooding velocity was 2 cm/s, system pressure 4.5 bar, and feedwater temperature about 40 ^{o}C. The plots show that at low flooding rates the influence of a sleeve-type 62 % blockage is hardly detectable and no additional quench front is produced. However, at the same flooding rate a plate-type 62 % blockage causes significantly lower temperature rises in a zone of at least 300 mm long immediately downstream of the blockage and the initiation of an additional quench front.

At higher flooding rates (6.7 cm/s) the sleeve blockage also produces enhanced cooling immediatly downstream of the blockage. This leads to somewhat reduced temperature rises in a zone of less than 100 mm long behind the upper end of the sleeve. Again, the plate blockage produces far greater cooling effects than do the sleeve. Here, the plate blockage causes a strong cooling improvement over a zone of more than 300 mm long with decreasing

cladding temperatures from the start of flooding and with early quenching. The degree of the improvement and the length of the affected zone depend on the steam velocity, the water content in the two-phase flow and the geometrical shape of the blockage. The water content increases with increasing flooding rate. Downstream of the plate blockage, an additional quench front was observed at flooding velocities of 2 cm/s and greater. A flooding velocity of 5 cm/s was necessary for the establishment of a separate quench front when a comparable sleeve blockage was used. More details are reported in References /14/ through /16/ and /25/ through /28/.

These results confirm the finding of the early PWR-FLECHT blocked bundle data /4/ as far as improved cooling behind plate blockages is concerned. They further show that it is important to perform experiments with slim rounded sleeve blockages similar to ballooned fuel rods in order to avoid taking unjustifiably high credit for the cooling effects downstream of the blockage.

9.2 EFFECTS OF BLOCKAGES WITH AND WITHOUT BYPASS (5x5 ROD BUNDLE)

Figure 4 shows arrangements of the eight test series performed using the 5x5 rod bundle array. To assess the effects of flow blockage caused by ballooned rods upon two-phase flow and local heat transfer, unblocked and blocked bundle test results are compared. For the unblocked bundle tests, two test series were performed to separate out the grid spacer effects possibly overlaying blockage effects. For simulation of the end of the refill phase, a selected axial temperature profile was established within the rod bundle (see Fig. 38). At beginning of reflood, the bundle power was switched to the corresponding decay heat transient when the water, which was fed at a constant rate into the lower bundle plenum, reached the lower end of the heated bundle. The feedwater temperature and the system pressure were both kept constant during each test run (see Fig. 39). However, at the beginning of reflood, the feedwater was heated up by the hot environment of the lower plenum. Nevertheless, some few seconds later the feed water temperature decreased and reached the desired value.

The resulting quench front for the test data plotted is shown in Fig. 40. There is no quench front moving from the top of the bundle towards the quench front rising from below because of the design of the upper bundle

plenum. The water entrained by the steam leaving the upper bundle grid plate is separated out from the steam flow and drained into the water collecting tank. No water leaving the bundle can fall back into the bundle. The geometry of a reactor is different for that area. The fuel rods end before the upper core support structures. However, the length of this separation space depends on the reactor design as well as the flow and the water deentrainment conditions. Therefore, the most pessimistic situation has been chosen for the tests: The water once left the bundle is lost for further possible cooling. From Fig. 39 it can be concluded that during flow pulsations within the bundle (occuring inspite of constant flooding rate), a certain amount of water above the top end of fuel rods would fall back into the bundle when the system pressure and the steam velocity at the bundle exit, respectively are at their instantaneous minimum.

Most of the results discussed below are reported in References /17/, /29/ through /43/.

9.2.1 BASE-LINE TESTS AND GRID SPACER EFFECTS, SERIES I AND II

The base-line tests have been performed to include the boundary conditions of the test facility and the operational procedure in the parametric study of the reflood conditions. Furthermore, the tests have made it possible to quantify the grid spacer effects. The axial and radial locations of the measuring positions are shown in Figures 22 through 24. The test parameters of both Series are listed in Tables 1 and 2.

9.2.1.1 MEASUREMENTS

Figure 41 shows cladding temperatures as a function of time after start of reflood for the unblocked bundle Test No. 216 including seven grid spacers (Series I). Four elevations about the bundle midplane have been chosen for the figure because the midplane grid spacer has been removed for Series II and replaced by various sleeve blockage arrays for Series III, IV, VII and VIII. For information about the radial temperature distribution in the bundle including two-phase flow effects, two measurements from different rods are plotted for three of these four elevations. The location of the rods is chosen such that they are placed either in the "blocked region" and/or in the "bypass region", for Series III, IV, V and VI. All axial elevations are

referenced to the top flange of the rod bundle.

From Series II, cladding temperatures are shown from test No. 229 in Fig. 42, measured at identical rods and elevations, respectively, as for Test No. 216 of Series I. The initial as well as the flooding conditions are the same. Closer comparison of the data from series I and II shows significant differences for Level 1925 mm, i.e. 60 mm downstream of the trailing edge of the midplane grid spacer of Series I, missing for Series II. The axial temperature profiles shown in Fig. 43 for three time steps are taken from the temperature transients of the afore-mentioned tests.

These pronounced grid spacer effects have been observed also in the FLECHT-SEASET 21 rod bundle experiments /44/, the THETIS reflooding experiments on a 49 rod cluster /11/, the ERSEC reflooding experiments on a 6x6 rod bundle investigating the effect of different grid spacers /45/, the REBEKA clad ballooning experiments /46/, and the NRU-MT-3 clad ballooning experiments /47/.

9.2.1.2 DISCUSSION OF THE GRID SPACER EFFECTS

Grid spacers represent coplanar blockages with blockage ratios of about 20 %. The coolant mass flux of the individual subchannels remains identical for the constricted areas, because no bypass exists as for clusters of ballooned rods in a PWR core. Inspite of the small blockage ratio of grid spacers, they produce high flow turbulence and dispersion of droplets due to their geometrical shape. Thin plates placed parallel to the flow direction are crossing in the center of each subchannel dividing it into four small flow areas.

Local enhancement of the cooling occurs mainly for the early portion of the reflood phase, disappearing approximately at the onset of film boiling. The axial extent of the effect decreases with increasing distance from the grid spacer, disappearing approximately 300 mm downstream of the trailing edge of the grid spacer.

The results show that the blockage arrays chosen for series III, IV, VII and VIII are sufficiently far away from the upstream grid spacer for a meaningful separate investigation of the blockage effects. Further analysis of the

grid spacer effects is made in Section 11.1.

9.2.2 SEPARATE EFFECTS OF BLOCKAGES WITH BYPASS, SERIES III AND IV

The flow diversion around ballooned fuel rods in the center of a PWR as shown in Fig. 3 indicates a certain coolant mass flux reduction for the blocked rod cluster. This effect may lead to reduced local cooling. However, a two-phase flow passing a blockage may lead to enhanced cooling for a given mass flux due to increased turbulence and droplet dispersion. Since the measurement of the local mass flux within a rod bundle (especially for a transient two-phase flow) generally can not be made accurate enough, the effect of flow diversion is hence investigated in Series III and IV.

To approximate the flow conditions of larger bundles with larger clusters of "ballooned" rods, a 3x3 rod cluster with sleeves for simulation of ballooned claddings was placed in a corner of the square bundle housing containing the 5x5 rod bundle. This geometry roughly corresponds to one quarter of a 10x10 rod bundle with a blocked 6x6 rod cluster in the center. But, since especially the cross flow downstream of the blocked section will differ in these two arrays, restrictions must be made for an extrapolation of the results for the 5x5 array to those for a 10x10 array. The conditions in the bypass region as well as upstream of the blockage and within the blockage may be closer to each other.

9.2.2.1 MEASUREMENTS, SERIES III

The axial and radial locations of the temperature measuring positions are shown in Figures 22 and 25. The tests performed as well as the corresponding parameters are listed in Table 3. Sample results of measurement of temperature transients in the region of the blockage for one of the tests are plotted in Fig. 44. Upstream of the blockage (Level 2125 mm), the maximum temperatures and quench times of the blocked rod cluster are almost the same as those of the bypass rod cluster. For the flooding conditions mentioned, a slight improvement of the cooling upstream of the blockage occurs probably due to water entrainment and breaking up of droplets at the leading edge of the blockage. At the midplane of the blockage (Level 2025 mm), the tempera-

ture transient measured in the bypass corresponds roughly to that of an unblocked bundle at the same elevation under identical flooding conditions. The temperatures of the sleeves exposed to the reduced coolant mass flux in the constricted subchannels are lower than those of the claddings in the bypass. However, the temperatures of the portion of the rods which are covered by the sleeves remain high throughout the whole period. Downstream of the blockage (Level 1925 mm), both the maximum temperature and quench time of the blocked rod cluster are affected by the blockage. The maximum temperature in the blocked rod cluster becomes slightly higher, and quenching occurs much later. Both effects are diminished further downstream.

9.2.2.2 DISCUSSION, SERIES III

The above description of the temperature transients for the test reported in Fig. 44 applies qualitatively equally well to all tests of Series III. Within the blockage, the steam filled gap of 0.8 mm width between the outer surface of the heater rods and the inner surface of the sleeves leads to an immediate decrease of the sleeve temperatures after the start of reflood. In the case of 90 % blockage, only a small portion of the sleeve surface is exposed to the coolant flow to achieve effective radial heat removal. Except for the short quenching period, axial heat conduction in the rod and the sleeve is negligible as suggested by experimental results and supported by corresponding analyses. The radial heat transfer through the gap between the rod and the sleeve is most important for the simulation quality of the array chosen /28/. For the blockage cooling, it can be concluded that the mass flux reduction due to flow diversion leads to delayed heat removal from the rods underneath the deformed claddings. However, the temperatures of the "lifted claddings" are lower than those of the undeformed claddings in the bypass during the most interesting part of the reflood period.

Downstream of the blockage, the difference in temperature rise between blocked and unblocked arrays is relatively small inspite of the close coplanar blockage arrangement and the high blockage ratio of 90 % over an axial length of 65 mm. Moreover, the region in which this difference can be detected is very limited. The most significant difference between the temperature transients so compared is found during the second half of the reflood period when cladding temperatures decrease in the unblocked array. The typical turnaround point as found in unblocked arrays rarely appears in the blocked

arrays. The reason for the delayed decrease of the cladding temperature downstream of the blockage is that a new quench front has to be initiated. When the top end of the sleeves is quenched, the portion of the rod which is covered by the sleeves stays hot. The axial propagation of the quench front due to heat conduction within the rod is interrupted by the sleeve. Therefore, precursory cooling downstream of the blockage has to bring the claddings to a lower temperature level than usually measured (compare temperature transients plotted for Level 1925 mm in Fig. 44). The quench front initiated downstream of the blockage proceeds faster than the quench front in the bypass rod cluster until they reach the same elevation at the same time somewhere further downstream. This quenching phenomenon found in the case of solid fuel rod simulators without gap between heat source and cladding and in the case of sleeves simulating deformed fuel rod claddings might be different from that found in the case of ballooned real fuel rods. The sleeve design adopted for the present investigation leads to rather conservative results concerning delayed quenching.

9.2.2.3 MEASUREMENTS, SERIES IV

With the 62 % blockage at a 3x3 rod cluster in a corner of a 5x5 rod bundle, a larger number of tests has been performed (see Table 4). The axial and radial locations of the temperature measuring positions are shown in Figures 22 and 26. The temperature transients plotted in Fig. 45 were measured from a test conducted with identical flooding conditions as for the test of 90 % blockage presented in Fig. 44. Most significant differences are the sleeve temperature and cladding temperature transients downstream of the blockage. The sleeves are quenched earlier than the claddings of the rods in the bypass. A new quench front is initiated downstream of the blockage before the main bundle quench front reaches the blockage level. The portion of the rod which is covered by a sleeve stays hot, indicating delayed heat removal from the blocked portion of the bundle.

9.2.2.4 DISCUSSION, SERIES IV

Figure 46 shows temperature transients, measured at exactly the same locations as in the previously described test, for a test performed with a lower flooding velocity, v = 2.2 cm/s, but the same system pressure as before. The sleeve temperature transient shows no more earlier quenching and both the

heat removal and the quenching downstream of the blockage are delayed. The transients are more similar to those shown in Fig. 44 for the test with 90 % blockage and a higher flooding velocity. The main difference between these two tests is that the maximum temperature downstream of the 62 % blockage remains at the same level as that measured for the bypass rod claddings.

The test performed with a flooding velocity of v = 5.8 cm/s (see Fig. 47) again shows earlier quenching of the sleeves as well as of the claddings downstream of the blockage. For a lower system pressure and the same flooding velocity, these effects are even more pronounced inspite of the longer duration of the total reflood phase (compare Fig. 47 with Fig. 48).

The test performed with the low pressure of 2 bar and the medium flooding velocity of 3.8 cm/s shows earlier quenching of the sleeves and delayed quenching of the rod portions downstream of the blockage (see Fig. 49). The test performed with the same flooding velocity and a high system pressure of 6 bar again shows earlier quenching for the sleeves as well as for the claddings downstream of the blockage (see Fig. 50). Both effects increase with increasing flooding velocity (compare Fig. 47 with Fig. 51).

9.2.3 COMBINED EFFECTS OF BLOCKAGES WITH BYPASS AND GRID SPACERS, SERIES V AND VI

It is evident from the data presented thus far that coolant channel blockages of 62 % and even 90 % in the arrays chosen scarcely cause increases in cladding temperatures for the flooding conditions applied. However, the exact mass flux distributions in the blocked and bypass regions of the bundle are unknown. The effects of droplet dispersion, cross flow, and fall back of droplets into subchannels with reduced steam velocity could not be individually distinguished in Series I through IV.

Series V and VI were designed for providing information about the combined effects of mass flux diversion and redistribution. For example, does the cross flow downstream of a 90 % blockage lead to a reduction in the temperature increase downstream of the blockage? Therefore, a grid spacer has been placed immediately downstream of a 90 % blockage in Series V. While the grid spacer hinders cross flow over a certain rod length, it, on the other hand, improves cooling downstream for a given mass flux.

If coplanar blockages were developed simultaneously at two different elevations in a rod cluster, would the main coolant mass flux bypass both blockages and thus cause a hot region between the two blockage elevations? To address this question, the array of Series VI was tested. It is known from investigations /46/ concerning the influence of thermalhydraulics on fuel rod behavior during a LOCA (REBEKA-program) that for such blockage configurations (not likely expected in a reactor), a grid spacer would normally be found between the two blockage elevations.

9.2.3.1 MEASUREMENTS, SERIES V AND VI

For these two test series, a sole system pressure of 4 bar was applied. The variation of flooding velocity as the most important parameter was found sufficient for the screening of additional effects. The axial and radial locations of the temperature measuring positions are shown in Figs. 22, 27, and 28. The complete sets of tests performed for Series V and VI are listed in Tables 5 and 6, respectively.

9.2.3.2 DISCUSSION, SERIES V AND VI

The results of a test of Series V as shown in Fig. 52 are compared with the results obtained from Series III, as shown in Fig. 44. It has to be mentioned that for Series V (as well as for Series VI) the 90 % blockage was placed 100 mm below the bundle midplane, i.e. below the elevation of the blockage midplane of Series III. This partially explains the earlier quenching of the sleeves for the tests of Series V but not observed for Series III. An additional difference between the results of Series V and those of Series III was found in the region downstream of the blockage. The slight increase of the maximum temperature downstream of the blockage remaining similar to that observed for Series III, there is no delayed quenching downstream of the blockage of Series V. The grid spacer placed downstream of the top end of the blockage does not hinder the slight increase of the maximum temperature compared with the situation in the bypass. This temperature difference is developing during the first half of the reflood phase and is recovered during the second half. The cooling situation in the region of the blockage which is followed by a grid spacer is essentially the same as that for an identical blockage which is not followed by a grid spacer. In the region of the blockage up to the leading edge of the midplane grid spacer

for Series VI, a similar observation on the cooling situation can be made. However, for Series VI the grid spacer effect leads to much lower temperatures at Level 2025 mm, upstream of the 62 % blockage (see Fig. 53). The temperature transients measured at the level of the 62 % blockage and downstream of it are shown in Fig. 54. The sleeve temperatures in the 62 % blockage as well as the cladding temperatures downstream are lower than the cladding temperatures in the bypass. This result is qualitatively consistent with the effects found in Series IV. However, the mass flux through the 62 % blockage, which is placed downstream of the 90 % blockage, must have been reduced in comparison with Series IV. Because of this, cladding temperatures become higher 200 mm downstream of the 62 % blockage as compared with those in the bypass. A second region of higher cladding temperatures can be found far downstream of the upper blockage.

Not all phenomena occuring in Series V and VI can be completely explained. More information is clearly needed, especially concerning the contributions of the entrained water to the local and integral heat removal in such bundle and blockage configurations. This problem will be approached below (Section 10) by analyzing the water carry over measured in the tests with different blockage geometries.

9.2.4 EFFECTS OF BLOCKAGES WITHOUT BYPASS, COOLING ENHANCEMENT FOR KNOWN MASS FLUX, SERIES VII AND VIII

For the blockage configurations with bypass presented up to this point, the coolant mass flux through the constricted subchannels is not readily determinable. This is not the case for the arrays of Series VII and VIII. At the bundle midplane all subchannels are blocked by identical sleeves of a design same as for the blockage arrays presented above. The mass flux transients for the constricted subchannels correspond then to those for the totally unblocked bundle.

Strictly speaking, this is not representative of the situation in the core of a reactor. However, in this arrangement the influence of blockage size on the two-phase flow cooling behaviors can nevertheless be investigated quantitatively for a given blockage shape.

9.2.4.1 MEASUREMENTS, SERIES VII AND VIII

The tests performed for Series VII and VIII with blockage ratios of 62 % and of 90 %, respectively are listed in Tables 7 and 8. The axial and radial locations of the measuring positions are shown in Figs. 22, 29, and 30. Tests with cooling by dry steam have also been included for the purpose of separating out the cooling enhancement of blockages for single-phase flow. However, the steam cooling tests were performed as steady state tests using a low bundle power because of the poor single-phase cooling. (The maximum temperature for the fuel rod simulators used was limited to 1050 ^{o}C). The separate steam supply available was not sufficient to remove the 120% ANS-Standard decay heat transient applied for the reflood tests presented.

9.2.4.2 DISCUSSION, SERIES VII AND VIII

For blockages without bypass, the coolant mass flux through the constricted subchannels is increased significantly compared with that of the constricted subchannels of identical blockages with bypass for identical flooding conditions. Inspite of this fact the cooling conditions within the blockage itself have been found to be essentially unchanged. Figure 55 shows temperature transients from a test of Series VII performed with the base case flooding conditions V = 3.8 cm/s, P = 4 bar). The sleeve temperature transient corresponds roughly to that shown in Fig. 45. The cooling conditions within the blockage are nearly the same for Series IV and VII. However, downstream of the blockage the cooling enhancement increases significantly for the blockage without bypass. This effect increases again for increased blockage ratio adopted for Series VIII (see Fig. 56). This is consistent with the results obtained with the 1x5 rod array briefly described in Section 9.1. The results of Series VII and VIII allow quantitative analyses of the blockage effects on a similar basis as for the grid spacer effect.

10. COMPARISON OF ALL ARRAYS WITH EACH OTHER

The main aims of the FEBA program are:

- To find out the order of magnitude of blockage effects on emergency core cooling (ECC);
- To provide a data base for modeling of blockage effects on ECC thermohydraulics.

Cladding temperature transients produce the first quantitative information about the rod bundle cooling behaviors. Therefore, some of the data already shown are compared with each other for some selected cases of interest.

To examine the effects of a 90 % blockage with bypass, temperature transients of Series III are compared with those of Series II, a bundle configuration without the midplane grid spacer. Figure 57 shows temperature transients measured in the 3x3 rod blockage zone, in the bypass zone, and data from the corresponding test of Series II. Upstream of the blockage (Level 2125 mm), the maximum temperatures and quench times are almost the same. At the midplane of the blockage (Level 2025 mm), the temperature transient measured in the bypass is lower than that of the unblocked bundle. The temperatures of the sleeves are lower than those of the claddings in the byass. Downstream of the blockage (Level 1925 mm) the maximum temperature in the blocked cluster becomes lower than that of the unblocked bundle. This comparison indicates that a 90 % blockage with bypass in the 5x5 rod bundle gives a better heat transfer in the first half of the reflood period where the peak cladding temperatures occur than in the unblocked bundle test.

Figures 58 through 61 again show further comparisons of temperature transients from different test series. Besides the different blockage effects, they might also provide information about the scatter of the data from one test to another. The possibilities of maintaining identical initial conditions as well as to reproduce identical transients are limited. Any analysis of experimental data would have to take into consideration this important point. Therefore, modeling of the complex thermal-hydraulic phenomena seems to be a problem of even more immense severity.

The cooling enhancement effect of blockages (see Section 9.2.2) seems to be smaller for single-phase flows than for two-phase flows. The main reason for this is the effectiveness of the water content of the two-phase flow on the heat removal from the heated rod bundles. Normally, a certain amount of the water fed into the lower portion of the bundle is carried by the steam flow to the upper end of the bundle without removing much heat along the way. With increasing number as well as size of flow obstacles, the amount of water carry over decreases and the overall heat removal increases. Locally, there might be decreased cooling depending on the geometrical conditions for flow split. However, reduced steam velocity in the wake of e.g. blockages

with bypass could allow the droplets to fall back. These droplets are dispersed and partially evaporated on approaching hot surfaces thus removing a significant amount of heat. This new cooling mechanism helps suppress the cooling problem in regions of reduced steam flow of the bundle. Additionally, droplets are dispersed at each flow obstacle leading to an increase in population of smaller droplets and, hence, enhanced cooling compared with single-phase flows.

The increase of evaporation of droplets due to blockages can be investigated quantitatively by comparing the time-dependent water carry over for the different blockage arrays. At first, the influence of the system pressure as well as of the flooding velocity for a given array as the base case are obtained. In Fig. 62, a plot of water carry over versus time is shown for three tests performed with the array of Series IV. For increased system pressure, the water carry over decreases because of the lower steam velocity mainly. Some cladding temperature transients of the tests chosen are shown in Figures 45, 49 and 50. The influence of the flooding velocity is demonstrated in Fig. 63. Cladding temperature transients of the corresponding tests are shown in Figures 45, 46 and 47.

The water carry over measured from three tests performed with identical flooding conditions (pressure and flooding velocity) but different blockage geometries is presented in Fig. 64. About 30 % of the water fed into the lower plenum has exited through the upper end of the bundle when the bundle midplane is quenched for the tests of Series IV. However, only 22 % is carried over at the same time in the comparable test of Series V with seven grid spacers and a 90 % blockage array. And for Series VI, with seven grid spacers and stacked 90 % and 62 % blockage arrays, only 14 % of the water injected leaves the bundle within a time span of about 250 s. In this bundle, the droplets hit the flow obstacles and became dispersed to contribute to an enhanced evaporative cooling, especially in the blocked rod cluster. Therefore, far downstream of the upper blockage, increased heating of the coolant is observed in comparison with the situation in the bypass at the same level. Just downstream of the upper blockage, cladding temperatures are lower than in the bypass and for an axial distance of 200 mm from the blockage the situation becomes just the opposite (see Fig. 54, Levels 1725 and 1525 mm).

From the data of Series VIII (all subchannels blocked, blockage ratio 90 %) it can be concluded, that the total water content of the flow passing through the blockage is evaporated inside and downstream of the blockage and consequently no water carry over is measurable during the early portion of the reflood phase of a LOCA as shown in Fig. 65. A comparison of temperature transients of a few sample tests is shown in the plots of Figures 45 and 56. The high evaporation rate inside and downstream of the blockage is believed to be responsible for the significant heat removal in that area. Far downstream, then, there is only single-phase steam cooling with greatly increased steam mass flux.

11. ANALYSES

For a better understanding of the different cooling mechanisms which take place during the reflooding phase, the two-phase flow can be roughly divided into several sequential flow regimes (see Fig. 66). Among them, the mist flow regime is the most critical one, where the maximum cladding temperatures are usually to be found. However, since the mist flow is produced in the bundle passage going all the way back to the quench front, the whole reflood transient would have to be analyzed.

From the temperature transient measurements, the duration of the mist flow regime can be obtained by the scheme described below. Since the highly dispersed mist flow is characterized by very low water content, the differential pressure measured over a fixed axial length of the bundle is used for the determination of the change of the water content. A rise of pressure difference indicates the increase of water content in the flow. This is particularly evident in the transition between mist flow cooling and film boiling regimes. Strictly speaking, there is no abrupt change of the flow conditions, and the "film boiling" period should be arranged into several subdivisions. However, the mist flow regime is relatively rather stable and therefore can be recognized fairly well from the differential pressure measurement. The differential pressure transient as well as the cladding and fluid temperature transients measured from the middle portion of the bundle are shown in Fig. 67. Three tests from Series II have been selected to demonstrate, in addition, the influence of the system pressure. The change of the slope of the differential pressure transient is clearly visible. The

upper bound of the transient indicates that the quench front has already passed and the corresponding portion of the bundle is completely flooded, i.e. the middle portion of the bundle of 545 mm length as mentioned in the legend of Fig. 67.

The plotted fluid temperatures show quenching of the fluid thermocouple probe tips at about the same time when the water content in the subchannels suddenly increases. However, some dryouts of the probe tips after the first quenching give evidence to the presence of superheated steam for even increasing content of water of saturation temperature in the flow. The quench times of the fluid temperature measuring probes at various bundle levels for the individual tests have been used for analysis of the duration of the mist flow regime to establish a correlation (see Section 11.1).

11.1 GRID SPACER EFFECT ON TWO-PHASE FLOW HEAT TRANSFER

The effect of grid spacers on cladding temperatures are to be described in Section 9.2.1. Analyzing possible mechanisms of droplet break-up and reformulation of the flow pattern during mist flow, two different situations can be found depending on the temperature of a grid spacer. For a hot, dry grid spacer, larger droplets arriving at the leading edge are split into a large number of small droplets which pass through the grid. For a cold, wet grid spacer on the other hand, some of the droplets are caught by the water film on the grid. This water film is blown to the trailing edge of the grid where smaller droplets are formed and entrained into the steam flow. Quenching of the grid marks the transition of mist cooling mechanism from the situation of a hot, dry grid spacer to that of a cold, wet grid spacer.

Figure 68 shows grid spacer temperature transients compared with cladding and fluid temperature transients for the lower as well as the upper portion of the bundle. The grid spacer temperatures were measured in subchannels close to the housing. Measuring Pos. 1 was placed at the grid spacer in subchannel surrounded by the housing and rods No.'s 21 and 22 (see Fig. 26). The data of Measuring Pos. 2 were recorded in subchannel surrounded by the housing and rods No.'s 4 and 5. The cladding and the fluid temperatures, measured at axial levels slightly different from those of the corresponding grid spacers, are used only for the purpose of providing a frame of reference for the flow boundary conditions. The grid spacer temperature is gener-

ally slightly lower than the fluid temperature at the same axial level. However, quenching of the grid occurs relatively late. This is true especially for the upper bundle portion. In general, the influence of the system pressure is not significant. Only for high flooding velocities earlier quenching of the grid spacers relative to the quenching of the fluid temperature probe can be observed in the upper bundle portion.

It can be concluded that for the lower bundle portion the quench time for a grid spacer is roughly about one third of the cladding quench time, and for the upper bundle portion it is roughly about two thirds. These relatively long grid spacer quench times are closely related to the standard operational procedure of the FEBA tests. There, the long heating-up period prior to reflood is bringing the grid spacers to an initial temperature level considerably higher than that measured from tests performed with a steep heating-up ramp. However, for the upper bundle portions and at low flooding rates, the grid spacers are mostly heated up due to radiation from the rods and heat transfer from the superheated steam (see Test No. 267 in Fig. 69). The relatively high initial grid spacer temperature measured in the FEBA tests seems to be rather realistic.

11.1.1 ENHANCEMENT OF MIST COOLING

An additional, possibly plausible mechanism of heat transfer during reflooding is the cooling effect of smaller droplets generated from the thermally relatively inactive large droplets which are intercepted by the grid spacers located at distributed intervals along the whole length of the bundle /32/. To check on the validity of this suggested physical model, a direct measurement of droplet dynamics across the grid spacer is needed. Such an endeavor would have been considered nearly unrealizable until the recent development by Lee and Srinivasan /48/ of a special Laser-Doppler anemometry technique for the in situ simultaneous measurement of velocity and size of relatively large particles in a dilute two-phase supension flow. Using this optical scheme, Lee et al. /49/ conducted a series of systematic studies of the influence of a simulation cold wet grid spacer on the droplet size, population and velocity distribution in the mist flow downstream for several preselected initial mean droplet sizes in the millimeter range in the mist flow upstream. Their results reveal that regardless of the initial mean droplet size in the mist flow upstream of the grid spacer the mean

droplet size in the mist flow downstream of the grid spacer has been found to assume a stabilized value on the order of 200 microns. The measured order-of-magnitude increase in the population of the smaller droplets in the mist flow downstream of the grid spacer is indeed due to the reentrainment of droplets from the accumulated liquid from the deposition on the cold grid spacer of some of the droplets, including some of the larger ones, in the initial flow upstream of the grid spacer.

To acertain the effect of enhanced mist cooling downstream of the grid spacer, further measurement and correlation of axial temperature distribution behind a grid spacer and an understanding of the transient natural convection in a slow vertical dispersed flow have long been anticipated /50/. Figure 70 shows the measured cladding temperature, fluid temperature, and heat transfer coefficient relative to the saturation temperature corresponding to the system pressure at an elevation of 590 mm close to the top end of heated bundle length for a test with a low flooding velocity of 2.2 cm/s and a system pressure of 4.1 bar. In much of the initial period of reflooding, in this case, the temperature of the vapor is higher than that of the cladding and consequently the convective heat transfer is acutally from the superheated steam to the cladding instead of the measured overall loss of heat from the cladding to the dispersed flow. The only exception to this is the fact that at the very beginning, the measured heat transfer is indeed from the flow to the cladding as expected. This discrepancy in much of this period excluding the very beginning can be attributed to the effect of evaporative cooling of the smaller droplets in the flow most likely due to the presence of the grid spacers in the subchannel.

11.1.2 CHARACTERISTIC TIME SCALE FOR MIST FLOW

As expected, the running time for a test varies greatly from test to test. In order to be able to analyze the test results on some rational basis, a suitable characteristic time scale would have to be found with particular attention paid to the mist flow portion of the transient. Since the quenching of the flow probe generally marks the end of the loosely defined mist flow region, the flow probe quench time seems to be the logical choice for the required characteristic time scale. Within the scatter of the experimental data due to the uncertainty in the determination of time of flow

probe quenching, the following correlation was established for the quench time of the flow probe:

$$T^*_Q = \sum_{i=0}^{2} \sum_{j=0}^{1} C_{ij} \cdot Re^{-j} \cdot P^{-1} \qquad (11\text{-}1)$$

where

$$T^*_Q = T_Q \cdot \left(\frac{V}{L}\right)$$

T_Q	Probe quench time
V	Flooding velocity at bundle inlet
L	Axial distance from bundle bottom end
C_{ij}	Coefficient
Re	Flooding Reynolds number (water at saturation)
P	Normalized system pressure

Figure 71 shows results of this empirical correlation, Eq. (11-1), compared with the experimental data base. The dimensionless probe quench time is plotted versus the system pressure with the flooding Reynolds number as the parameter. The correlation fits the data with a mean error of 1.5 % and a standard deviation of 15 %. Close to the bundle midplane, the compared data are in good agreement for all flooding conditions. For axial position upstream and downstream of the bundle midplane, the probe quench time is slightly overpredicted and underpredicted, respectively.

11.1.3 MIST COOLING ENHANCEMENT DOWNSTREAM OF GRID SPACER

A transient heat balance based on rod power, stored heat and heat release to the coolant leads to the local surface heat flux q_{total}. For the determination of q_{total} the local cladding and fluid temperatures and the physical properties of the heater rod materials are taken into account. On the other hand, a transient mass balance leads to the determination of the local vapor mass flux, m_v :

$$\dot{m}_i = \dot{m}_v + \dot{m}_{co} + \dot{m}_b \qquad (11\text{-}2)$$

where

$\dot{m}_i$	Mass flux of injected water
$\dot{m}_v$	Mass flux of vapor
$\dot{m}_{co}$	Mass flux of carry-over
$\dot{m}_b$	Mass flux of water stored in bundle deduced from differential pressure measurement

By the use of this local vapor mass flux together with the local flow properties and physical properties of vapor under local flow conditions, we can obtain the local vapor heat transfer coefficient, h_v, with reference to the local vapor temperature from the Dittus-Boelter correlation equation for single-phase convective heat transfer /51/:

$$Nu_v = 0.023 \cdot Re_v^{0.8} \cdot Pr_v^{0.4} \qquad (11\text{-}3)$$

where

$Nu_v = \frac{h_v \cdot d_H}{k_v}$	Vapor Nusselt number
h_v	Vapor heat transfer based on difference between cladding and vapor temperatures
d_H	Hydraulic diameter of subchannel
k_v	Vapor thermal conductivity
$Re_v = \frac{U_v \cdot d_H}{\nu_v}$	Vapor flow Reynolds number
$U_v = \frac{\dot{m}_v}{A \cdot \rho_v}$	Vapor Velocity
$\dot{m}_v$	Vapor mass flux

A	Cross-section area of bundle
ρ_v	Vapor density
ν_v	Vapor kinematic viscosity
Pr_v	Vapor Prandtl number

The local droplet heat flux, $\dot{q}_d$, can then be determined as follows:

$$\dot{q}_d = \dot{q}_{total} - h_v \cdot (T_c - T_v) \qquad (11\text{-}4)$$

where T_c and T_v are the measured cladding and vapor temperatures, respectively.

Within the scatter of the data due to the various experimental uncertainties, the following correlation was established for the local droplet heat transfer:

$$Nu_d = \sum_{m=1}^{4} \sum_{n=0}^{3} \sum_{p=1}^{4} C_{mnp} \cdot Re_\ell^{-p} \cdot Re^{-n} \cdot (T')^m \qquad (11\text{-}5)$$

where

$Nu_d = \frac{d_H \cdot \dot{q}_d}{k \cdot (T_v - T_s)}$	Droplet Nusselt number
d_H	Hydraulic diameter of subchannel
$\dot{q}_d$	Droplet heat flux
k	Thermal conductivity of vapor
T_v	Vapor temperature
T_s	Saturation temperature of water
C_{mnp}	Coefficient
$Re_\ell = \frac{U_v \cdot \ell}{\nu_v}$	Vapor flow Reynolds number

$U_v = \frac{\dot{m}_v}{A \cdot \rho_v}$ Vapor velocity

$\dot{m}_v$ Vapor mass flux

A Cross section area of bundle

ρ_v Vapor density

ℓ Distance downstream of leading edge of grid spacer

ν_v Vapor kinematic viscosity

$Re = \frac{v \cdot d_H}{\nu}$ Flooding Reynolds number (water at saturation)

$T' = \frac{T}{T_Q}$ Normalized time

T Time

T_Q Flow probe quench time

Figure 72 shows results of this correlation Eq. (11-5), compared with the experimental data base. The droplet Nusselt number is plotted versus the normalized flooding time. The parameter is the local vapor flow Reynolds number based on the downstream distance from the leading edge of the grid spacer. For the total range of flooding parameters, the correlation fits the data with a mean error of 0.5 % and a standard deviation of 7 %. The plot presents a comparison among droplet Nusselt numbers determined for four axial locations which are 100, 200, 300 and 400 mm downstream of the bundle midplane. A system pressure of 4.1 bar and a flooding velocity of 3.8 cm/s have been selected.

The following observations can be made:

- Heat transfer improvement due to fine droplets downstream of a grid spacer,
- Heat transfer improvement decrases with increasing axial distance downstream of a grid spacer,
- Heat transfer improvement decreases with increasing time after start of flooding.

11.2 BLOCKAGE EFFECTS ON TWO-PHASE FLOW HEAT TRANSFER

With respect to cladding deformation during reflood and the coolability of blockages already formed, the heat transfer conditions at the very beginning of reflood are most important. Therefore, this brief analysis is concentrated on the mist flow regime. For a flooding rate of as low as 2 cm/s in some test series, water already is carried through the whole bundle length. The content of water in the early two-phase mixture generally is very low. However, its cooling effect is of great importance. As discussed above, some of the droplets entrained by the steam are intercepted by flow obstacles such as grid spacers, ballooned claddings, burst lips etc., and dispersed or reentrained. The larger surface to volume ratio for decreased size of droplets as well as increased turbulence favor enhanced evaporation, i.e. heat removal for a given mass flux. Moreover, there may be such other phenomena as, in the wake of blockages with bypass, the falling back of larger droplets due to gravity into regions of reduced steam velocity, their dispersion on approaching hot surface and steam jets leaving the constricted subchannels. Modeling of such phenomena needs to be restricted to those of most significant effects.

Analysis of the experimental data shows the following trends for the heat transfer conditions around blockages:

- Two-phase flow passing a coolant channel constriction leads to enhanced cooling due to enhancements of turbulence and droplet dispersion.
- Therefore, the coolant mass flux reduction through blocked subchannels due to flow diversion for blockages with bypass would not as seriously influence cladding temperatures within and downstream of blockages as in the case of single-phase flow.
- For the 90 % blockage ratio only maximum cladding temperatures downstream of the blockage are slightly higher than in the bypass area at corresponding elevations.
- Within the blockage (90 % as well as 62 %) the cladding temperatures are lower than in the bypass except for a short period just before the bundle quench front arrives at the blockage elevation.

- The 62 % blockage with bypass leads to lower cladding temperatures within and downstream of the blockage for most of the flooding conditions carried out.

Heat transfer analysis usually produces heat transfer coefficients based on either the saturation temperature or the local fluid temperature. However, this method is not always adequate to describe the heat transfer conditions during the mist flow regime. Since, especially for low flooding rates, the steam is highly superheated and the droplets are at the saturation temperature, an accurate description of the heat removal from the rod claddings to the two separate components of the mixture is difficult. Therefore, the surface heat flux seems to be a more adequate result for presentation of data evaluated from the measurements. Figure 73 shows the trends described above as normalized heat flux blocked/unblocked (for the conditions downstream of blockages) versus normalized time, i.e. the correlation developed for analysis of the grid spacer effect (see Section 11.1). The analysis of the experimental data obtained for blockages is being continued. However, this has to be done in close cooperation with efforts in improving the existing scheme of modeling which has not yet included many of the phenomena found in the measurements.

The quality of evaluation and analyses of data depends on how far the effects detected are relevant for reactor conditions. It is a valuable practice to compare the data obtained from different test series with each other as well as with the results of complementary experimental programs. The results presented from the 2D/3D-Program /52/, and, especially from the FLECHT-SEASET /53/, as well as the THETIS-program /11/ show trends consistent with those of the FEBA results. A number of individual characteristics of the different programs, e.g. different fuel rod and hence fuel rod simulator and bundle designs, different blockage designs and configurations, and, different operational procedures for the tests, make difficult direct comparisons of data measured. However, the data can be compared qualitatively by examining trends in the data /12/. The trends are consistent so far including their magnitude. Computer code models being in development actually for grid spacer and blockage heat transfer can be validated using extended data bases and different rod geometries, /54,55,56/.

12. SUMMARY OF THE RESULTS

The results obtained from reflooding rod bundles with severe coolant channel blockages with bypass show that blockages of 62 % and even 90 % in the arrays chosen scarcely cause increased cladding temperatures for flooding velocities as low as 2 cm/s. This finding contributes directly to the question of the extent to which coolant channel blockages influence emergency core cooling during the reflood phase of a LOCA. However, emphasis has been placed on separating out individual cooling effects for improved understanding of the two-phase flow heat transfer in complex rod bundle geometries. The size as well as the shape of blockages are essential parameters investigated qualitatively using a 5 rod row. The most pessimistic shape of blockages - corresponding to idealized cladding deformations from ballooning tests - have been maintained for several consecutive test series. The grid spacer effect has been separated out as well as included in the experimental investigation of blockage effects. The local conditions of the two-phase flow showing relatively high steam superheat - inspite of the presence of water droplets - have been found to be essential for further computer code modeling. Connected with this problem are the water entrainment mechanisms, since the water carried over leaves the bundle as a significant heat sink unused. Flow obstacles as grid spacers and blockages reduce the water carry over.

The data base established from reflooding a 5x5 rod bundle of German PWR dimensions includes blocked as well as unblocked bundle data. The main reflood parameters such as the system pressure and the flooding velocity have been varied in the range of 2 through 6 bar, and 2.2 through 5.8 cm/s, respectively. For the bundle power 120 % of the ANS Standard reactor decay heat transient has been applied.

The results can be summarized as follows:

- Obstacles in the coolant flow channels increase the dispersed flow cooling effectiveness in a limited region downstream of the obstacles.
- Downstream of spacer grids this effect leads to lower cladding temperatures.
- Downstream of partial blockages, cladding temperatures depend on both effects of increased dispersed flow cooling and local mass flux reduction.

- For subchannel blockage ratios of 90 %, the mass flux reduction dominates slightly leading to a moderate increase of cladding temperatures (50 K) just downstream of the blockage compared with the same axial position in the bypass. However, compared with unblocked bundle conditions there is no increase of the maximum cladding temperatures for 90 % blockages of 65 mm axial length.
- For subchannel blockage ratios of 62 % the increased dispersed flow cooling dominates leading to lower cladding temperatures downstream of the blockage compared with the same axial position in the bypass.
- For both blockage ratios, the temperatures of the blockage sleeves - simulating ballooned fuel rod claddings - are lower than those of the unlifted claddings in the bypass inspite of the delayed heat removal from the heat sources in the blockage.
- A grid spacer a short distance downstream of a 90 % blockage reduces the axial extension of increased cladding temperatures downstream of the blockage, and the effect of delayed heat removal disappears.
- An additional 62 % blockage downstream of a 90 % blockage shows similar characteristics as mentioned above for the separate 62 % blockage. It leads to lower cladding temperatures.
- Far downstream of the double blockage, cladding temperatures increase slightly compared with the bypass conditions due to the loss of water content in the coolant. However, the maximum temperatures remain below the maximum temperatures of unblocked bundles.
- Water carry over is reduced with increasing number and size of flow obstacles in a bundle. This explains quantitatively the moderate influence of severe flow blockages on the maximum cladding temperatures.
- The results obtained from bundle tests with blockage ratios of 62 % and 90 %, respectively, for all coolant subchannels confirm quantitatively the cooling enhancement downstream of blockages for given mass fluxes. As expected, the improvement of heat removal downstream of such blockages is significantly higher than that downstream of a grid spacer. The essential part of the effect occurs in the early phase of reflood characterized by mist cooling. The blockage of all bundle subchannels at the bundle midplane is not representative of any situation in the core of a reactor. However, the influence of blockage size on the two-phase flow cooling behaviors can be verified quantitatively using the data of these test series.

13. CONCLUSIONS

- The coolability of PWR fuel rod clusters blocked up to 90 % is not a severe reflood cooling problem even for flooding velocities as low as 2 cm/s.
- Lower blockage ratios, e.g. 62 %, lead to lower cladding temperatures in the blocked region than in unblocked rod clusters.
- Grid spacers increase the dispersed flow cooling effectiveness of the early portion of the reflood phase significantly.
- The results of the systematical investigations provide data for computer code model development and assessment concerning the blockage and grid spacer effects during reflooding PWR cores.

14. REFERENCES

[1] Fiege, A.:
"Fuel Behavior under Loss-of-Coolant-Accident Conditions"
KfK 3442 B, Jan.1983

[2] Ihle, P.; Rust, K.:
"FEBA - Flooding Experiments with Blocked Arrays,
Data Report 1, Test Series I Through IV"
KfK 3658, March 1984

[3] Ihle, P.; Rust, K.:
"FEBA - Flooding Experiments with Blocked Arrays,
Data Report 2, Test Series V Through VIII"
KfK 3659, March 1984

[4] Cadek, F. F.; Dominics, D. P.; Leyse, R. H.:
"PWR FLECHT Final Report"
WCAP-7665, April 1971

[5] Hein, D.:
"PKL I Findings - PKL II Plans"
9th Water Reactor Safety Research Information Meeting, Gaithersburg, MD,
Oct. 26-30, 1981

[6] Cermak, J. O.; et al.:
"PWR Full Length Emergency Cooling Heat Transfer (FLECHT)
Group 1 Test Report"
WCAP-7435, Jan. 1970

[7] Creer, J. M.; Bates, J. M.:
"Effects of Sleeve Blockages on Air Velocity Distributions in an Unheated
7x7 Rod Bundle"
BNWL-1975, Jan. 1976

[8] Creer, J. M.; et al.:
"Effects of Sleeve Blockages on Axial Velocity and Intensity of Turbulence
in an Unheated 7x7 Rod Bundle"
BNWL-1965, Jan. 1976

[9] Davis, P. R.:
"Experimental Study of the Effect of Flow Restrictions in a Small Rod
Bundle under Emergency Core Coolant Injection Conditions"
Nuclear Technology, Vol. 1, Aug. 1971, pp. 551-556

[10] Loftus, M. J.; et al.:
"PWR FLECHT-SEASET, 21-Rod Bundle Flow Blockage Task, Data and Analysis
Report"
NUREG/CR-2444, EPRI NP-2014, WCAP-9992, Vol. 1, Sept. 1982

[11] Pearson, K. G.; Cooper, C. A.; Jowitt, D.; Kinneir, J. H.:
"Flooding Experiments on a 49-Rod Cluster Containing a Long 90% Blockage"
AEEW-R 1591, Jan. 1983

[12] Ogden, D. M.:
"Review of FEBA Blockage Data"
11th Water Reactor Safety Research Information Meeting, Gaithersburg, MD, Oct. 24-28, 1983

[13] Hofmann, G.; et al.:
"Untersuchungen zum Einfluß der Größe und Form von Kühlkanalblockaden auf die Kernnotkühlung in der Flutphase eines Kühlmittelverluststör= falles"
In: Halbjahresberichte des Projektes Nukleare Sicherheit:
KfK 2050, Aug. 1974, S. 190-195
KfK 2130, Mai 1975, S. 231-239
KfK 2195, Sept. 1975, S. 284-304

[14] Malang, S.; et al.:
"Untersuchungen zum Einfluß der Größe und Form von Kühlkanalblockaden auf die Kernnotkühlung in der Flutphase eines Kühlmittelverluststör= falles"
In: Halbjahresberichte des Projektes Nukleare Sicherheit:
KfK 2262, Juni 1976, S. 318-333
KfK 2375, Nov. 1977, S. 380-393
KfK 2435, April 1977, S. 377-391

[15] Ihle, P.; Rust, K.:
"FEBA - Flooding Experiments with Blocked Arrays, Influence of Blockage Shape"
ANS-Transactions - ENC '79, Vol. 31, May 1979, pp. 398-400

[16] Hofmann, G.; Ihle, P.; Rust, K.:
"Influence of Coolant Channel Disturbances on Transient Two-Phase Flow in Rod Bundles Investigated in Reflood Experiments"
Proc. of XVIIIth IAHR-Congress, Cagliari, Italy, Sept. 10-14, 1979, Vol. 4, pp. 445-451

[17] Ihle, P.; et al.:
"Untersuchungen zum Einfluß der Größe und Form von Kühlkanalblockaden auf die Kernnotkühlung in der Flutphase eines Kühlmittelverluststör= falles"
In: Halbjahres- bzw. Jahresberichte des Projektes Nukleare Sicherheit:
KfK 2500, Dez. 1977, S. 404-417
KfK 2600, Mai 1978, S. 401-415
KfK 2700, Nov. 1978, S. 4200/121-153
KfK 2750, Okt. 1979, S. 4200/145-165
KfK 2800, Feb. 1980, S. 31-32 und 87-88
KfK 2850, Aug. 1980, S. 33-35 und 97-99
KfK 2950, Aug. 1981, S. 4200/184-200
KfK 3250, Juni 1982, S. 4200/122-137
KfK 3350, Juli 1983, S. 4200/163-173

[18] Malang, S.:
"HETRAP - A Heat Transfer Analysis Program"
ORNL-TM-4555, Sept. 1974

[19] Rust, K.; Malang, S.; Götzmann, W.:
"PEW - Ein FORTRAN IV-Rechenprogramm zur Bereitstellung physikalischer Eigenschaften von Werkstoffen für LWR-Brennstäbe und deren Simulatoren"
KfK-Ext. 7/76-1, Dez. 1976

[20] Ihle, P.; Müller, St.:
"Experience with Steam Temperature and Water Detection Probes for Transient Mist Flow in a Hot Bundle"
NUREG/CP-0014, Vol. 2, Oct. 1980, pp. 970-981

[21] Reimann, J.; John, H.; Müller, St.:
"Impedance Probe for Detecting Flow Regime and Measuring the Phase Distribution in Horizontal Air-Water and Steam-Water Flow"
Two-Phase Flow Instrumentation Review Group Meeting, Troy, NY, March 13-14, 1978

[22] Müller, St.:
"Verfahren und Einrichtung zum Identifizieren einer Zweiphasenströmung"
DE-PS 25 58 588, Nov. 1977

[23] Müller, St.:
"Verfahren und Einrichtung zum Identifizieren einer Zweiphasenströmung"
Jahrestagung Kerntechnik '78, Hannover, 4.-7. April 1978, S. 174-177

[24] Rust, K.; et al.:
"DAS - Ein Daten-Auswerte-System"
(to be published as KfK-Report)

[25] Ihle, P.; Malang, S.; Rust, K.; Schmidt, H.:
"Der Einfluß von Kühlkanalblockaden auf den Wärmeübergang während der Flutphase eines Kühlmittelverluststörfalles"
Jahrestagung Kerntechnik '77, Mannheim, 29. März - 1. April 1977, S. 201-204

[26] Ihle, P.; Malang, S.; Rust, K.:
"Thermalhydraulic Tests with Bundles of Ballooned Rods Simulating the Reflood Phase of a LOCA"
Proc. of Topical Meeting on Thermal Reactor Safety, Sun Valley, ID, July 31 - Aug. 4, 1977, Vol. 2, pp. 720-732

[27] Ihle, P.; Malang, S.; Rust, K.:
"Thermalhydraulic Tests with Bundles of Ballooned Rods"
Conference on Heat and Fluid Flow in Water Reactor Safety, Manchester, Great Britain, Sept. 13-15, 1977, Paper C213/77

[28] Ihle, P.; Malang, S.; Rust, K.:
"Reflood Experiments with Blocked Bundle of Ballooned Rods"
ASME Winter Annual Meeting on Nuclear Reactor Safety Heat Transfer, Atlanta, GA, Nov. 27 - Dec. 2, 1977

[29] Ihle, P.; Müller, St.:
"Transient Two-Phase Flow Conditions in Heated Rod Bundles"
CONF-800403, Vol. 1, April 1980, pp. 419-426

[30] Ihle, P.; Rust, K.:
"Einfluß der Stababstandshalter auf den Wärmeübergang in der Flutphase eines DWR-Kühlmittelverluststörfalles"
Jahrestagung Kerntechnik '80, Berlin, 25. - 27. März 1980, S. 145-148

[31] Ihle, P.; Rust, K.:
"Einfluß der Stababstandshalter auf den Wärmeübergang in der Flutpha=
se eines DWR-Kühlmittelverluststörfalles"
KfK 3178, Juni 1980

[32] Ihle, P.; Rust, K.; Lee, S. L.:
"Mist Core Cooling During the Reflood Phase of PWR-LOCA"
NUREG/CP-0027, Vol. 3, Feb. 1983, pp. 1801-1809

[33] Ihle, P.; Rust, K.; Lee, S. L.:
"Experimental Investigation of Reflood Heat Transfer in the Wake of Grid Spacers"
NUREG/CP-0043, April 1983, pp. 417-443

[34] Lee, S. L.; Ihle, P.; Rust, K.:
"On the Importance of Grid Spacer Induced Mist Cooling on the Suppression of Core Peak Cladding Temperature During Reflood of PWR"
Proc. of ASME/JSME - Thermal Engineering Joint Conference, Honolulu, HI March 20-24, 1983, Vol. 3, pp. 381-385

[35] Rust, K.; Ihle, P.:
"Heat Transfer and Fluid Flow During Reflooding of Blocked Arrays"
NUREG/CP-0014, Vol. 2, Oct. 1980, pp. 970-981

[36] Ihle, P.; Politzky, H. M.; Rust, K.:
"FEBA - Flooding Experiments with Blocked Arrays, Heat Transfer in Partly Blocked 25 Rod Bundle"
ASME 19th National Heat Transfer Conference on Experimental and Analyti=
cal Modeling of LWR Safety Experiments, Orlando, FL, July 27-30, 1980,
HTD-Vol. 7, pp. 129-138

[37] Ihle, P.:
"Flooding Experiments in Blocked Arrays, FEBA - Recent Results and Future Plans"
8th Water Reactor Safety Research Information Meeting, Gaithersburg, MD, Oct. 27-31, 1980

[38] Ihle, P.; Rust, K.:
"Flow Blockage Effects on Reflood Heat Transfer in 25 Rod Bundles"
Proc. of 7th International Heat Transfer Conference, München, Sept. 6-10, 1982, ,Vol. 5, pp. 475-479

[39] Fiege, A.:
"Stand und Ergebnisse der Untersuchungen zum LWR Brennstabverhalten bei Kühlmittelverluststörfällen"
KfK 3422, Okt. 1982

[40] Ihle, P.; Rust, K.:
"Flutexperimente mit blockierten Anordnungen, Stand des Programmes und neue Ergebnisse"
Jahrestagung Kerntechnik '82, Mannheim, 4. - 6. Mai 1982, S. 97-100

[41] Ihle, P.; Rust, K.:
"Influence of Flow Blockages on Emergency Core Cooling"
ASME-Paper 82-HT-66, June 1982

[42] Rust, K.; Ihle, P.; Lee. S. L.:
"Comparison of FEBA Test Data with RELAP4/MOD6 Postcalculations"
Proc. of Second International Topical Meeting on Nuclear Reactor Thermal-Hydraulics, Santa Barbara, CA, Jan. 11-14, 1983, Vol. 1, pp.731-739

[43] Ihle, P.:
"Degraded Core Heat Transfer"
Proc. of Second International Topical Meeting on Nuclear Reactor Thermal-Hydraulics, Santa Barbara, CA, Jan. 11-14, 1983, Vol. 1, pp. 49-59

[44] Loftus, M. J.; Hochreiter, L. E.; Utton, D. B.; Young, M. Y.:
"Spacer Grid Heat Transfer Effects During Reflood"
NUREG/CP-0043, April 1983, pp. 445-475

[45] Clement, P.; Deruaz, R.; Veteau, J. M.:
"Reflooding of a PWR Bundle, Effect of Inlet Flow Rate Oscillations and Spacer Grids"
NUREG/CP-0027, Vol. 3, Feb. 1983, pp. 1763-1770

[46] Erbacher, F. J.; Neitzel, H. J.; Wiehr, K.:
"Effects of Thermohydraulics on Clad Ballooning, Flow Blockage and Cool= ability in a LOCA"
OECD-NEA-CSNI/IAEA Specialists' Meeting on Water Reactor Fuel Safety and Fission Product Release in Off-Normal and Accident Conditions,
Risø National Laboratory, Denmark, May 16-20, 1983

[47] Mohr, C. L.; et al.:
"LOCA Simulation in the National Research Universal Reactor Program"
NUREG/CR-2528, PNL-4166, April 1983

[48] Lee, S. L.; Srinivasan, J.:
"An LDA Technique for in Situ Simultaneous Velocity and Size Measurement of Large Spherical Particles in a Two-Phase Suspension Flow"
Int. J. Multiphase Flow, Vol. 8, No. 1, p. 47 (1982)

[49] Lee, S. L.; Rob, K.; Cho, S.:
"LDA Measurement of Mist Flow Across Grid Spacer Plate Important in Loss-of-Coolant Accident Reflood of Pressurized Water Reactor"
Proc. of International Symposium on Application of Laser-Doppler Anemo= metry to Fluid Mechanics, Lisbon, Portugal, June 1982, p. 5.3.1

[50] Tong, S. L.; Bennet, G. L.:
"NRC Water Reactor Safety Research Program"
Nuclear Safety, Vol. 18, No. 1, p. 1 (1977)

[51] Welty, J. R.:
"Engineering Heat Transfer"
John Wiley & Sons, New York (1978)

[52] Joint NRC, JAERI, BMFT 2D/3D Program:
"SCTF Core I Test Results" (JAERI)
9th Water Reactor Safety Research Information Meeting, Gaithersburg, MD, Oct. 26-30, 1981

[53] Loftus, M. J.; Hochreiter, L. E.; Lee, N.:
"FLECHT-SEASET 21-Rod Bundle, Flow Blockage Heat Transfer During Reflood"
Proc. of Second International Topical Meeting on Nuclear Reactor Thermal-Hydraulics, Santa Barbara, CA, Jan. 11-14, 1983, Vol. 1, pp. 646-656

[54] Hochreiter, L. E.:
"FLECHT-SEASET Blocked Bundle Test and Analysis"
11th Water Reactor Safety Research Information Meeting, Gaithersburg, MD, Oct. 24-28, 1983

[55] Lee, S. L.; Cho, S. K.; Sheen, H. J.; Issapour, I.:
"Measurements of Grid Spacer Enhanced Droplet Cooling Under Reflood Conditions in a PWR"
11th Water Reactor Safety Research Information Meeting, Gaithersburg, MD, Oct. 24-28, 1983

[56] Kelly, J. M.:
"COBRA-TF: Flow Blockage Heat Transfer Program"
11th Water Reactor Safety Research Information Meeting, Gaithersburg, MD, Oct. 24-28, 1983

TEST SERIES I

Base Line Tests With Undisturbed Bundle Geometry,
7 Grid Spacers

Test No.	Flooding Velocity (cold) cm/s	System Pressure bar	Feedwater Temp.[1] °C 0-30 s	Feedwater Temp.[1] °C End	Cladding Temp.[2] °C Initial	Housing Temp.[3] °C Initial	Remarks
210	2.8	4.2	48	39	717	588	
214	5.8	4.1	45	37	773	635	cf. Data Report 1
216	3.8	4.1	48	37	787	640	cf. Data Report 1
218	5.8	2.1	42	37	757	666	cf. Data Report 1
219	5.8	6.1	50	37	751	661	
220	3.8	6.1	49	37	789	699	cf. Data Report 1
221	2.8	6.1	51	37	784	712	
222	5.8	6.1	43	36	747	647	cf. Data Report 1
223	3.8	2.2	44	36	763	671	cf. Data Report 1
227	3.8	6.1	53	38	770	690	

1) Measured in the lower plenum
2) Measured at axial level 2025 mm, rod No. 9, TC No. 2
3) Measured at axial level 2025 mm

Table 1 FEBA 5x5 rod bundle: Main test parameters of test series I

TEST SERIES II

Investigation of the Effects of a Grid Spacer,
Without Grid Spacer at the Bundle Midplane

Test No.	Flooding Velocity (cold) cm/s	System Pressure bar	Feedwater Temp.[1] °C 0-30 s	Feedwater Temp.[1] °C End	Cladding Temp.[2] °C Initial	Housing Temp.[3] °C Initial	Remarks
229	5.7	4.1	50	37	747	700	cf. Data Report 1
229	3.8	4.1	53	38	778	722	cf. Data Report 1
230	5.8	6.1	48	37	791	710	cf. Data Report 1
231	3.8	6.2	54	40	758	674	cf. Data Report 1
233	5.8	2.0	47	37	789	740	cf. Data Report 1
234	3.8	2.0	46	37	767	696	cf. Data Report 1

1) Measured in the lower plenum
2) Measured at axial level 2025 mm, rod No. 9, TC No. 2
3) Measured at axial level 2025 mm

Table 2 FEBA 5x5 rod bundle: Main test parameters of test series II

TEST SERIES III

Investigation of the Effects of a 90% Flow Blockage With Bypass,
Blockage at the Bundle Midplane of 3x3 Rods Placed in the Corner
of the 5x5 Rod Bundle,
Without Grid Spacer at the Bundle Midplane

Test No.	Flooding Velocity (cold) cm/s	System Pressure bar	Feedwater Temp.[1] °C 0-30 s	Feedwater Temp.[1] °C End	Cladding Temp.[2] °C Initial	Housing Temp.[3] °C Initial	Remarks
235	5.8	6.2	46	37	775	740	cf. Data Report 1
236	3.8	6.2	48	37	796	760	cf. Data Report 1
237	5.6	4.2	45	37	758	699	Flooding Velocity not Constant
238	5.7	4.1	49	37	779	700	cf. Data Report 1
239	3.8	4.1	49	37	796	725	cf. Data Report 1
240	5.8	2.0	46	40	768	688	cf. Data Report 1
241	3.8	2.0	42	37	774	709	cf. Data Report 1
242	3.9	2.0	40	36	660	526	Low Initial Temp.
243	3.9	2.0	76	74	617	506	Low Initial Temp., High Feedwater Temp.

1) Measured in the lower plenum
2) Measured at axial level 2025 mm, rod No. 9, TC No. 2
3) Measured at axial level 2025 mm

Table 3 FEBA 5x5 rod bundle: Main test parameters of test series III

TEST SERIES IV

Investigation of the Effects of a 62% Flow Blockage With Bypass,
Blockage at the Bundle Midplane of 3x3 Rods Placed in the Corner
of the 5x5 Rod Bundle,
Without Grid Spacer at the Bundle Midplane

Test No.	Flooding Velocity (cold) cm/s	System Pressure bar	Feedwater Temp.[1] °C 0-30 s	Feedwater Temp.[1] °C End	Cladding Temp.[2] °C Initial	Housing Temp.[3] °C Initial	Remarks
261	5.7	2.0	57	42	761	745	cf. Data Report 1
262	3.8	2.0	54	43	718	674	cf. Data Report 1
263	3.8	3.9	61	43	737	635	cf. Data Report 1
264	5.7	3.9	63	41	794	696	cf. Data Report 1
266	3.8	3.9	125	45	368	275	Low Initial Temp., Max. Rod Power = 24.5 W/cm, Const. until t = 85 s
267	2.2	4.0	69	45	649	560	cf. Data Report 1
268	3.8	5.9	76	44	761	697	cf. Data Report 1
269	5.7	5.9	73	44	758	627	cf. Data Report 1
270	9.5	3.8	48	41	786	687	High Flooding Velocity
272	3.0	4.0	57	41	701	722	Max. Rod Power = 20.5 W/cm, Const.
273	3.0	4.0	57	41	767	616	Max. Rod Power = 20.5 W/cm, Const.

1) Measured in the lower plenum
2) Measured at axial level 2025 mm, rod No. 9, TC No. 2
3) Measured at axial level 2025 mm

Table 4 FEBA 5x5 rod bundle: Main test parameters of test series IV

TEST SERIES V

Investigation of the Effects of a 90% Flow Blockage With Bypass, Blockage at Axial Level 2125 mm of 3x3 Rods Placed in the Corner of the 5x5 Rod Bundle,
Grid Spacer at the Bundle Midplane

Test No.	Flooding Velocity (cold) cm/s	System Pressure bar	Feedwater Temp.[1] °C 0-30 s	Feedwater Temp.[1] °C End	Cladding Temp.[2] °C Initial	Housing Temp.[3] °C Initial	Remarks
281	5.7	3.9	75	48	794	709	cf. Data Report 2
282	3.8	3.9	77	45	791	634	cf. Data Report 2
284	2.2	3.9	69	45	655	550	cf. Data Report 2
285	3.8	3.9	101	80	719	576	High Feedwater Temp.
286	2.2	3.9	96	79	666	561	High Feedwater Temp.

1) Measured in the lower plenum
2) Measured at axial level 2025 mm, rod No. 9, TC No. 2
3) Measured at axial level 2025 mm

Table 5 FEBA 5x5 rod bundle: Main test parameters of test series V

TEST SERIES VI

Investigation of the Effects of 90% and 62% Flow Blockages With Bypass, 90% Blockage at Axial Level 2125 mm, 62% Blockage at Axial Level 1925 mm of 3x3 Rods Placed in the Corner of the 5x5 Rod Bundle, Grid Spacer at the Bundle Midplane

Test No.	Flooding Velocity (cold) cm/s	System Pressure bar	Feedwater Temp.[1] °C 0-30 s	Feedwater Temp.[1] °C End	Cladding Temp.[2] °C Initial	Housing Temp.[3] °C Initial	Remarks
275	3.8	3.9	61	43	674	410	Low Initial Temp.
276	3.8	3.9	73	43	746	547	cf. Data Report 2
277	2.1	3.9	73	46	567	350	Low Initial Temp.
278	4.8	3.9	75	43	646	405	Flooding Velocity not Constant

1) Measured in the lower plenum
2) Measured at axial level 2025 mm, rod No. 9, TC No. 2
3) Measured at axial level 2025 mm

Table 6 FEBA 5x5 rod bundle: Main test parameters of test series VI

TEST SERIES VII

Investigation of the Effects of a 62% Flow Blockage Without Bypass, Blockage at the Bundle Midplane of all Rods of the 5x5 Rod Bundle

Test No.	Flooding Velocity (cold) cm/s	System Pressure bar	Feedwater Temp.[1] °C 0-30 s	Feedwater Temp.[1] °C End	Cladding Temp.[2] °C Initial	Housing Temp.[3] °C Initial	Remarks
321	5.8	2.1	47	40	790	660	cf. Data Report 2
322	3.8	2.1	54	41	758	615	cf. Data Report 2
324	3.8	4.1	56	42	782	623	cf. Data Report 2
325	5.8	4.1	61	46	783	605	cf. Data Report 2
327	2.2	4.1	55	35	675	560	cf. Data Report 2
329	3.8	5.9	63	41	759	640	cf. Data Report 2
330	5.8	5.9	65	44	753	601	cf. Data Report 2

1) Measured in the lower plenum

2) Measured at axial level 1925 mm, rod No. 17, TC No. 2

3) Measured at axial level 2025 mm

Test series includes steady state and transient steam cooling tests for which low bundle power and system pressures of 2, 4 and 6 bar were selected.

Table 7 FEBA 5x5 rod bundle: Main test parameters of test series VII

TEST SERIES VIII

Investigation of the Effects of a 90% Flow Blockage Without Bypass, Blockage at the Bundle Midplane of all Rods of the 5x5 Rod Bundle

Test No.	Flooding Velocity (cold) cm/s	System Pressure bar	Feedwater Temp.[1] °C 0-30 s	Feedwater Temp.[1] °C End	Cladding Temp.[2] °C Initial	Housing Temp.[3] °C Initial	Remarks
333	5.8	5.9	60	43	780	651	cf. Data Report 2
334	3.8	5.9	66	43	789	652	cf. Data Report 2
336	5.8	4.1	53	41	747	671	cf. Data Report 2
337	3.8	4.0	57	42	795	647	cf. Data Report 2
338	2.2	4.1	61	44	627	547	cf. Data Report 2
340	5.8	2.2	54	41	808	683	cf. Data Report 2
341	3.8	2.2	52	41	792	661	cf. Data Report 2
342	2.2	2.2	51	41	690	607	cf. Data Report 2

1) Measured in the lower plenum

2) Measured at axial level 1925 mm, rod No. 17, TC No. 2

3) Measured at axial level 2025 mm

Test series includes steady state and transient steam cooling tests for which low bundle power and system pressures of 2, 4 and 6 bar were selected.

Table 8 FEBA 5x5 rod bundle: Main test parameters of test series VIII

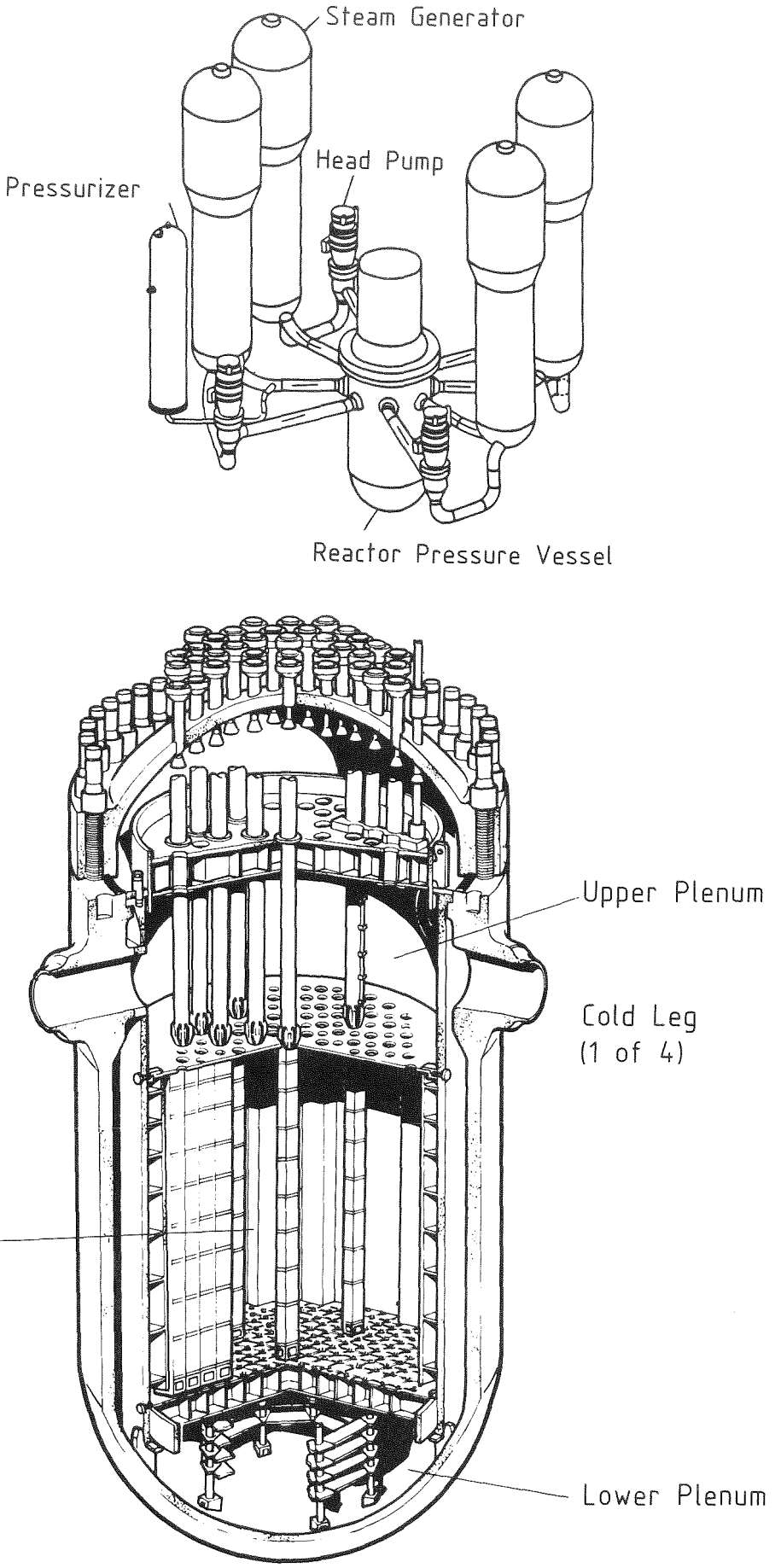

Fig. 1 4-loop steam generator system and pressure vessel with installations of a PWR

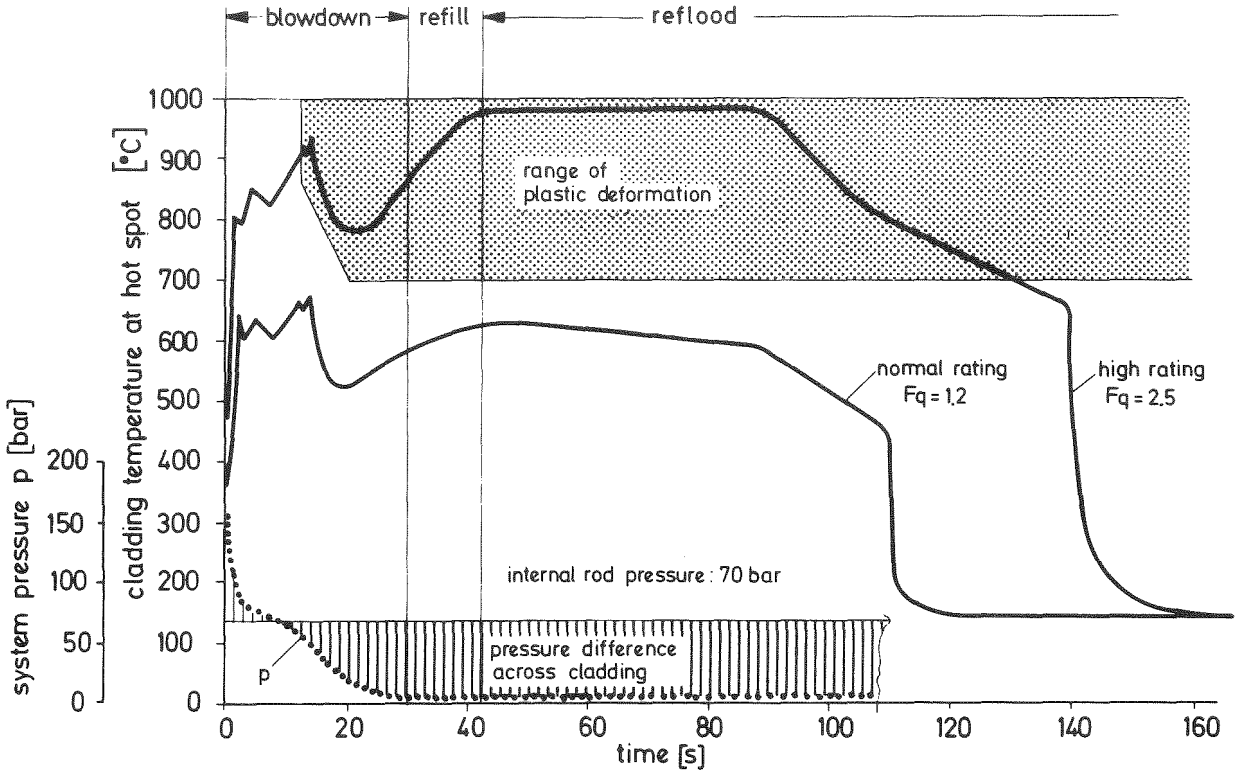

Fig. 2 Fuel rod cladding loading in a 2F-cold leg break LØCA

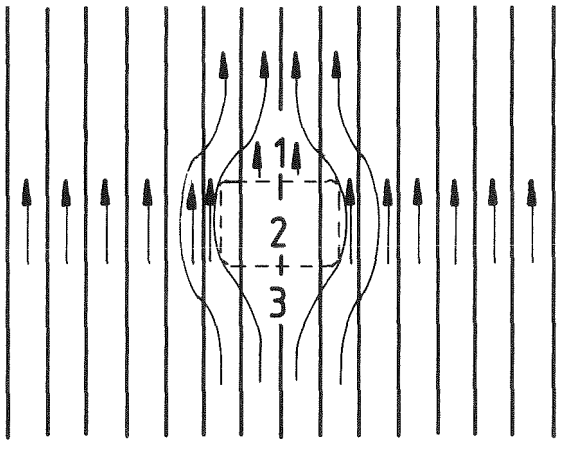

1 Droplet Fall Back?

2 Reduced Mass Flow to Which Extent?

3 Droplet Deentrainment?

Fig. 3 Sketch of a PWR core with reflood flow diversion at coolant channel constrictions in in the center

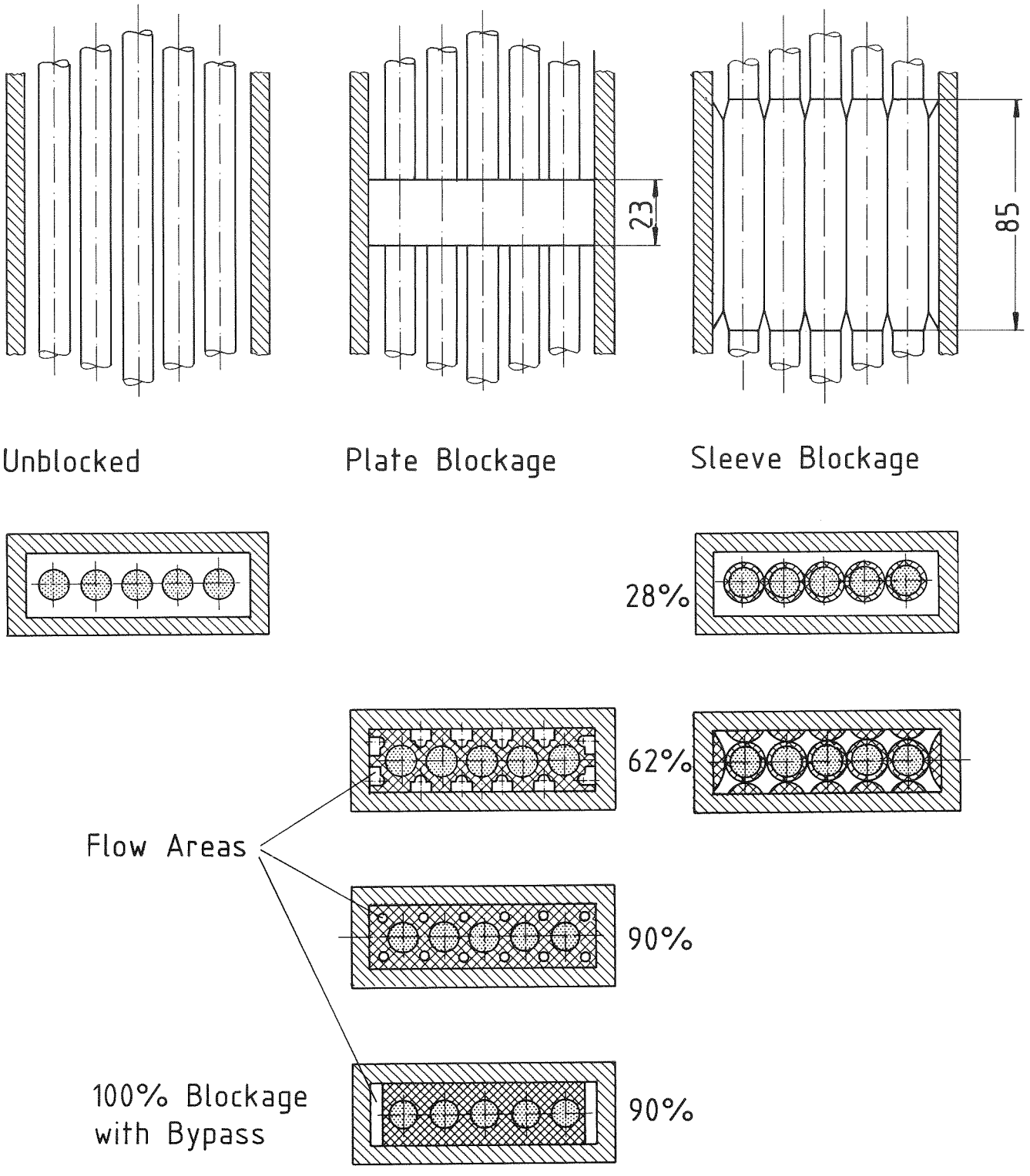

Fig. 4 5 rod row: Plate and sleeve blockages

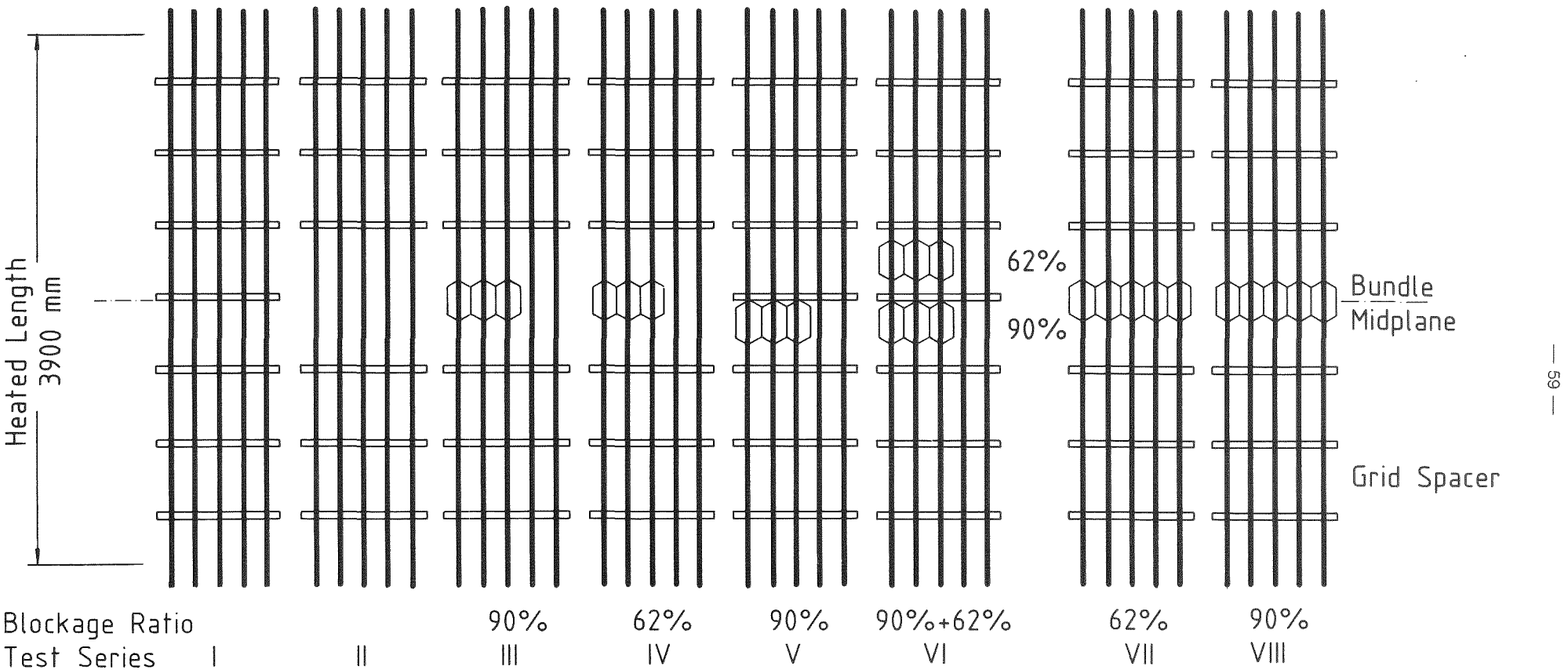

Fig. 5 5x5 rod bundle: Bundle geometries of test series I through VIII axial arrangement of grid spacers and sleeve blockages

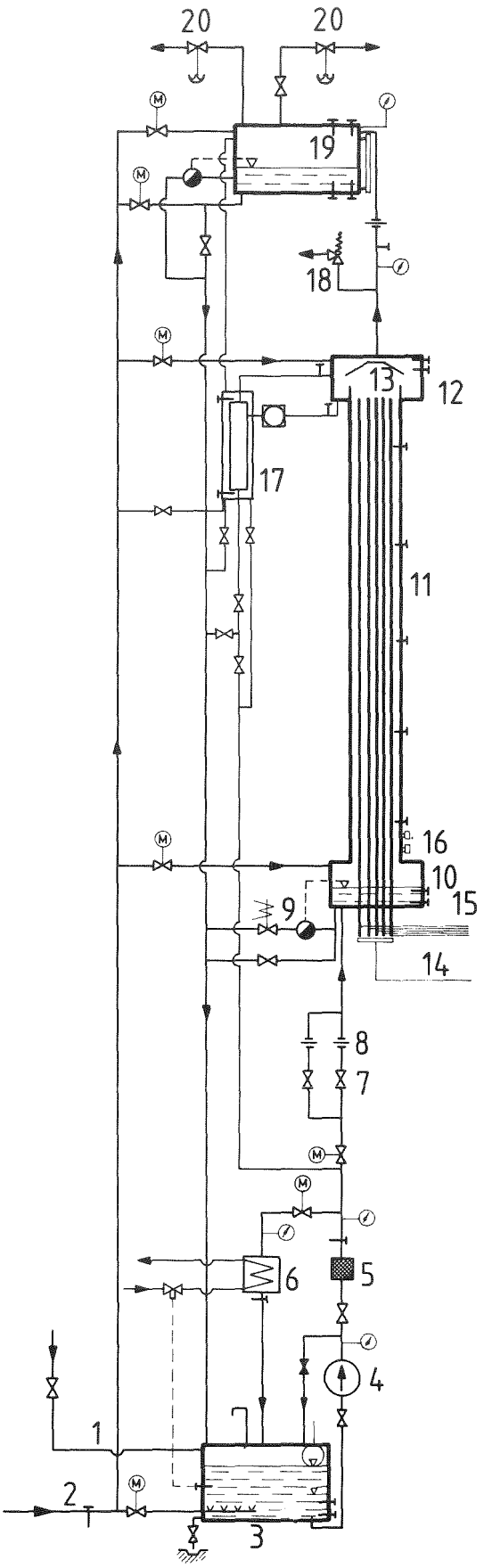

LEGEND

1 Water Supply
2 Steam Supply
3 Storage Tank
4 Water Pump
5 Filter
6 Heat Exchanger
7 Throttle Valve
8 Turbine Meter
9 Water Level Regulation Valve

10 Lower Plenum
11 Test Section
12 Upper Plenum
13 Water Separator

14 Power Supply
15 Rod Instrumentation Exits
16 Water Level Detector
17 Water Collecting Tank
18 Outlet Valve
19 Buffer
20 Pressure Regulator

Fig. 6 FEBA test loop

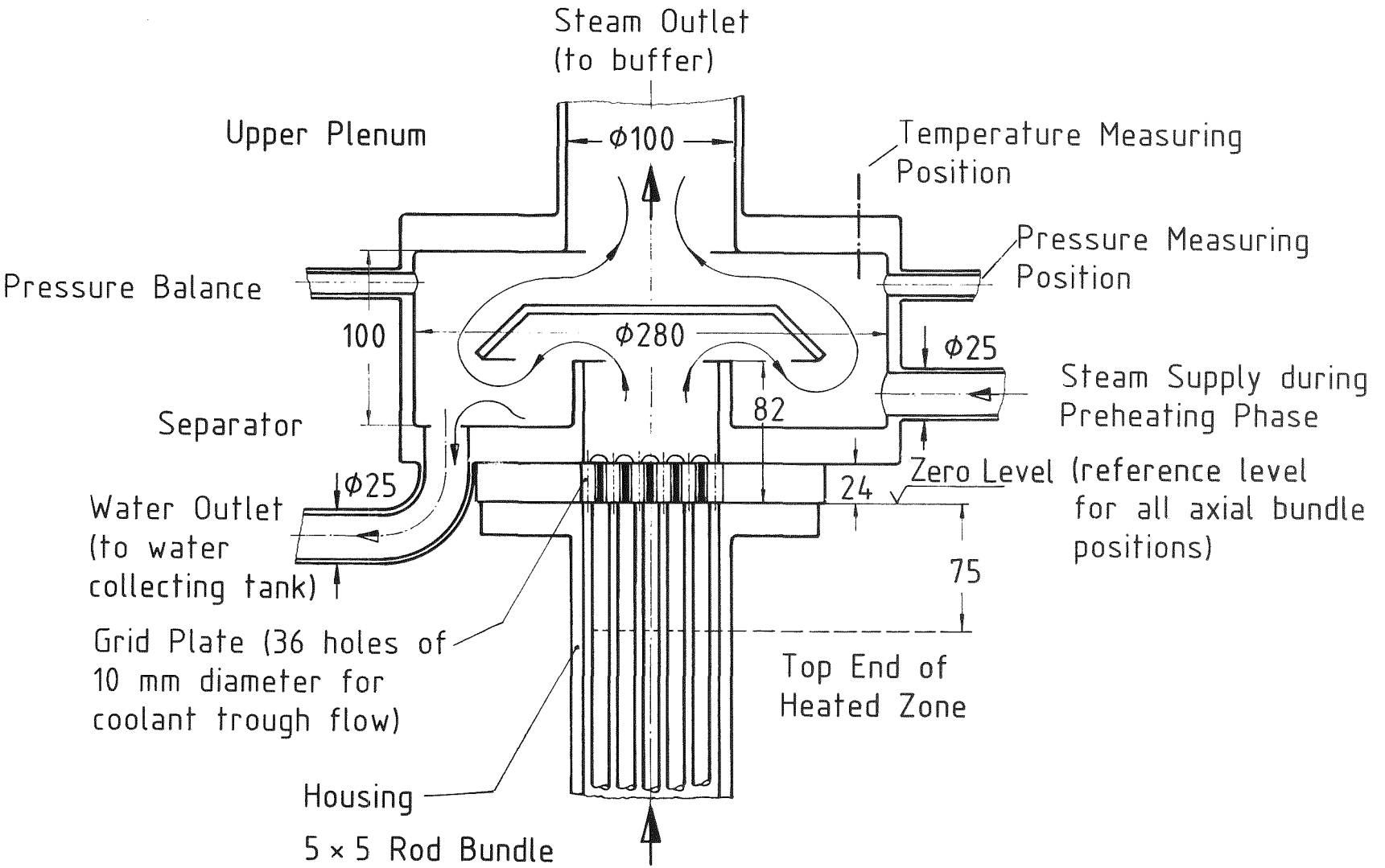

Fig. 7 5x5 rod bundle: Upper bundle end and upper plenum

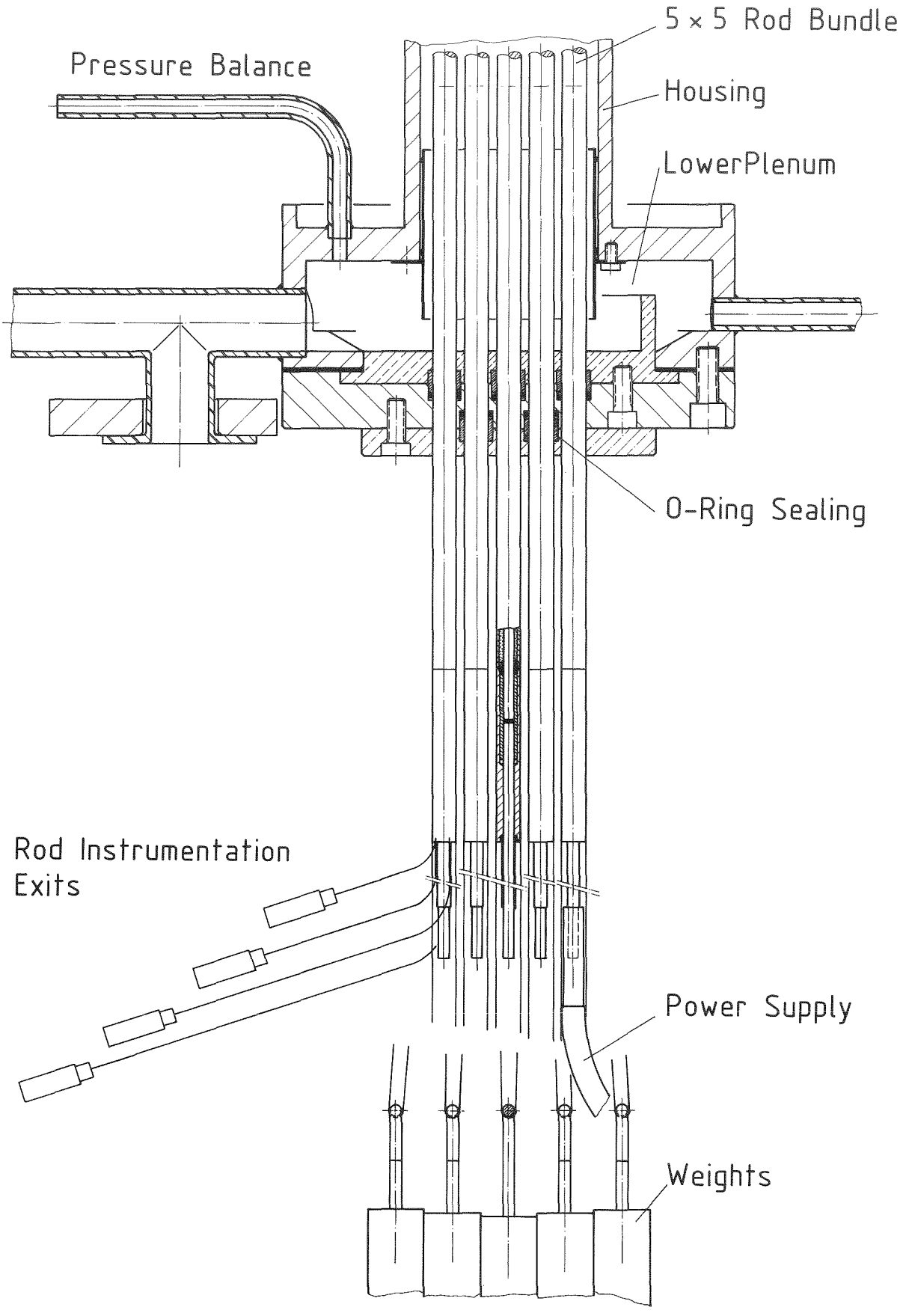

Fig. 8 5x5 rod bundle: Lower bundle end and lower plenum

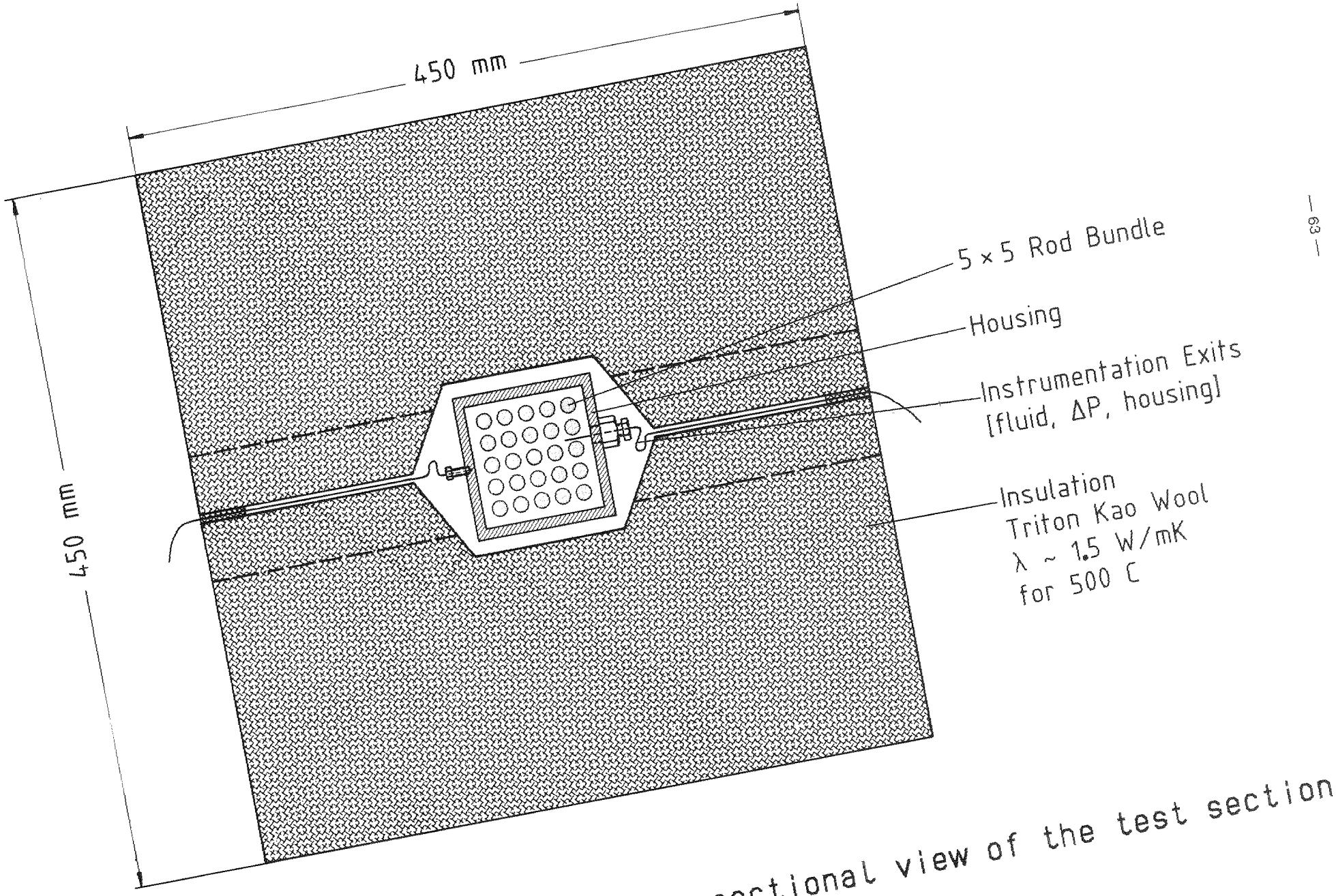

Fig. 9 5x5 rod bundle: Cross-sectional view of the test section

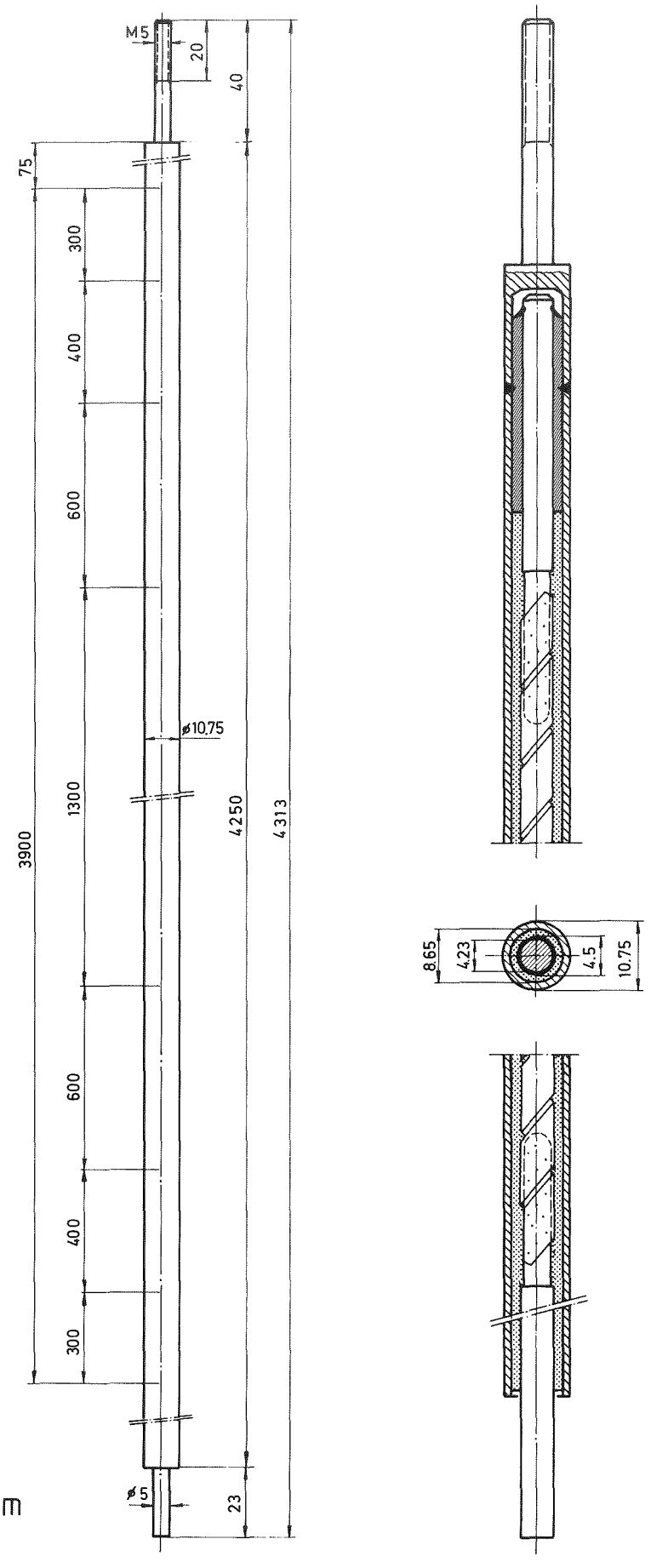

Dimensions in mm

Fig. 10 Longitudinal cross section of the FEBA heater rod

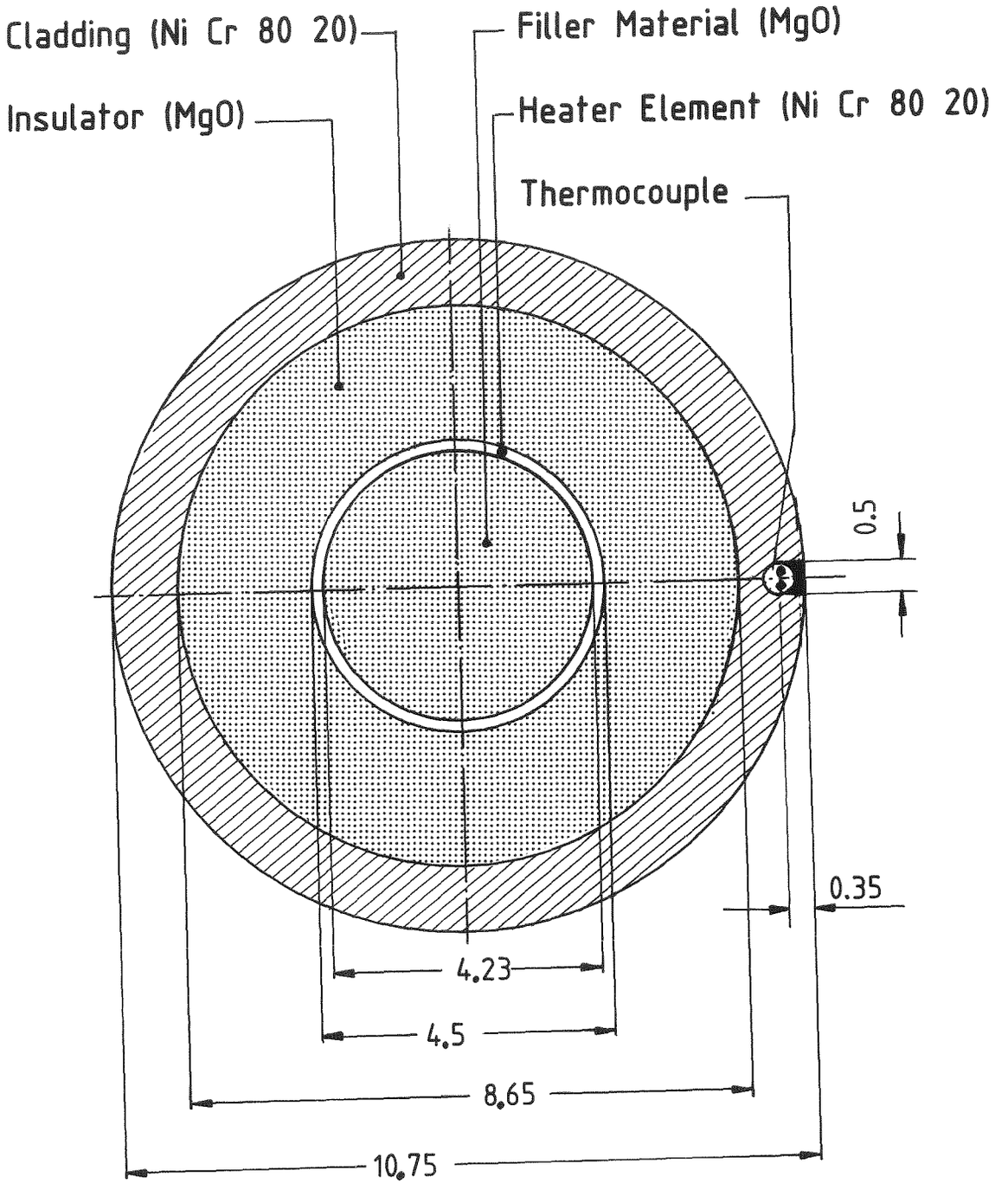

Dimensions are in millimeters

Fig. 11 Cross section of the FEBA heater rod

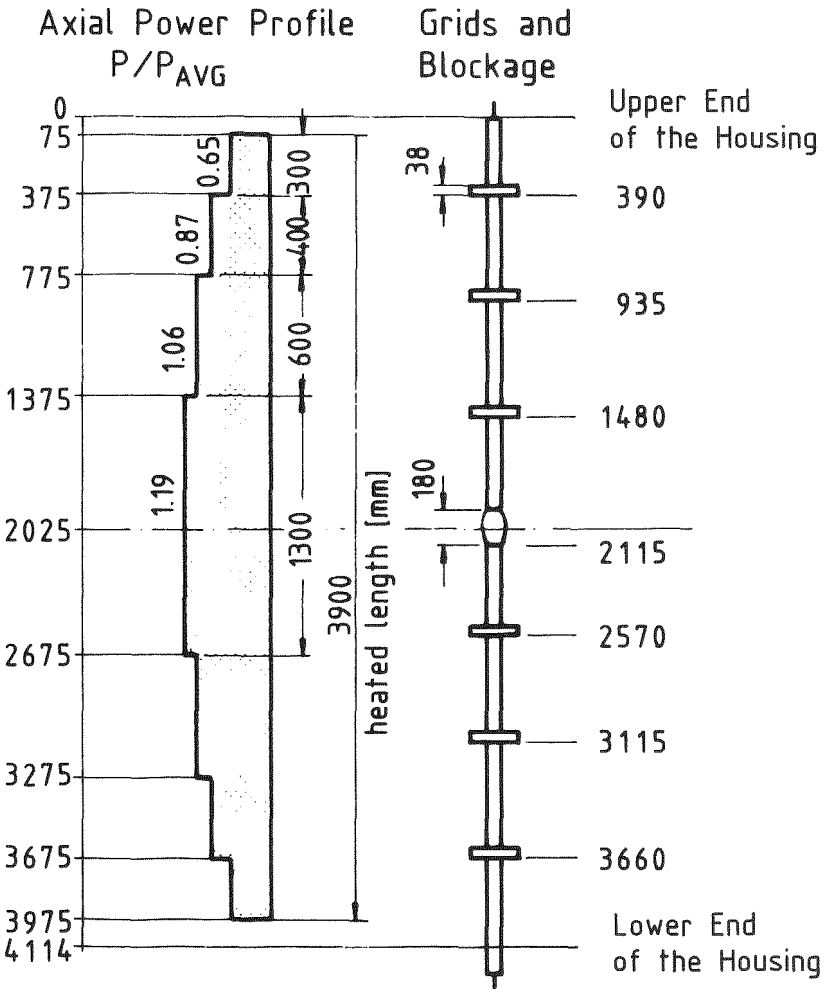

Fig. 12 Layout of the FEBA heater rod

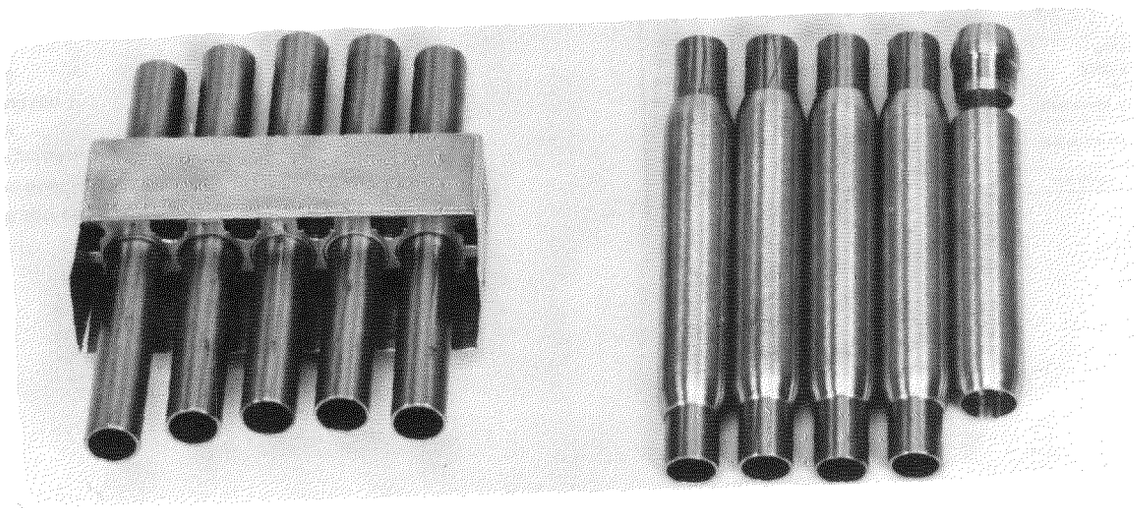

62% Plate Blockage
Used in 1x5 Rod Row

62% Sleeve Blockage
Used in 1x5 Rod Row

Fig. 13 5 rod row: Photographies of flow blockage devices

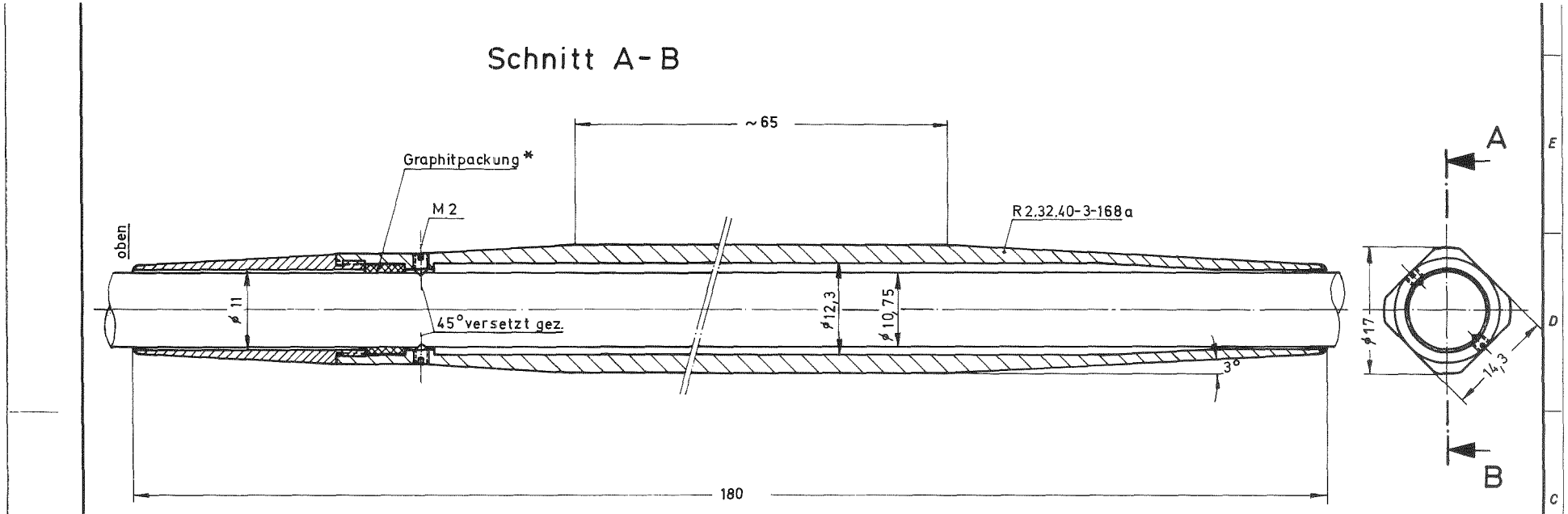

* gefertigt aus Burgmann-Rotatherm-Dichtungsband, geriffelt, 5 mm breit - Art. Nr. 0902
Fa. Feodor Burgmann
Dichtungswerk
819 Wolfratshausen 1
Postfach 1240

Teil	Stück	Benennung	Werkstoff	Abmessung	Zeichngs.-Nr. Norm	Bemerkung
Oberflächenzeichen	~ ▽ ▽▽ ▽▽▽ ▽▽▽▽		Freimaßtoleranz	bis 6 / über 6 bis 30	über 30 bis 100 / über 100 bis 300 / über 300 bis 1000 / über 1000 bis 2000	
Rauhtiefe max. in µ	1000	40	10	4	1,6		± 0,1	± 0,2	± 0,3	± 0,5	± 0,8	± 1,2

1979	Tag	Name	Werkstoff	Gesellschaft für Kernforschung m. b. H 7500 Karlsruhe Postfach 947	Zugeh. Zchng.
gez	5.3.	Kreuzinger H.	45.71		
gepr.					Ersatz für
ges					Ersetzt durch

Maßstab	Benennung	Zeichnungs-Nr.
2:1	Stabblockade-90% (montiert)	R2.32.40-3-172

Paßmaß Abmaß

Buch-stabe | Kommt vor | Änderung | Tag | Name

Fig. 14 5x5 rod bundle: Working drawing of the 90% blockage device

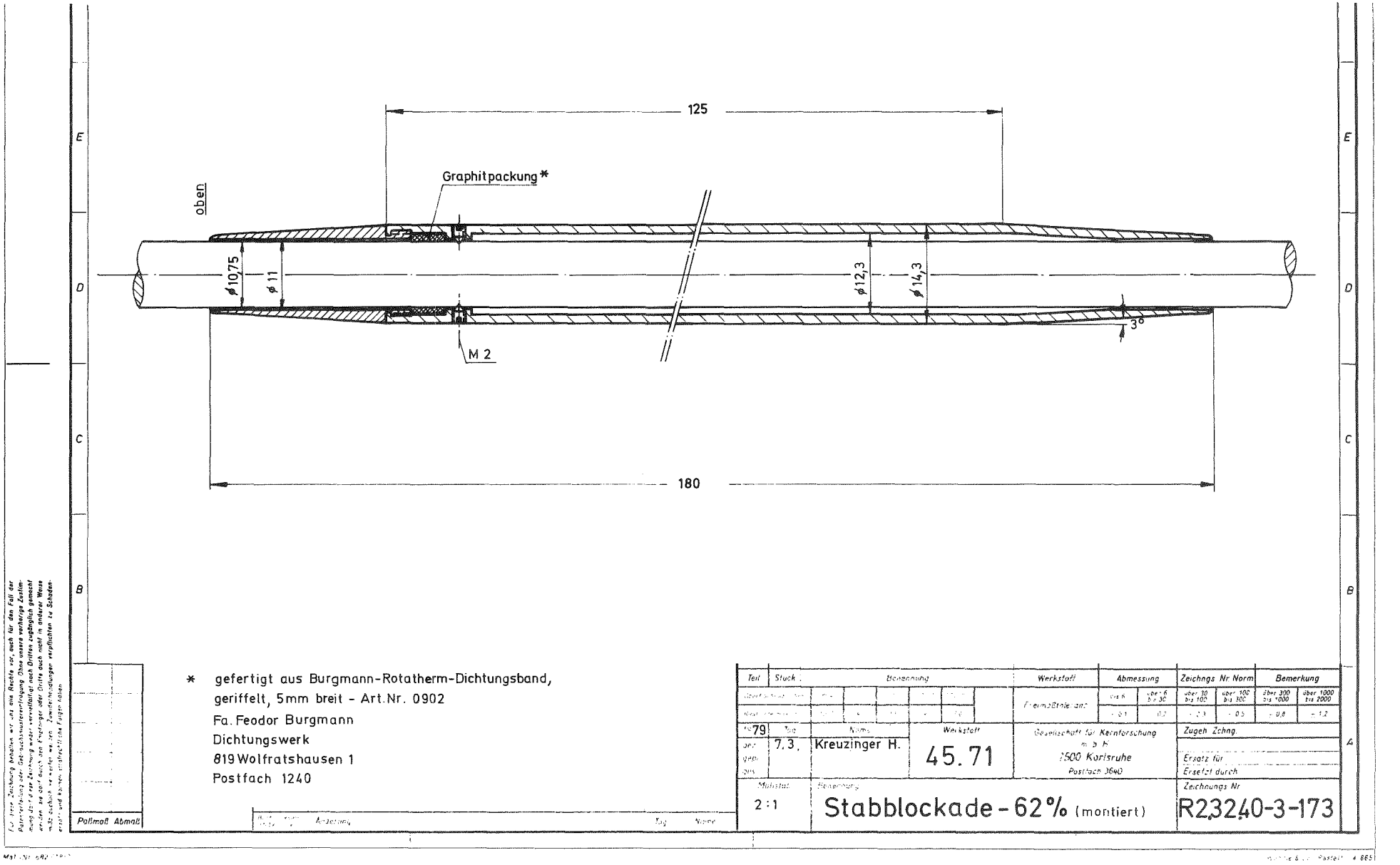

Fig. 15 5x5 rod bundle: Working drawing of the 62% blockage device

Cross Section
at Midplane of the Bundle

Local Blockage Ratio 90%
Overall Blockage Ratio 31%

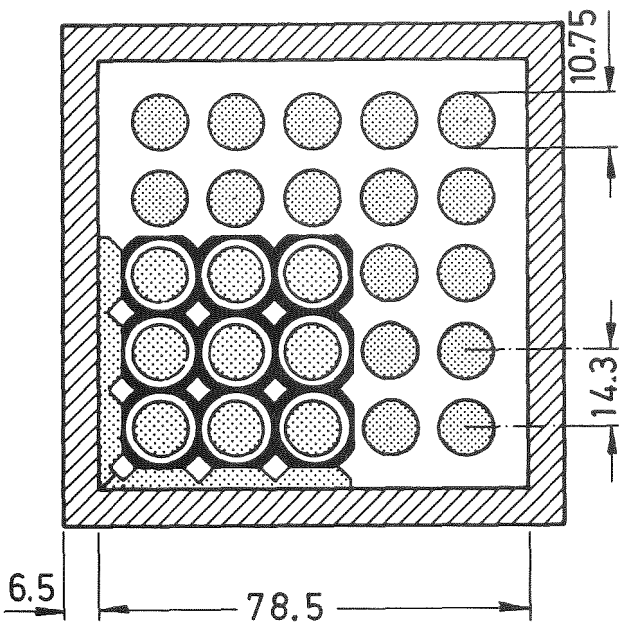

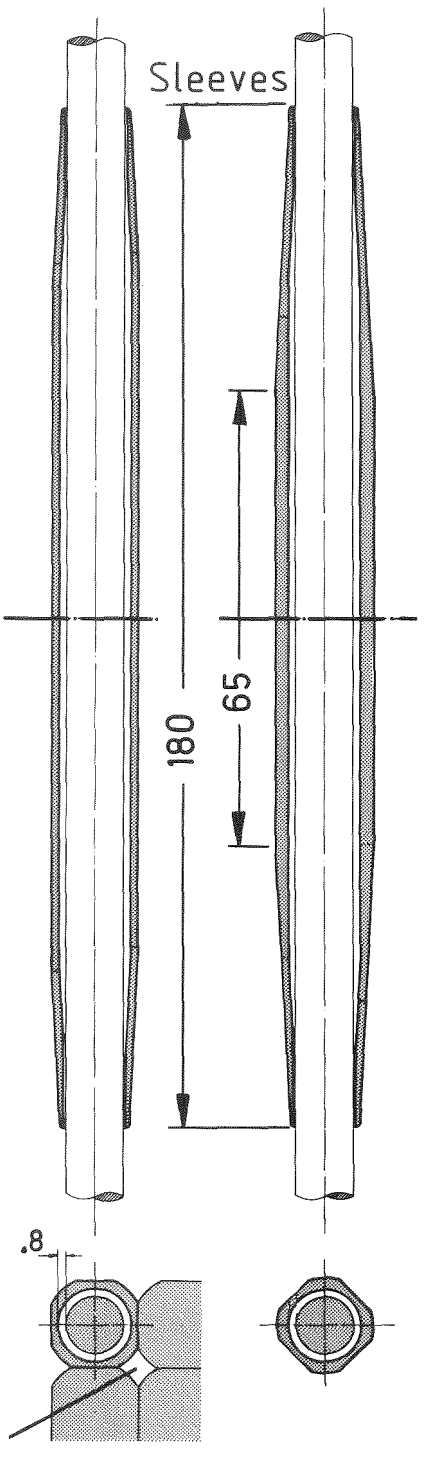

Bundle Data :

Pitch	14.3	mm
Rod Diameter	10.75	mm
Heated Length	3900	mm

Fig. 16 5x5 rod bundle: Array of the 90% partial blockage achieved with sleeves

Cross Section
at Midplane of the Bundle

Local Blockage Ratio 62%
Overall Blockage Ratio 20%

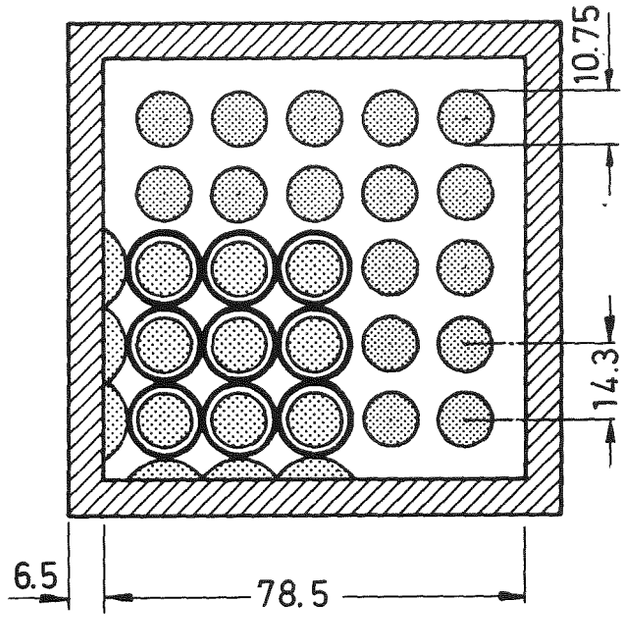

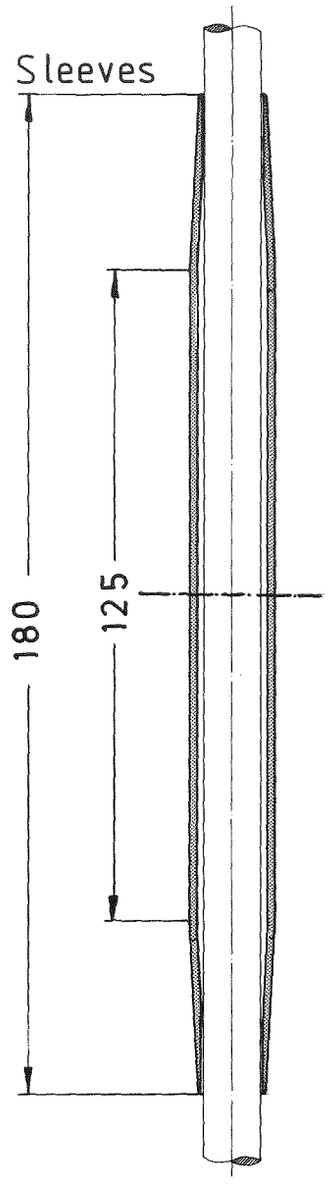

Bundle Data :

Pitch	14.3	mm
Rod Diameter	10.75	mm
Heated Length	3900	mm

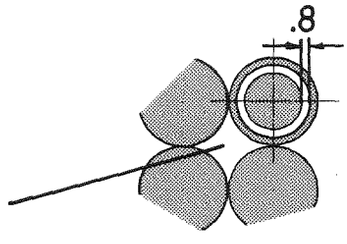

Fig. 17 5x5 rod bundle: Array of the 62% partial blockage achieved with sleeves

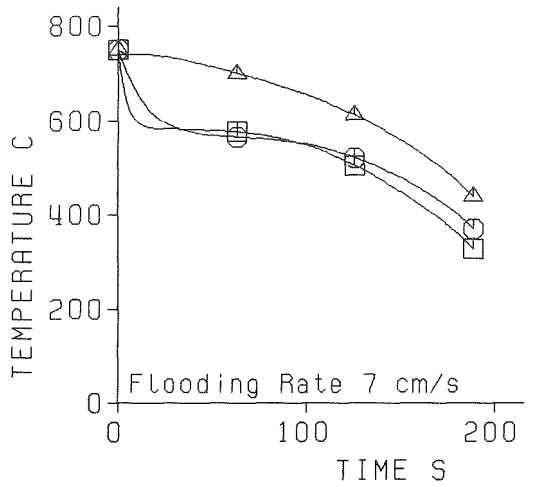

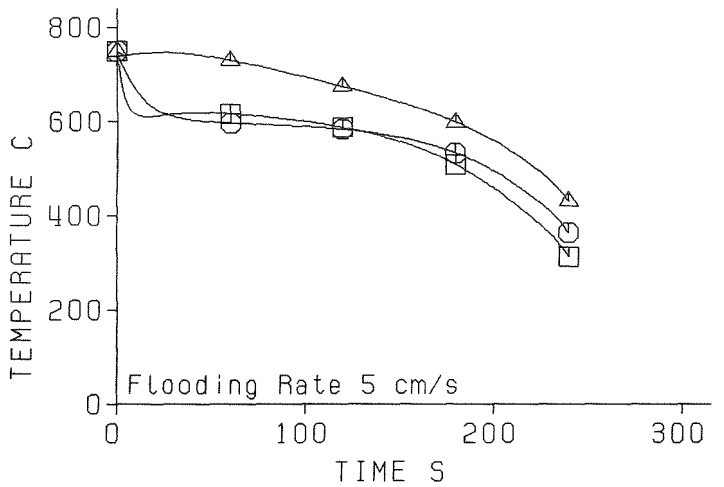

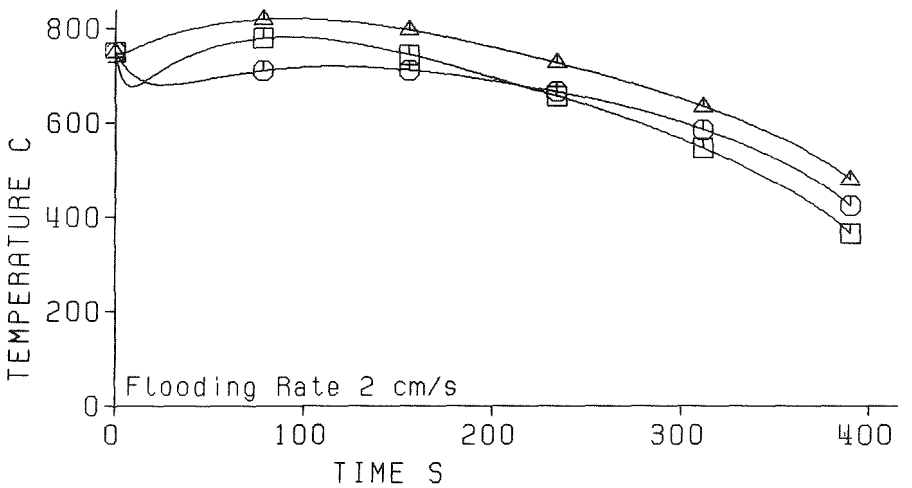

Cladding Deformations
Lead to a 62% Blockage
of Coolant Subchannels

□ Deformed Fuel Rod

⏀ Heater Rod Deformation
Simulated by a Hollow Sleeve

△ Heater Rod Deformation
Simulated by a Solid Sleeve

Gap Conductance:
H = 0.02 W/(cm**2*K)

Fig. 18 Influence of deformed claddings and flooding rates on surface temperatures

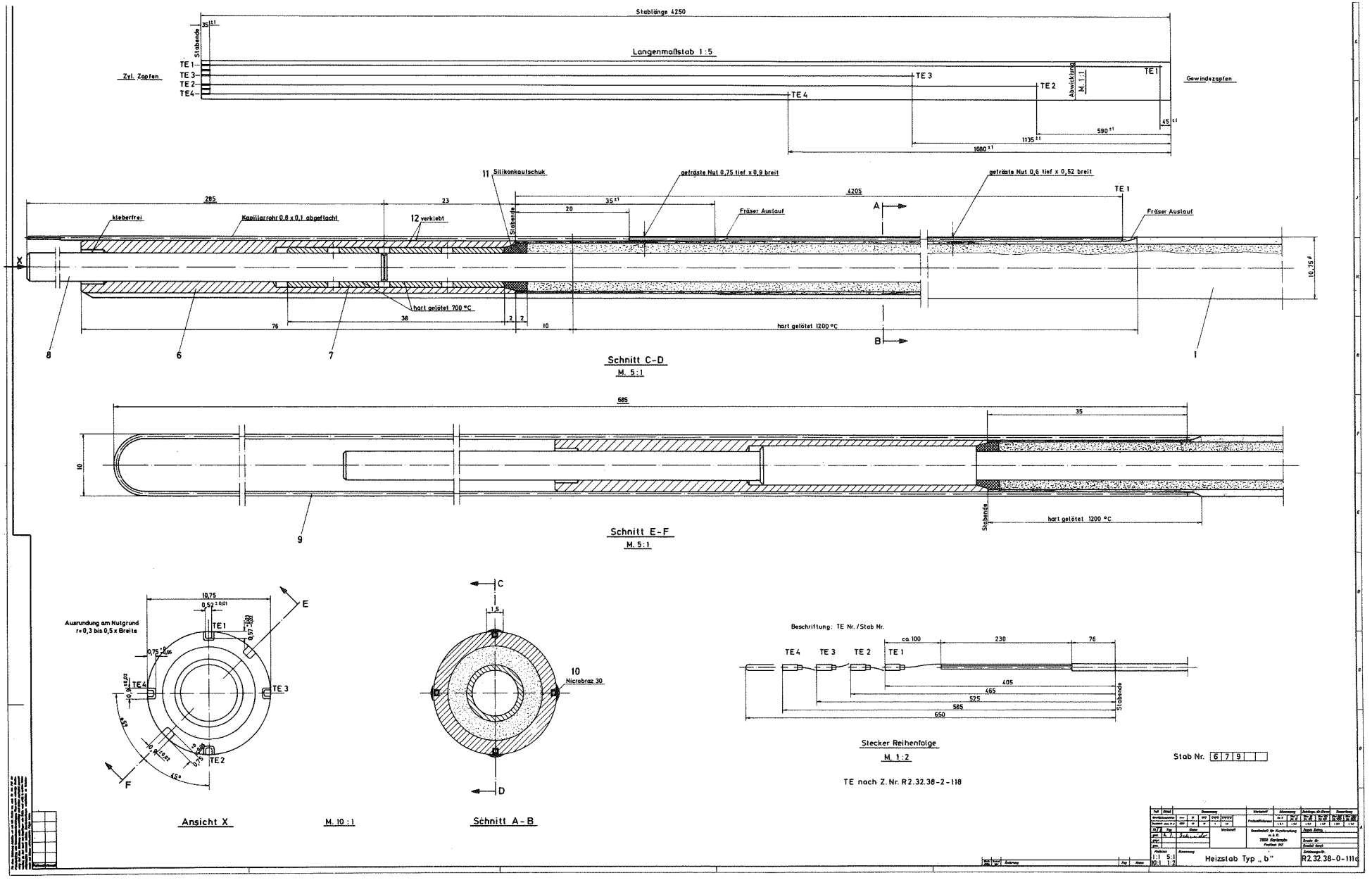

Fig. 19 Working drawing of an instrumented FEBA heater rod (type b of the cladding instrumentation)

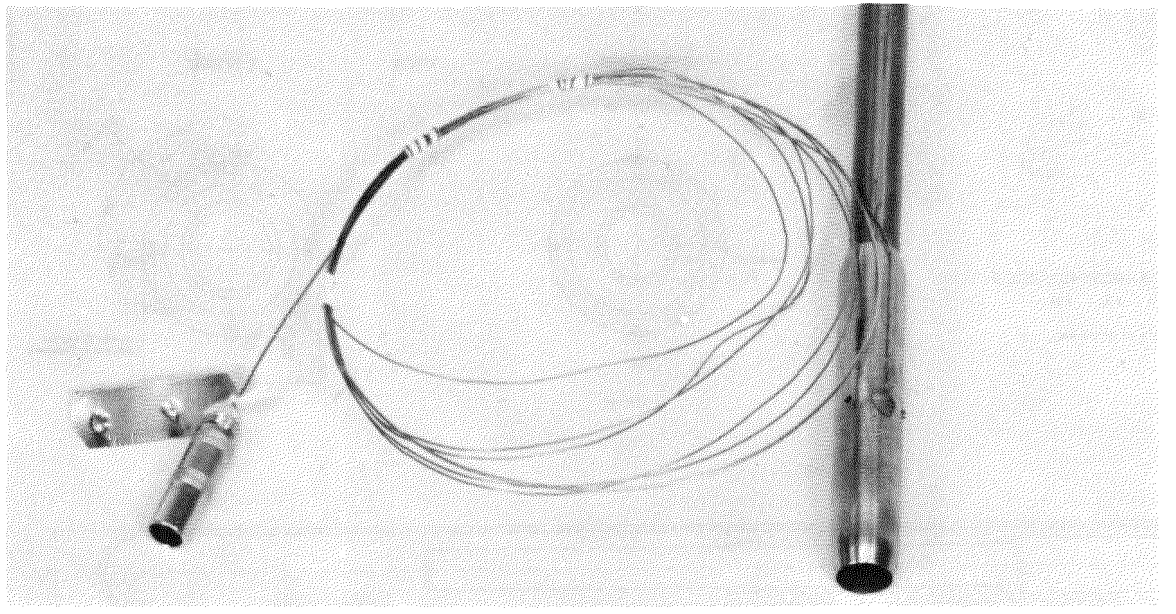

Instrumented
62% Sleeve Blockage
Used in 1x5 Rod Row

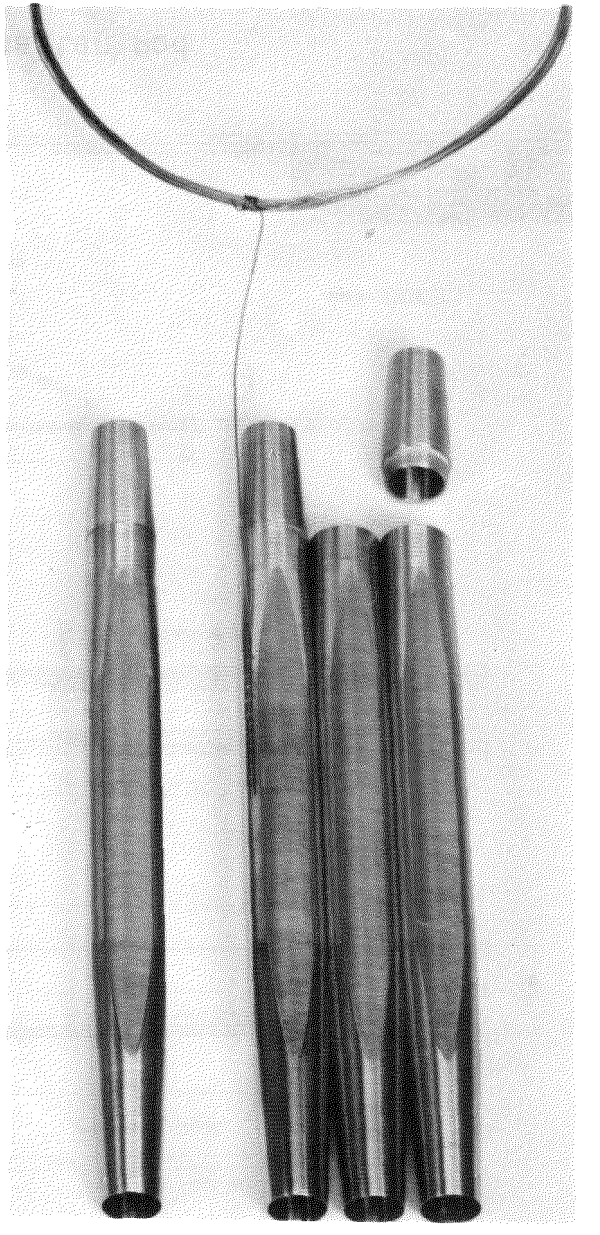

Instrumented
90% Sleeve Blockage
Used in 5x5 Rod Bundle

Fig. 20 Photographies of instrumented flow blockage devices

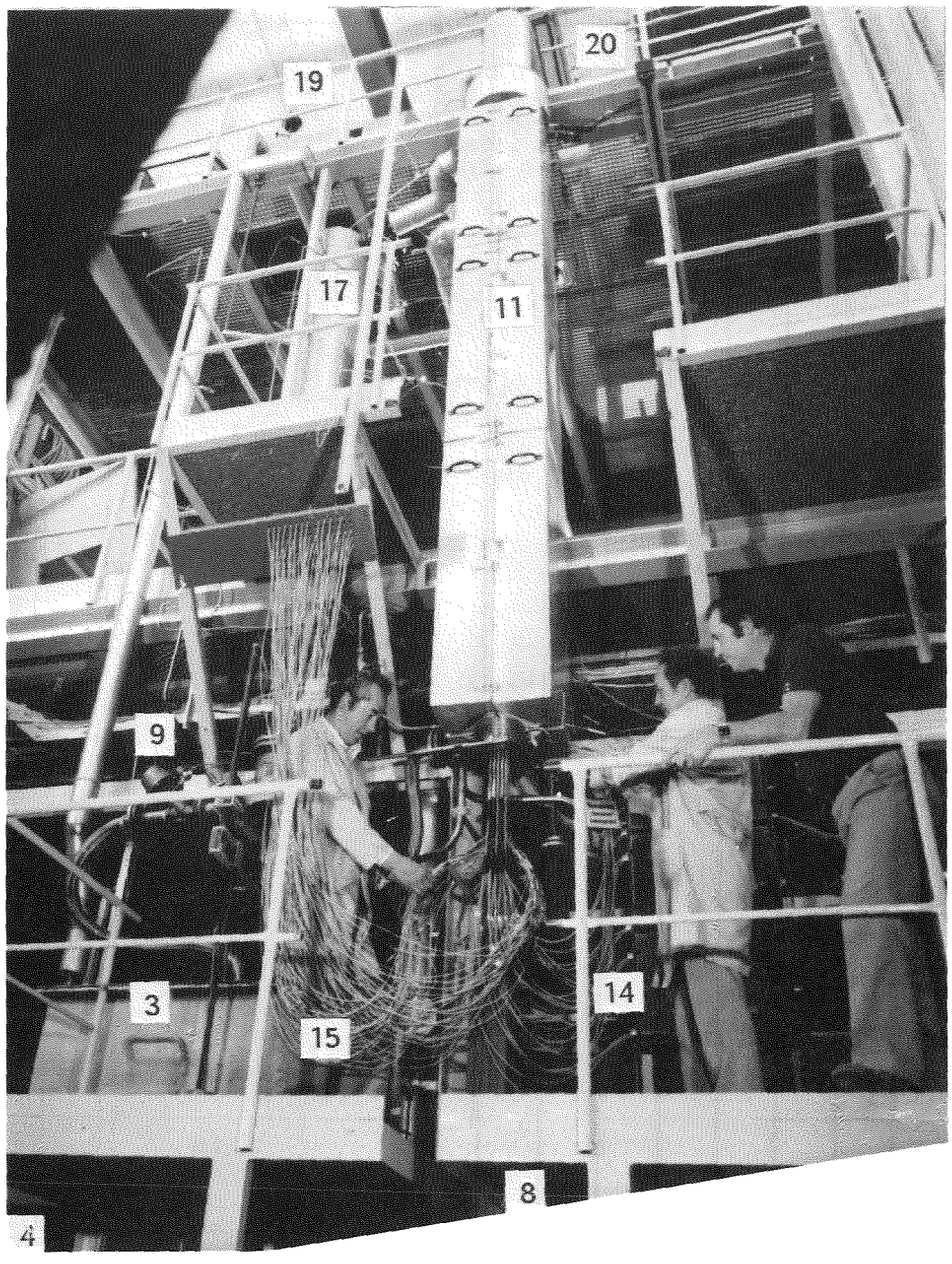

3 Storage Tank
4 Water Pump
8 Turbine Meter
9 Water Level Regulation Valve
11 Test Section
14 Power Supply
15 Rod Instrumentation Exits
17 Water Collecting Tank
19 Buffer
20 Pressure Regulator

Fig. 21 Photography of the FEBA test rig

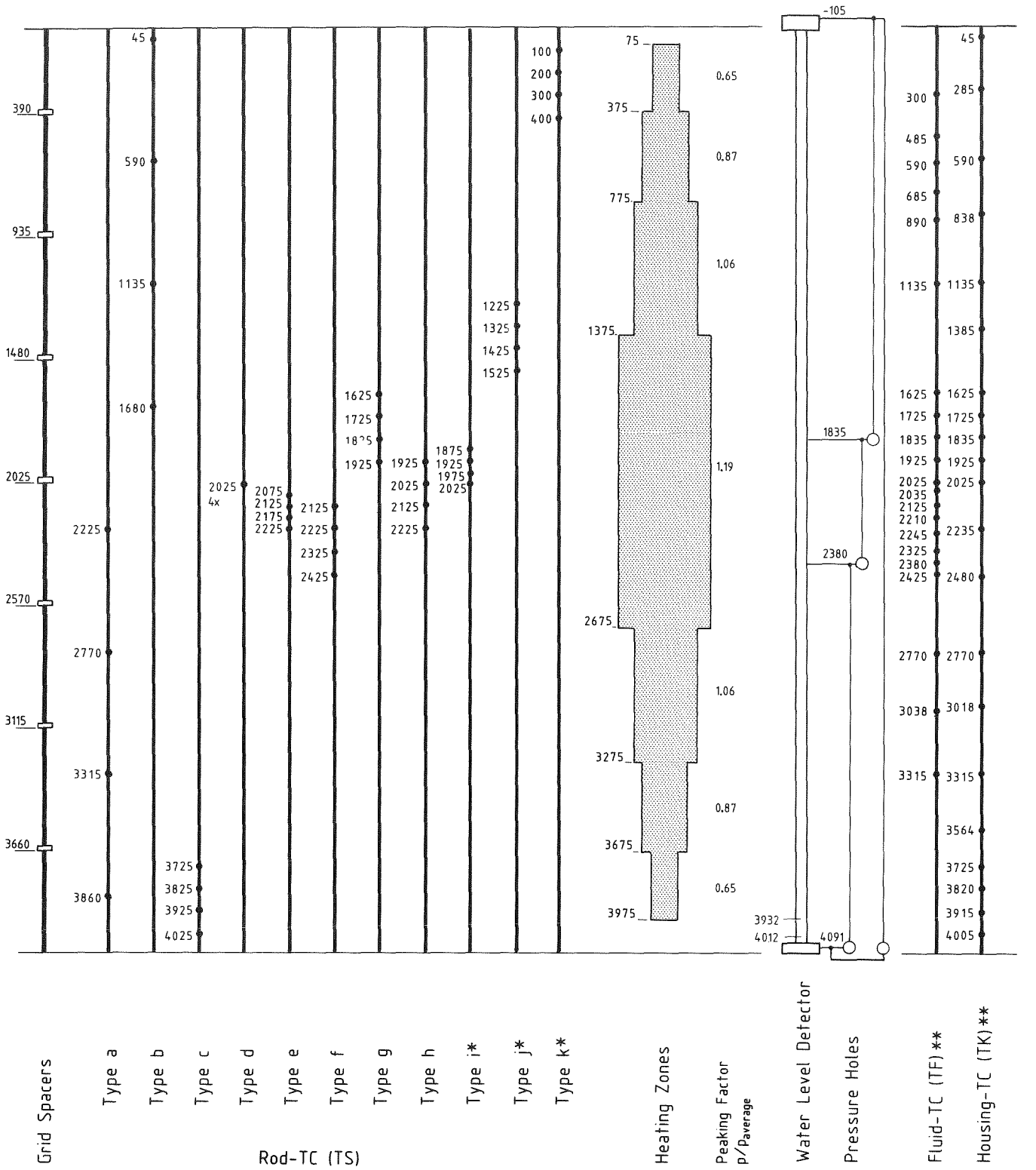

* in Test Series V through VIII only

** not all positions set for the individual tests

Fig. 22 5x5 rod bundle: Axial levels of the measuring positions

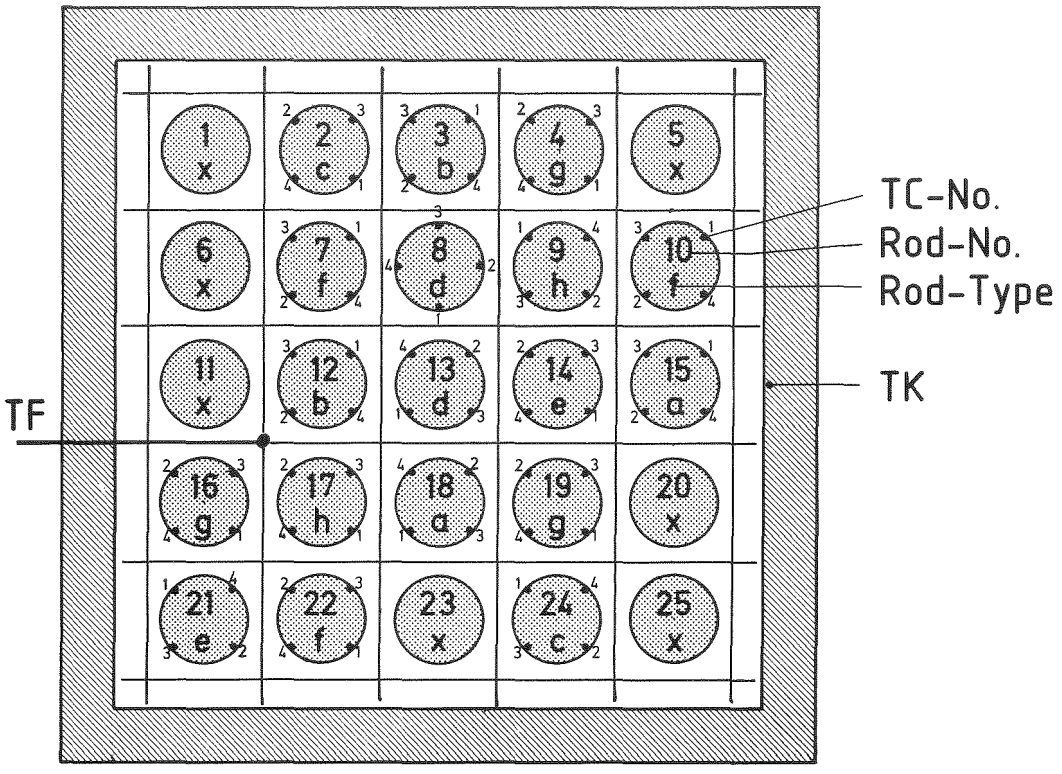

Rod Type	TC No.	Axial Level mm
a	1	2225
	2	2770
	3	3315
	4	3860
b	1	45
	2	590
	3	1135
	4	1680
c	1	3725
	2	3825
	3	3925
	4	4025
d	1	2025
	2	2025
	3	2025
	4	2025

Rod Type	TC No.	Axial Level mm
e	1	2075
	2	2125
	3	2175
	4	2225
f	1	2125
	2	2225
	3	2325
	4	2425
g	1	1625
	2	1725
	3	1825
	4	1925
h	1	1925
	2	2025
	3	2125
	4	2225

Rod Type	TC No.	Axial Level mm
x	without TC's	

Fig. 23 5x5 rod bundle: Radial and axial location of cladding, fluid and housing TC's for test series I

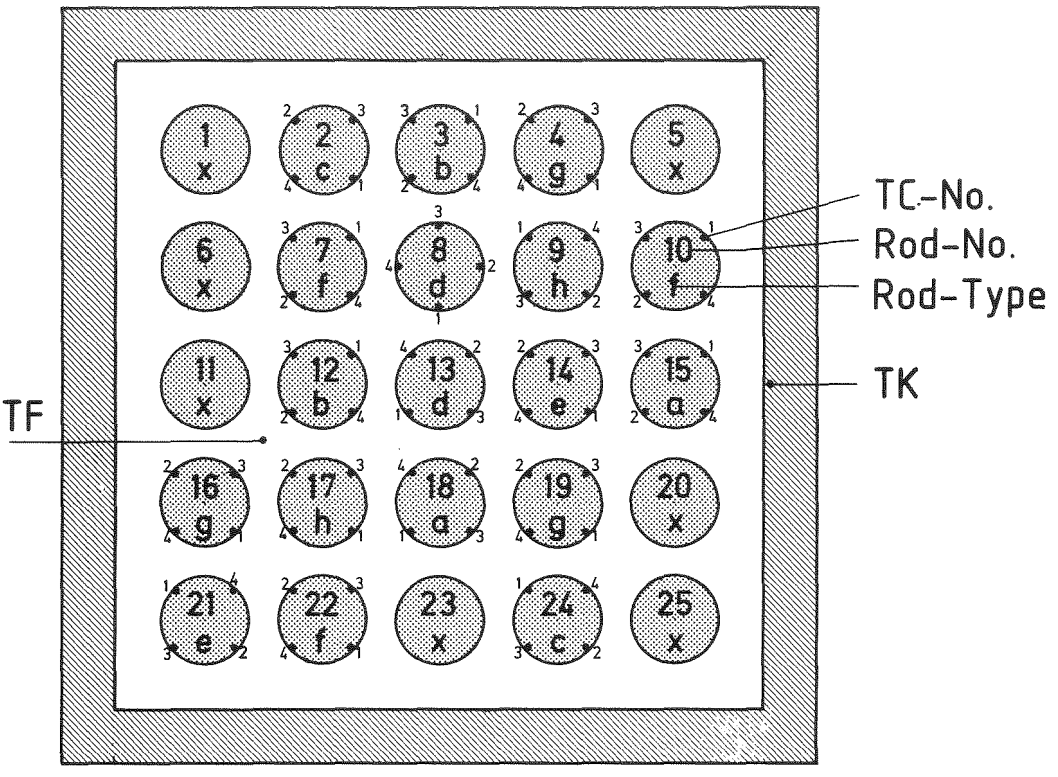

Rod Type	TC No.	Axial Level mm
a	1	2225
	2	2770
	3	3315
	4	3860
b	1	45
	2	590
	3	1135
	4	1680
c	1	3725
	2	3825
	3	3925
	4	4025
d	1	2025
	2	2025
	3	2025
	4	2025

Rod Type	TC No.	Axial Level mm
e	1	2075
	2	2125
	3	2175
	4	2225
f	1	2125
	2	2225
	3	2325
	4	2425
g	1	1625
	2	1725
	3	1825
	4	1925
h	1	1925
	2	2025
	3	2125
	4	2225

Rod Type	TC No.	Axial Level mm
x	without TC's	

Fig. 24 5x5 rod bundle: Radial and axial location of cladding, fluid and housing TC's for test series II

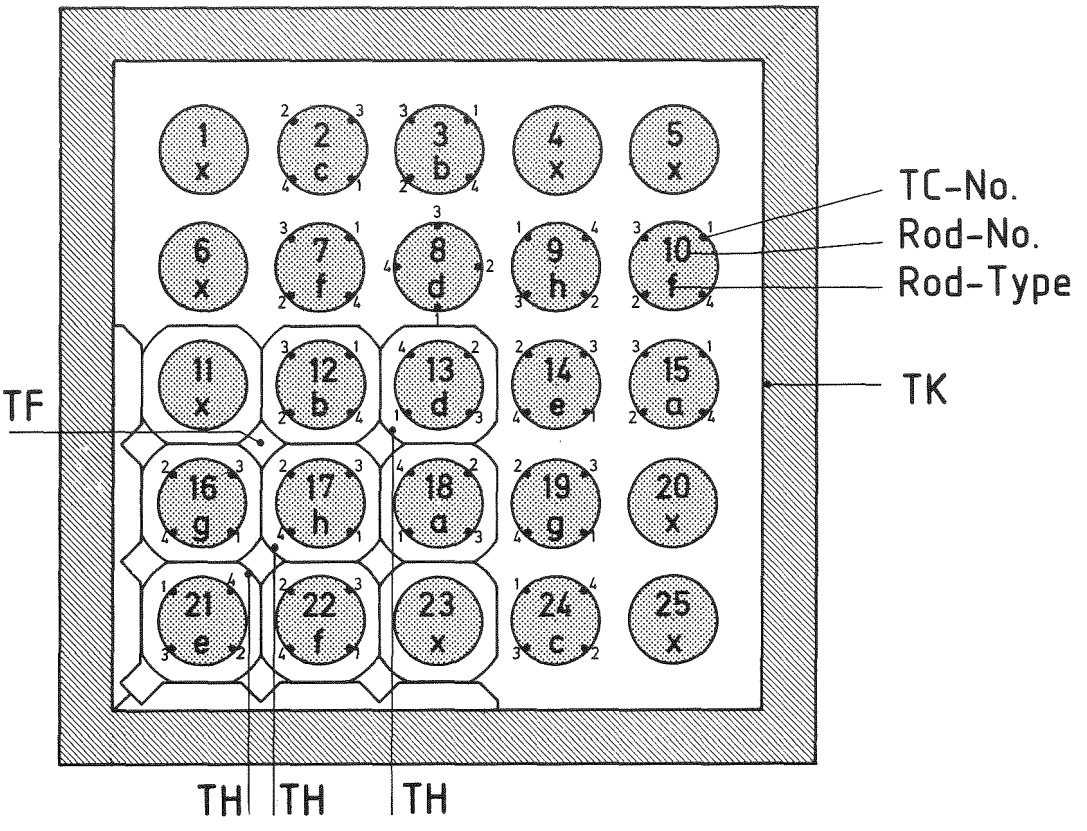

Rod Type	TC No.	Axial Level mm
a	1	2225
	2	2770
	3	3315
	4	3860
b	1	45
	2	590
	3	1135
	4	1680
c	1	3725
	2	3825
	3	3925
	4	4025
d	1	2025
	2	2025
	3	2025
	4	2025

Rod Type	TC No.	Axial Level mm
e	1	2075
	2	2125
	3	2175
	4	2225
f	1	2125
	2	2225
	3	2325
	4	2425
g	1	1625
	2	1725
	3	1825
	4	1925
h	1	1925
	2	2025
	3	2125
	4	2225

Rod Type	TC No.	Axial Level mm
x	without TC's	

Fig. 25 5x5 rod bundle: Radial and axial location of cladding, sleeve, fluid and housing TC's for test series III

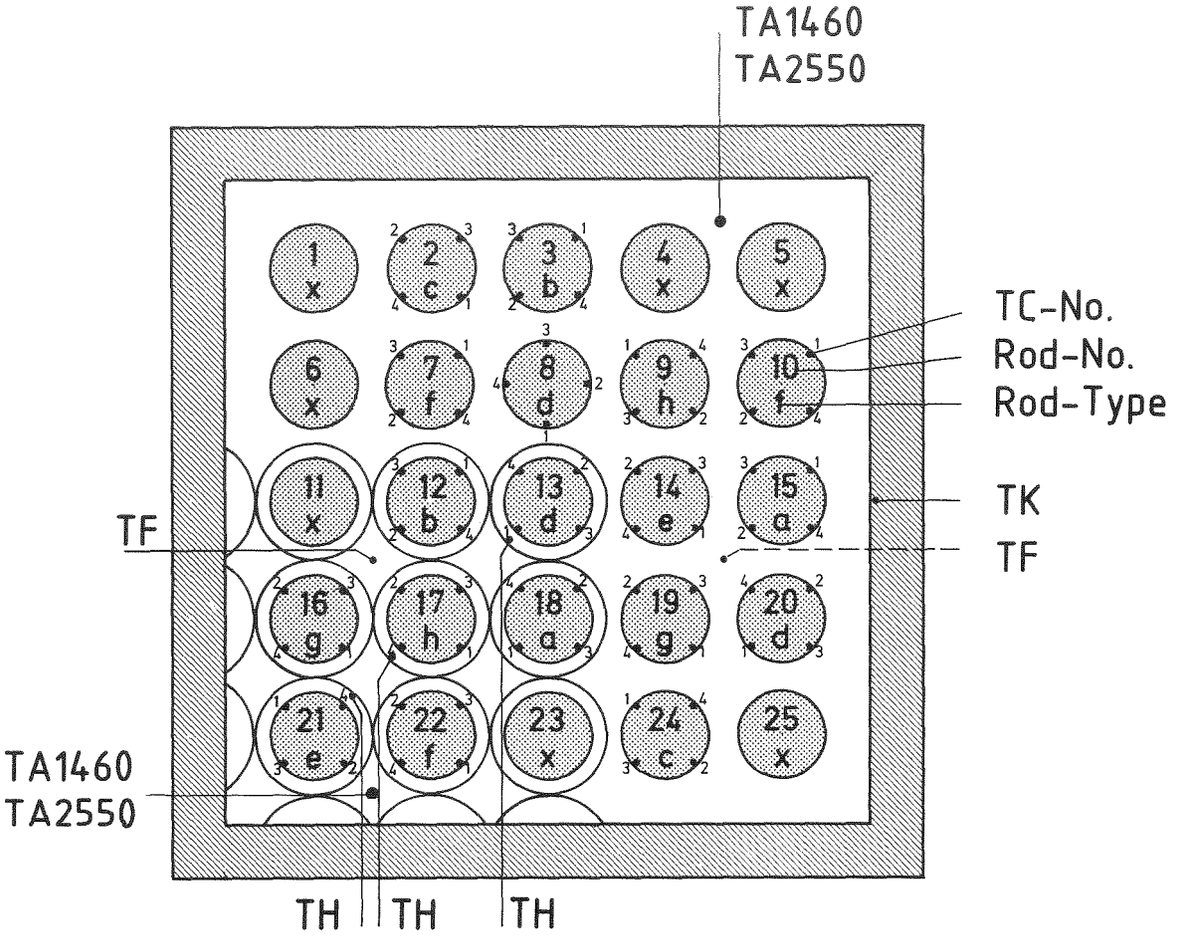

Rod Type	TC No.	Axial Level mm
a	1	2225
	2	2770
	3	3315
	4	3860
b	1	45
	2	590
	3	1135
	4	1680
c	1	3725
	2	3825
	3	3925
	4	4025
d	1	2025
	2	2025
	3	2025
	4	2025

Rod Type	TC No.	Axial Level mm
e	1	2075
	2	2125
	3	2175
	4	2225
f	1	2125
	2	2225
	3	2325
	4	2425
g	1	1625
	2	1725
	3	1825
	4	1925
h	1	1925
	2	2025
	3	2125
	4	2225

Rod Type	TC No.	Axial Level mm
x	without TC's	

Fig. 26 5x5 rod bundle: Radial and axial location of cladding, sleeve, spacer, fluid and housing TC's for test series IV

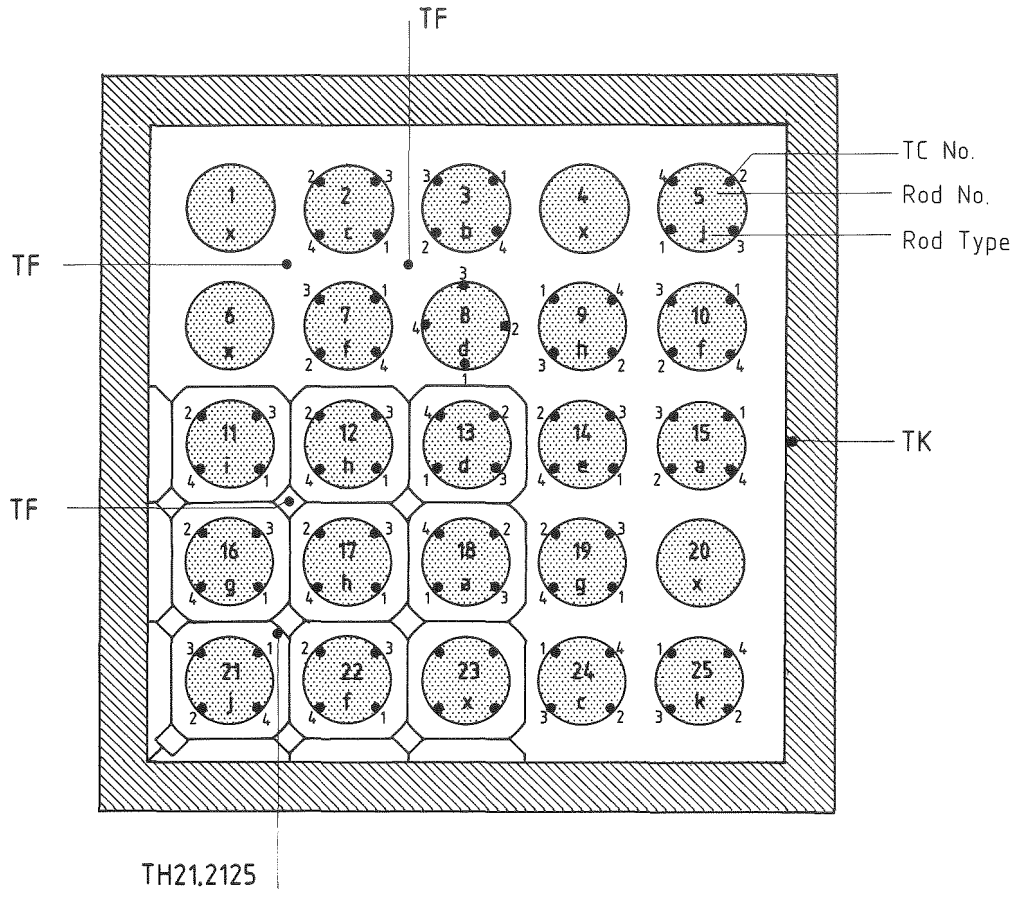

Rod Type	TC No.	Axial Level mm
a	1	2225
	2	2770
	3	3315
	4	3860
b	1	45
	2	590
	3	1135
	4	1680
c	1	3725
	2	3825
	3	3925
	4	4025
d	1	2025
	2	2025
	3	2025
	4	2025

Rod Type	TC No.	Axial Level mm
e	1	2075
	2	2125
	3	2175
	4	2225
f	1	2125
	2	2225
	3	2325
	4	2425
g	1	1625
	2	1725
	3	1825
	4	1925
h	1	1925
	2	2025
	3	2125
	4	2225

Rod Type	TC No.	Axial Level mm
i	1	1875
	2	1925
	3	1975
	4	2025
j	1	1225
	2	1325
	3	1425
	4	1525
k	1	100
	2	200
	3	300
	4	400
x	without TC's	

Fig. 27 5x5 rod bundle: Radial and axial location of cladding, sleeve, fluid and housing TC's for test series V

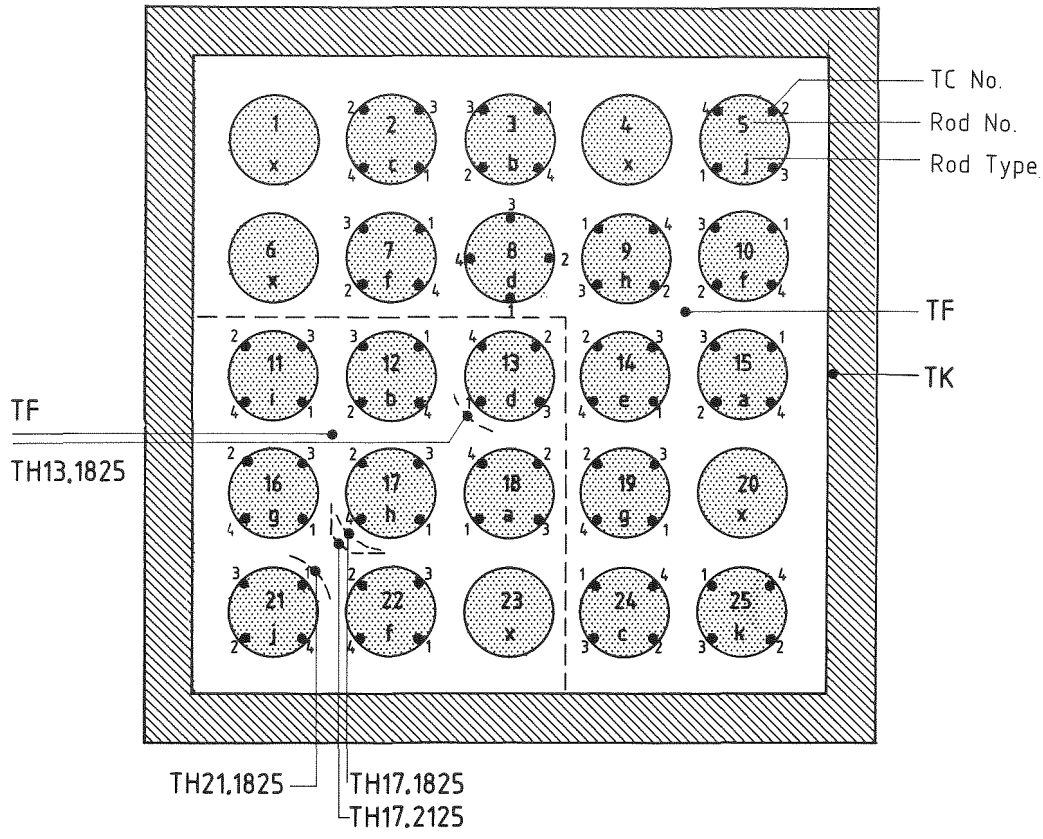

Rod Type	TC No.	Axial Level mm
a	1	2225
	2	2770
	3	3315
	4	3860
b	1	45
	2	590
	3	1135
	4	1680
c	1	3725
	2	3825
	3	3925
	4	4025
d	1	2025
	2	2025
	3	2025
	4	2025

Rod Type	TC No.	Axial Level mm
e	1	2075
	2	2125
	3	2175
	4	2225
f	1	2125
	2	2225
	3	2325
	4	2425
g	1	1625
	2	1725
	3	1825
	4	1925
h	1	1925
	2	2025
	3	2125
	4	2225

Rod Type	TC No.	Axial Level mm
i	1	1875
	2	1925
	3	1975
	4	2025
j	1	1225
	2	1325
	3	1425
	4	1525
k	1	100
	2	200
	3	300
	4	400
x	without TC's	

Fig. 28 5x5 rod bundle: Radial and axial location of cladding, sleeve, fluid and housing TC's for test series VI

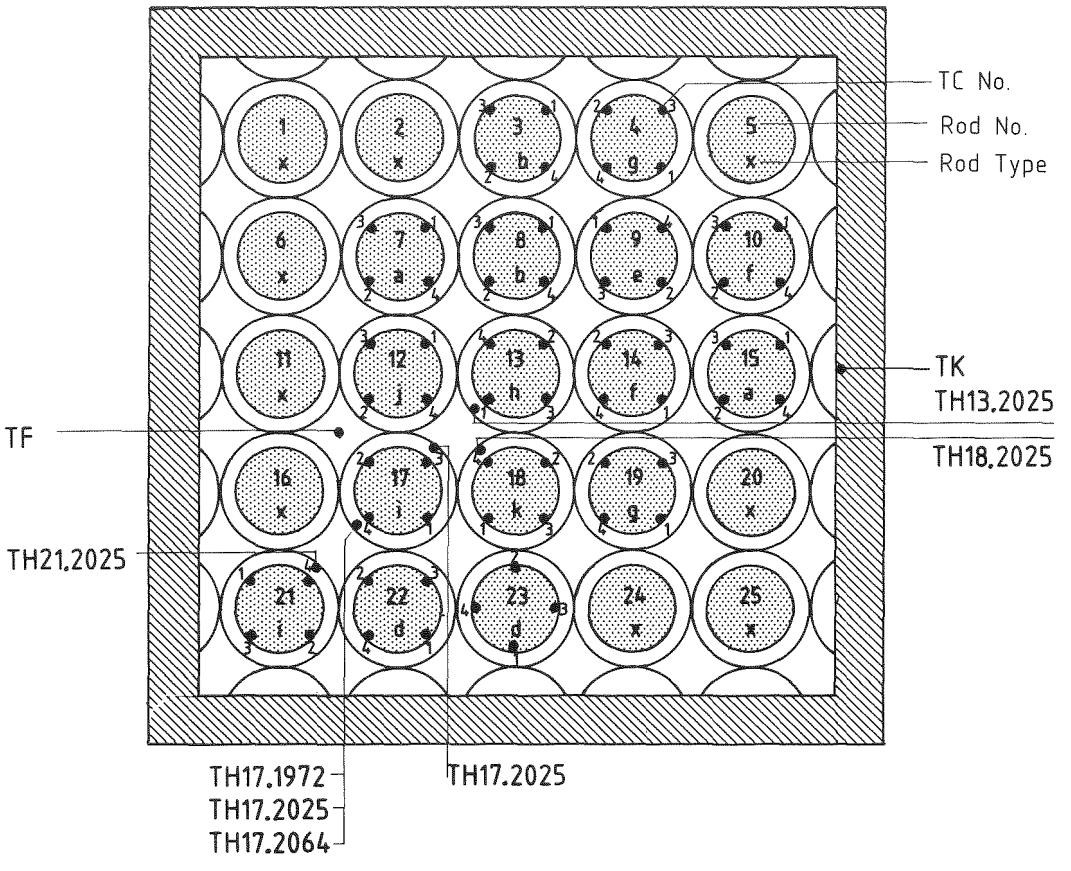

Rod Type	TC No.	Axial Level mm
a	1	2225
	2	2770
	3	3315
	4	3860
b	1	45
	2	590
	3	1135
	4	1680
c	1	3725
	2	3825
	3	3925
	4	4025
d	1	2025
	2	2025
	3	2025
	4	2025

Rod Type	TC No.	Axial Level mm
e	1	2075
	2	2125
	3	2175
	4	2225
f	1	2125
	2	2225
	3	2325
	4	2425
g	1	1625
	2	1725
	3	1825
	4	1925
h	1	1925
	2	2025
	3	2125
	4	2225

Rod Type	TC No.	Axial Level mm
i	1	1875
	2	1925
	3	1975
	4	2025
j	1	1225
	2	1325
	3	1425
	4	1525
k	1	100
	2	200
	3	300
	4	400
x	without TC's	

Fig. 29 5x5 rod bundle: Radial and axial location of cladding, sleeve, fluid and housing TC's for test series VII

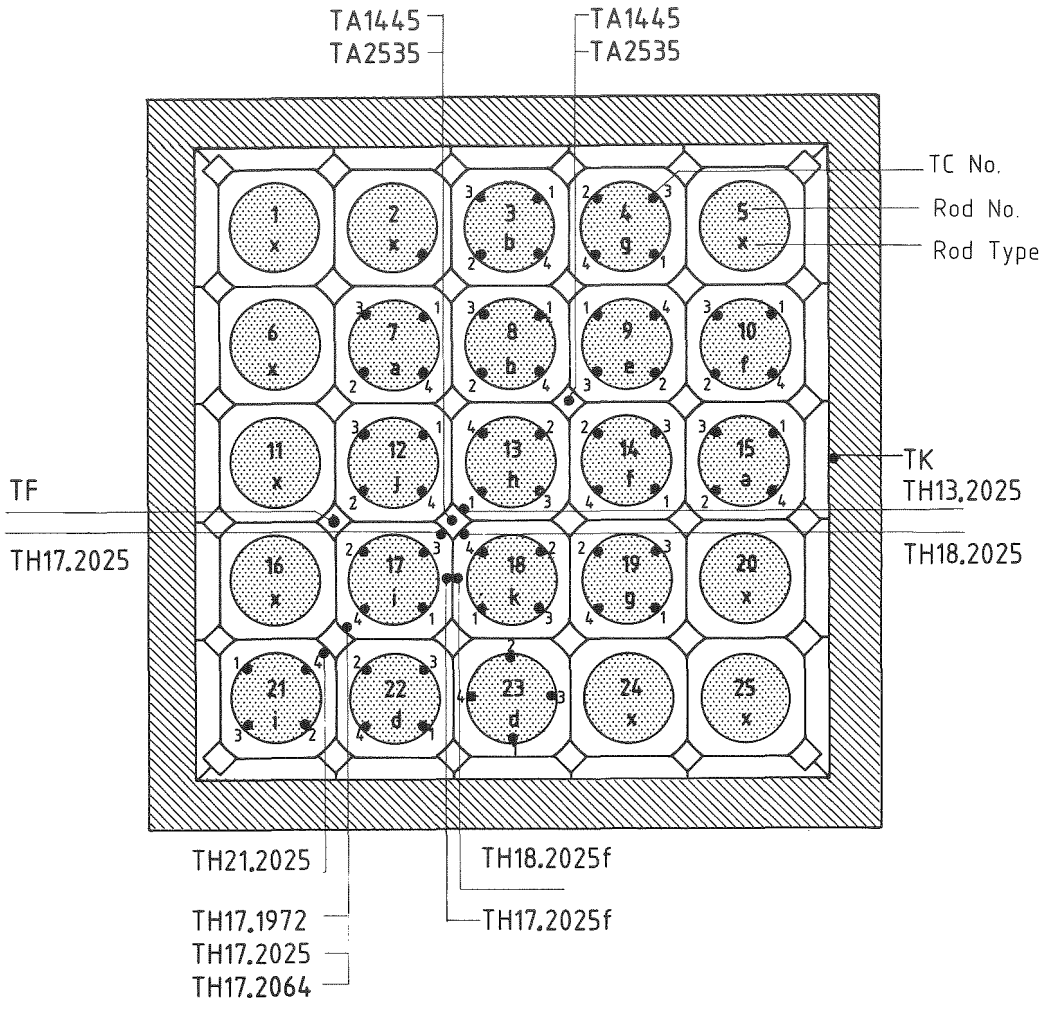

Rod Type	TC No.	Axial Level mm
a	1	2225
	2	2770
	3	3315
	4	3860
b	1	45
	2	590
	3	1135
	4	1680
c	1	3725
	2	3825
	3	3925
	4	4025
d	1	2025
	2	2025
	3	2025
	4	2025

Rod Type	TC No.	Axial Level mm
e	1	2075
	2	2125
	3	2175
	4	2225
f	1	2125
	2	2225
	3	2325
	4	2425
g	1	1625
	2	1725
	3	1825
	4	1925
h	1	1925
	2	2025
	3	2125
	4	2225

Rod Type	TC No.	Axial Level mm
i	1	1875
	2	1925
	3	1975
	4	2025
j	1	1225
	2	1325
	3	1425
	4	1525
k	1	100
	2	200
	3	300
	4	400
x	without TC's	

Fig. 30 5x5 rod bundle: Radial and axial location of cladding, sleeve, spacer, fluid and housing TC's for test series VIII

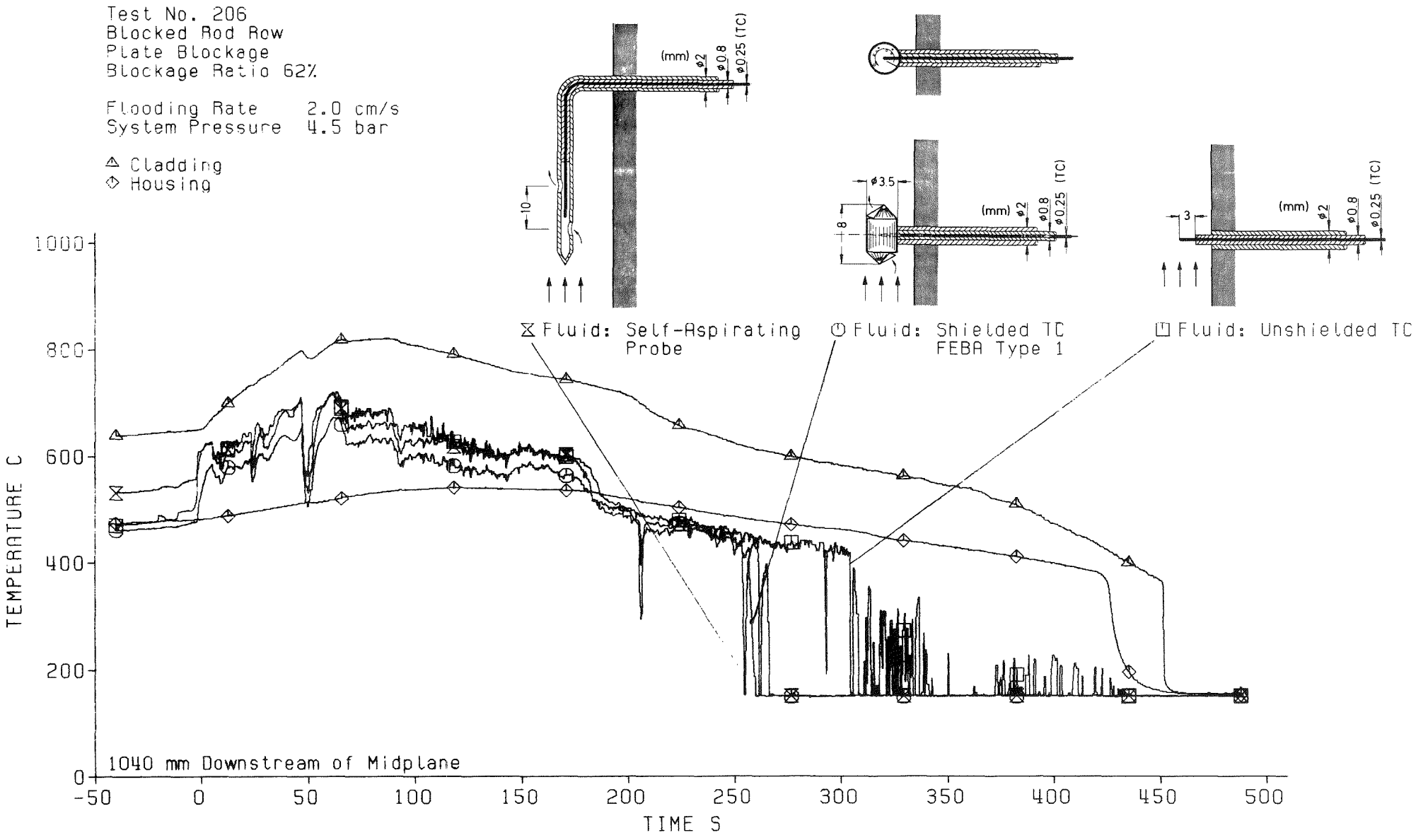

Fig. 31 5 rod row: Comparison of different fluid measuring devices

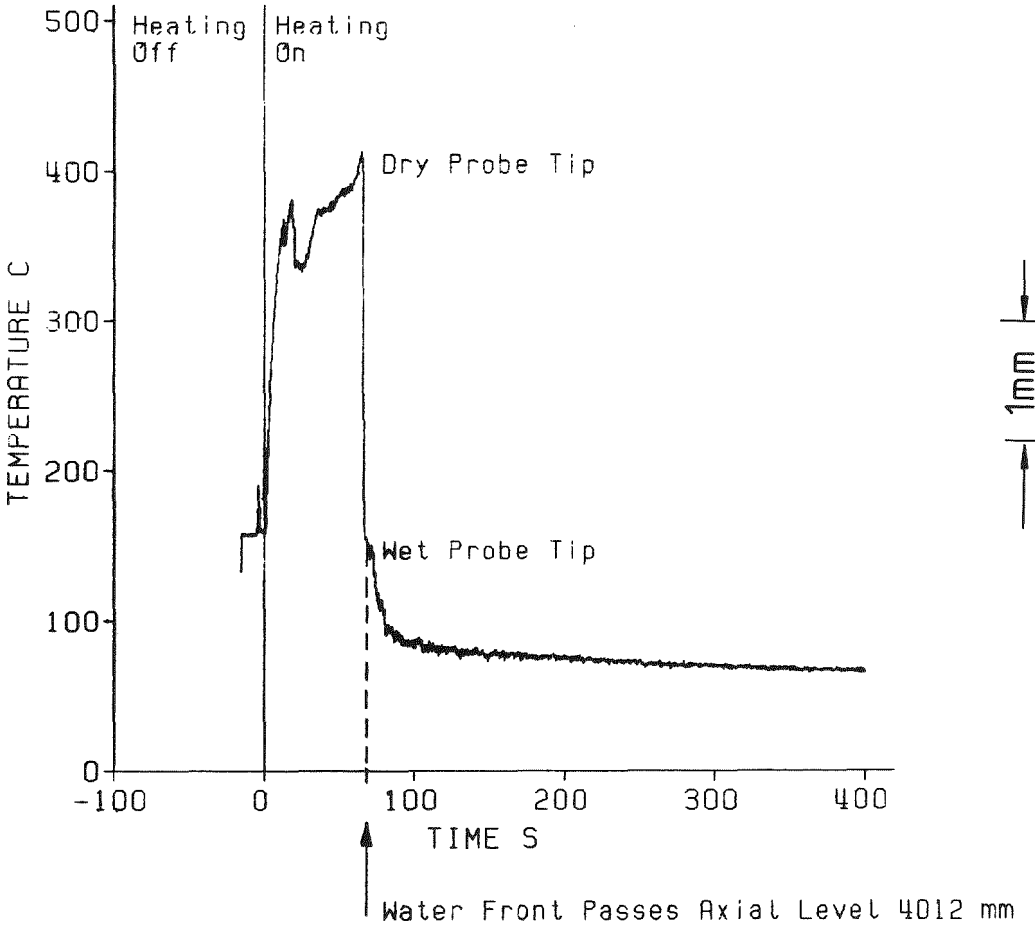

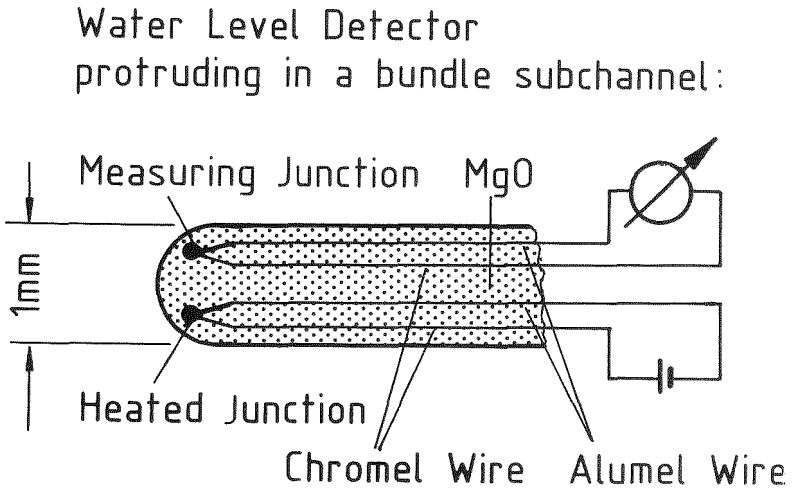

FEBA Test No. 266
Flooding Velocity 3.8 cm/s
System Pressure 3.9 bar
Feedwater Temperature 40 C

Fig. 32 Scheme and signal of the water level detector

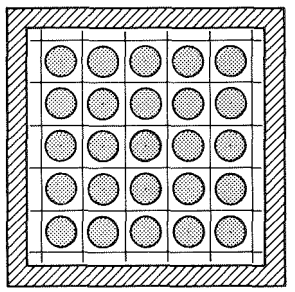

Test Series I
Test Series II

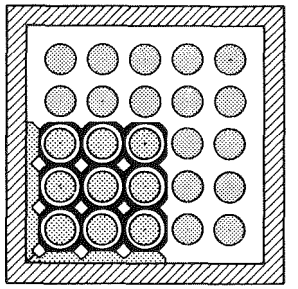

Test Series III
Test Series V
Test Series VI
90% Blockage

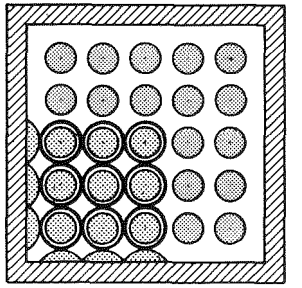

Test Series IV
Test Series VI
62% Blockage

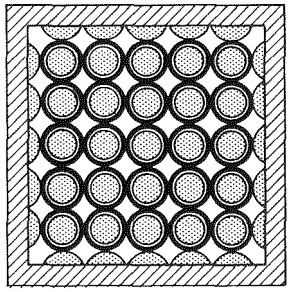

Test Series VII
62% Blockage

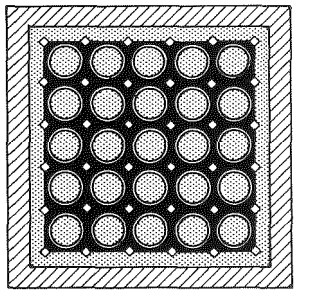

Test Series VIII
90% Blockage

FLOODING PARAMETERS

Test Series		I	II	III	IV	V	VI	VII	VIII
Flooding Velocity (cold bundle) Constant During Each Test	cm/s	3.8, 5.8	3.8, 5.8	3.8, 5.8	3.8, 5.8 (2.2, 10.)	2.2, 3.8 5.8	2.2, 3.8 5.8	3.8, 5.8 (2.2)	3.8, 5.8 (2.2)
System Pressure Constant During Each Test	bar	2, 4, 6	2, 4, 6	2, 4, 6	2, 4, 6 (4)	4	4	2, 4, 6 (4)	2, 4, 6 (2, 4)
Feedwater Temperature Constant During Each Test	°C	40 °C, some few tests with 80 °C							
Max. Cladding Temperature (at start of reflooding)	°C	between 700 and 800 °C, some few tests between 600 and 700°C							
Max. Housing Temperature (at start of reflooding)	°C	between 600 and 700 °C, some few tests between 500 and 600°C							
Bundle Power	kW	at start of reflooding 200 kW, 120% ANS decay heat transient 40 s after shutdown, some few tests with constant bundle power							

Steam Cooling Tests

Test series VII and VIII include steady state and transient tests for which low bundle power and system pressures of 2, 4 and 6 bar were selected.

Fig. 33 5x5 rod bundle: Test matrix of test series I through VIII

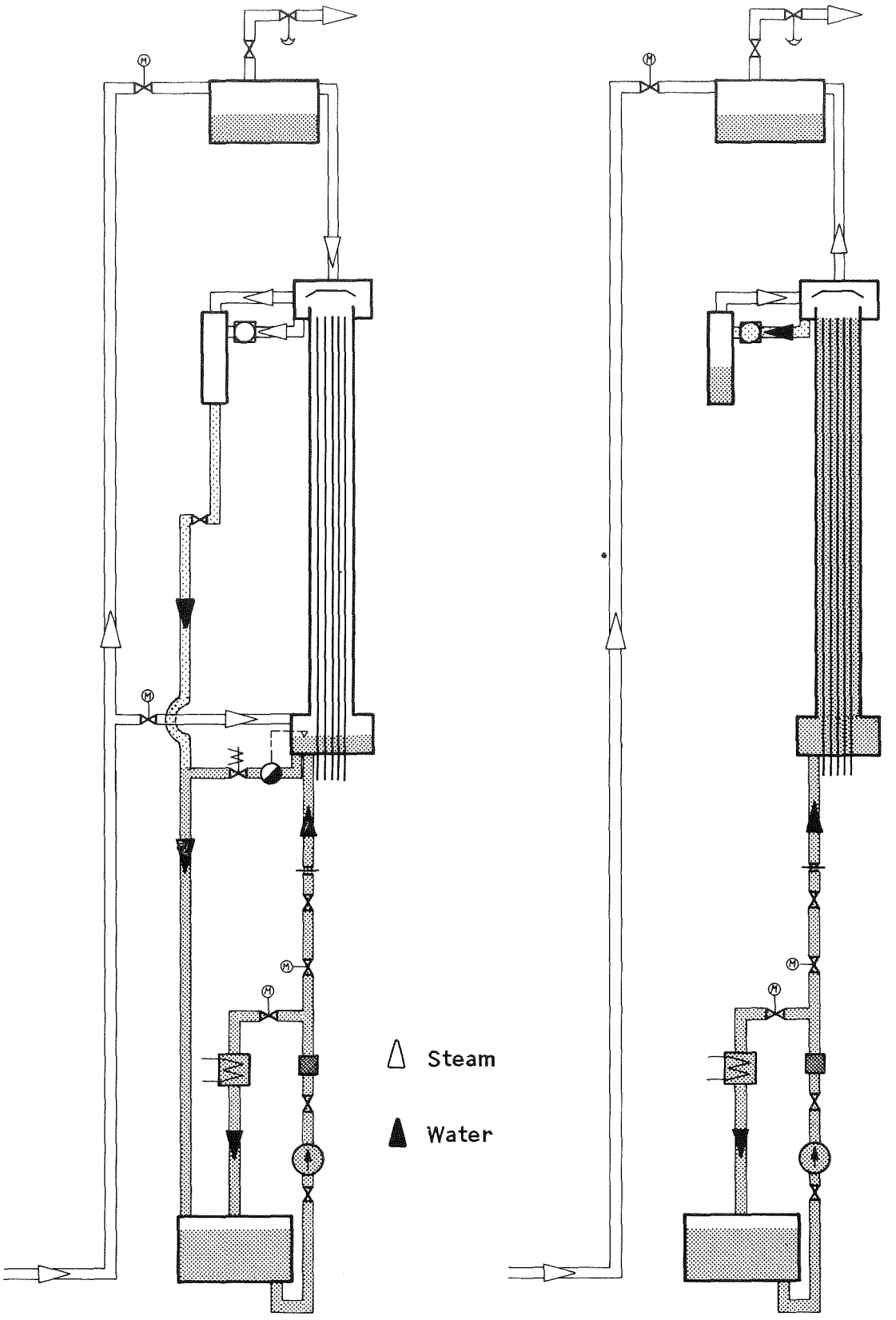

Fig. 34 Flow scheme during operational procedure of FEBA reflood experiments

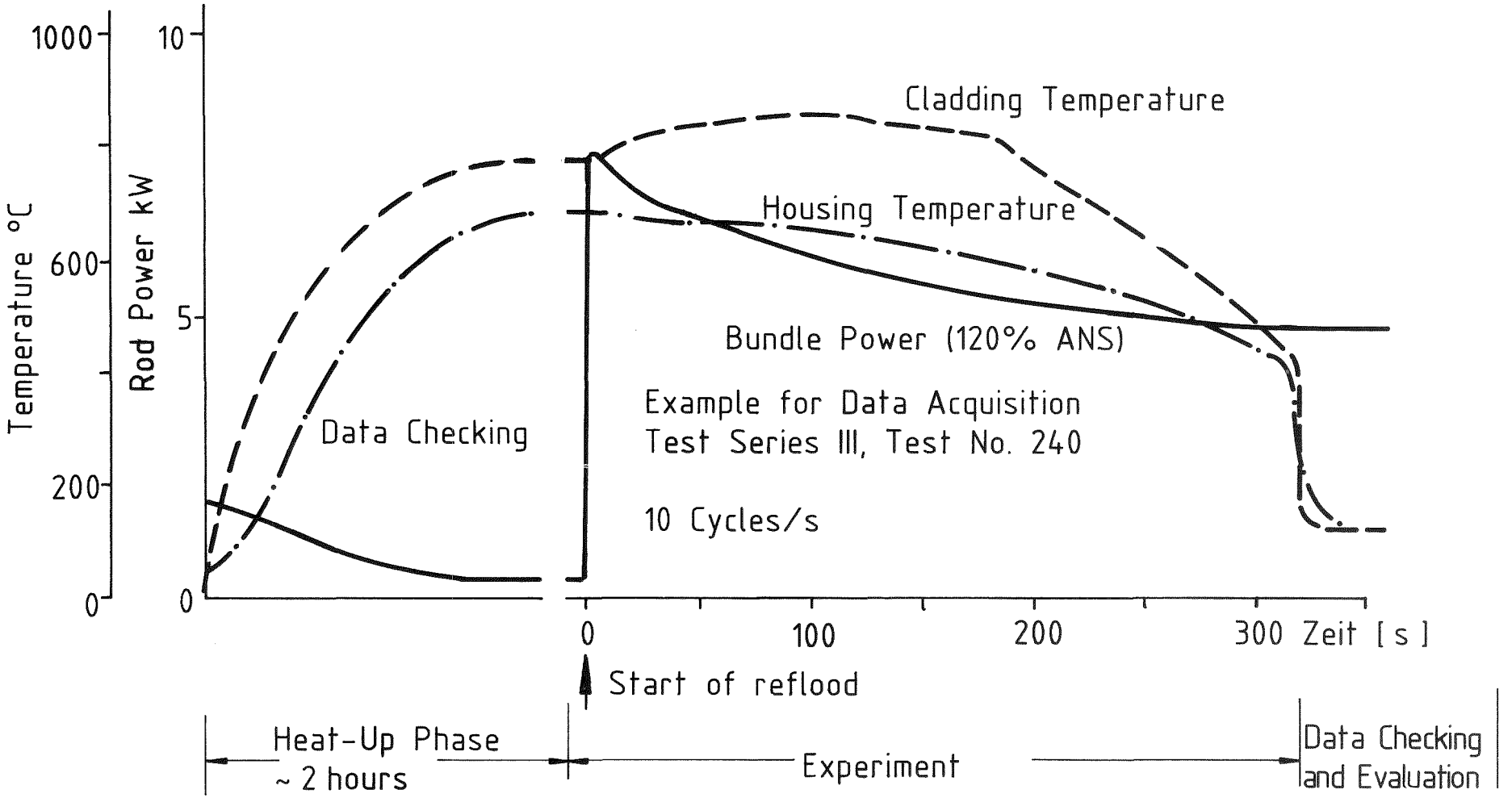

Fig. 35 5x5 rod bundle: Operational procedure of FEBA experiments

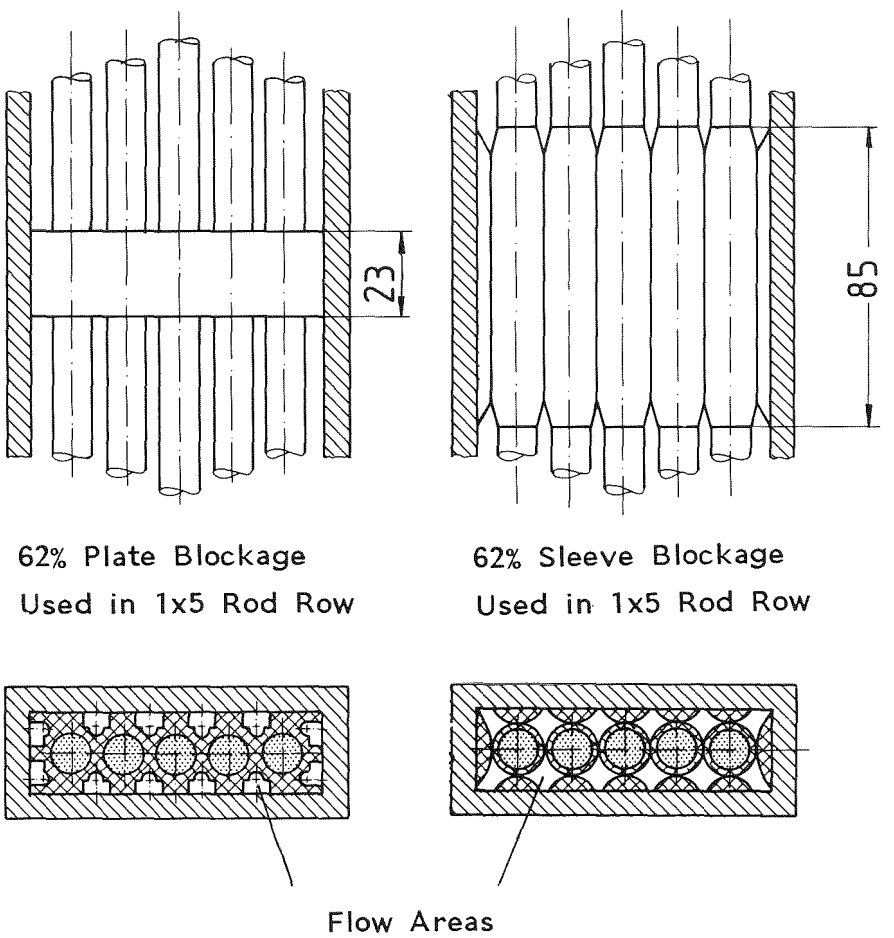

Fig. 36 5 rod row: Plate and sleeve blockage

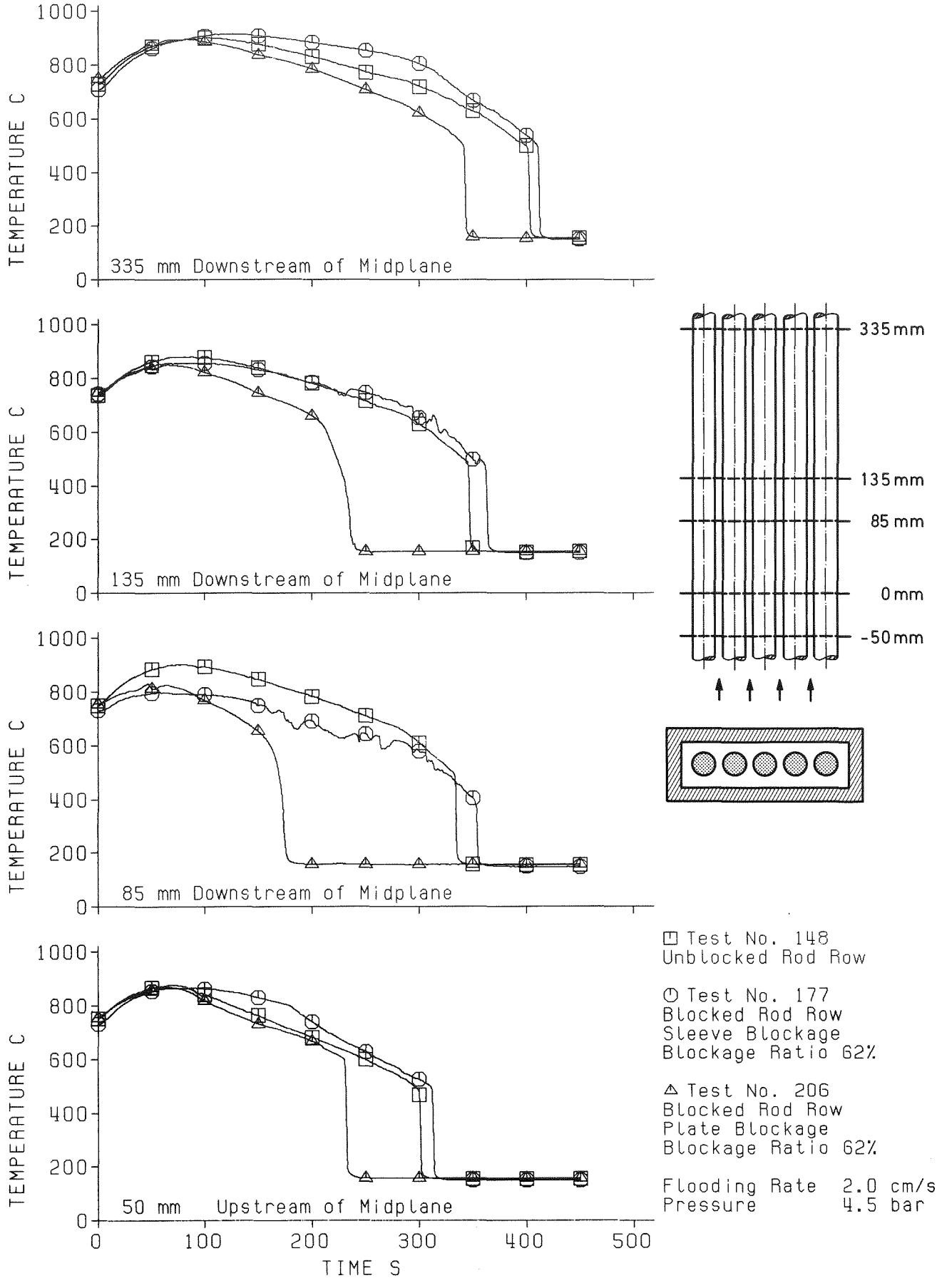

Fig.37 5 rod row: Influence of blockage shape on cladding temperatures

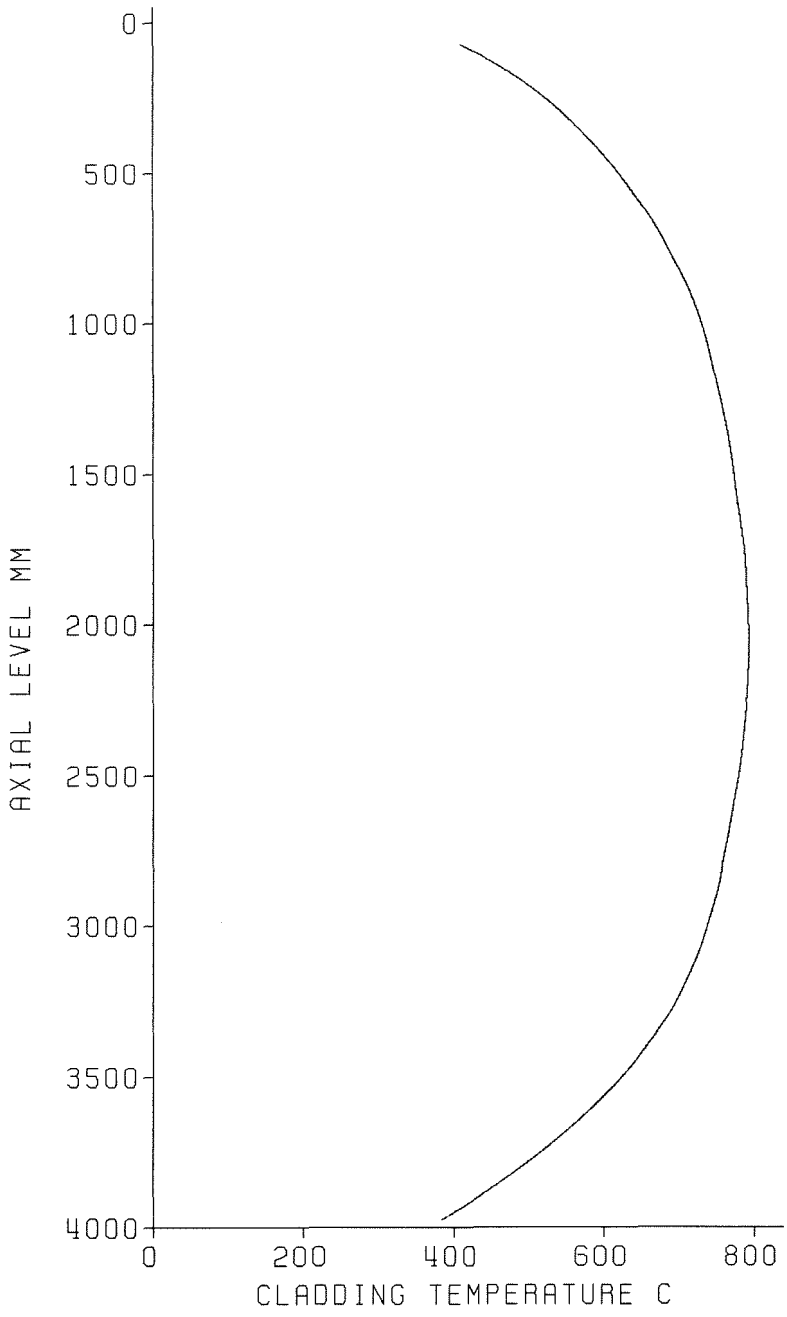

Test No. 216
7 Grid Spacers
Unblocked Bundle

Flooding Rate 3.8 cm/s
System Pressure 4.0 bar

Fig 38 5x5 rod bundle: Test series I, initial axial clad temperature profile

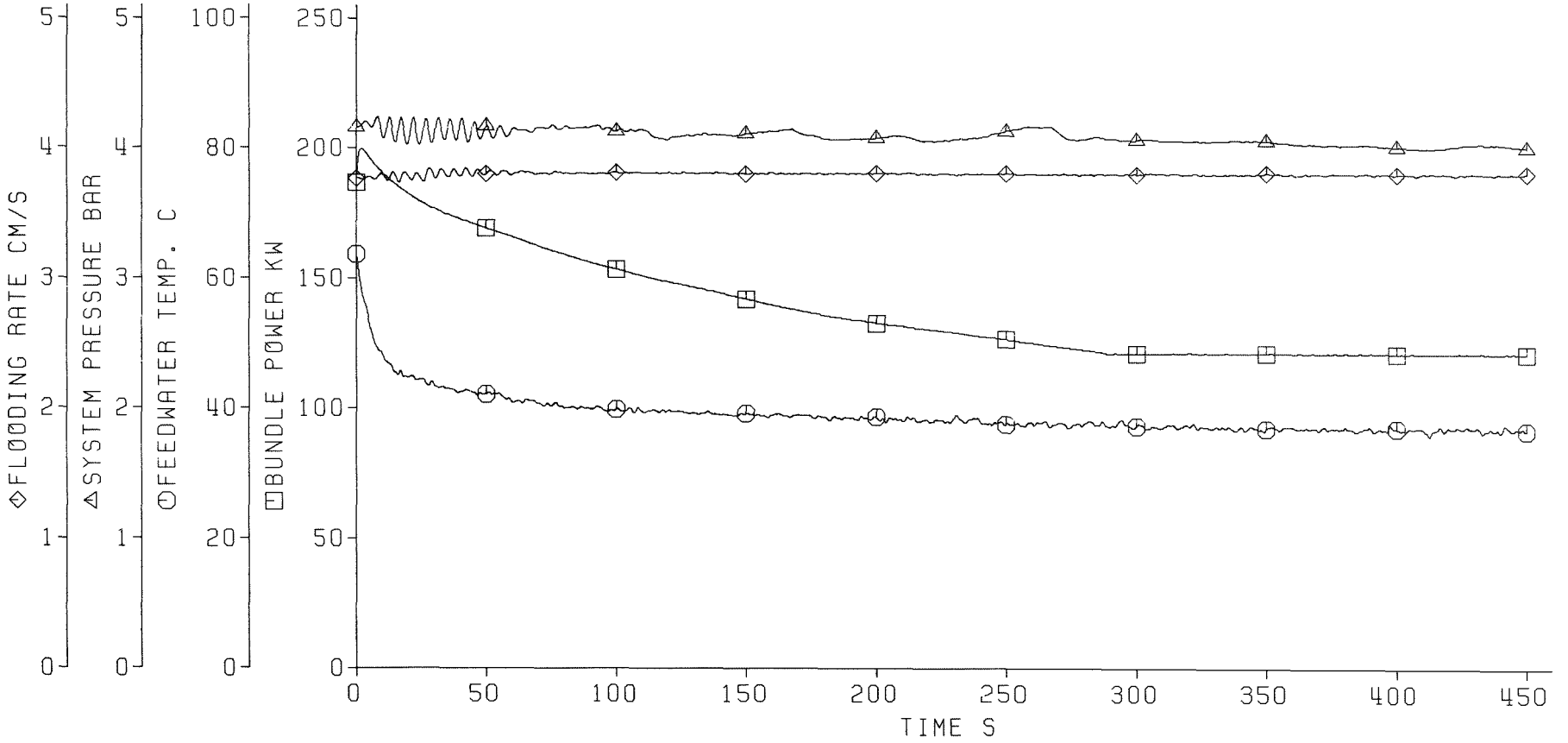

Fig.39 5x5 rod bundle: Test series I, flooding parameters

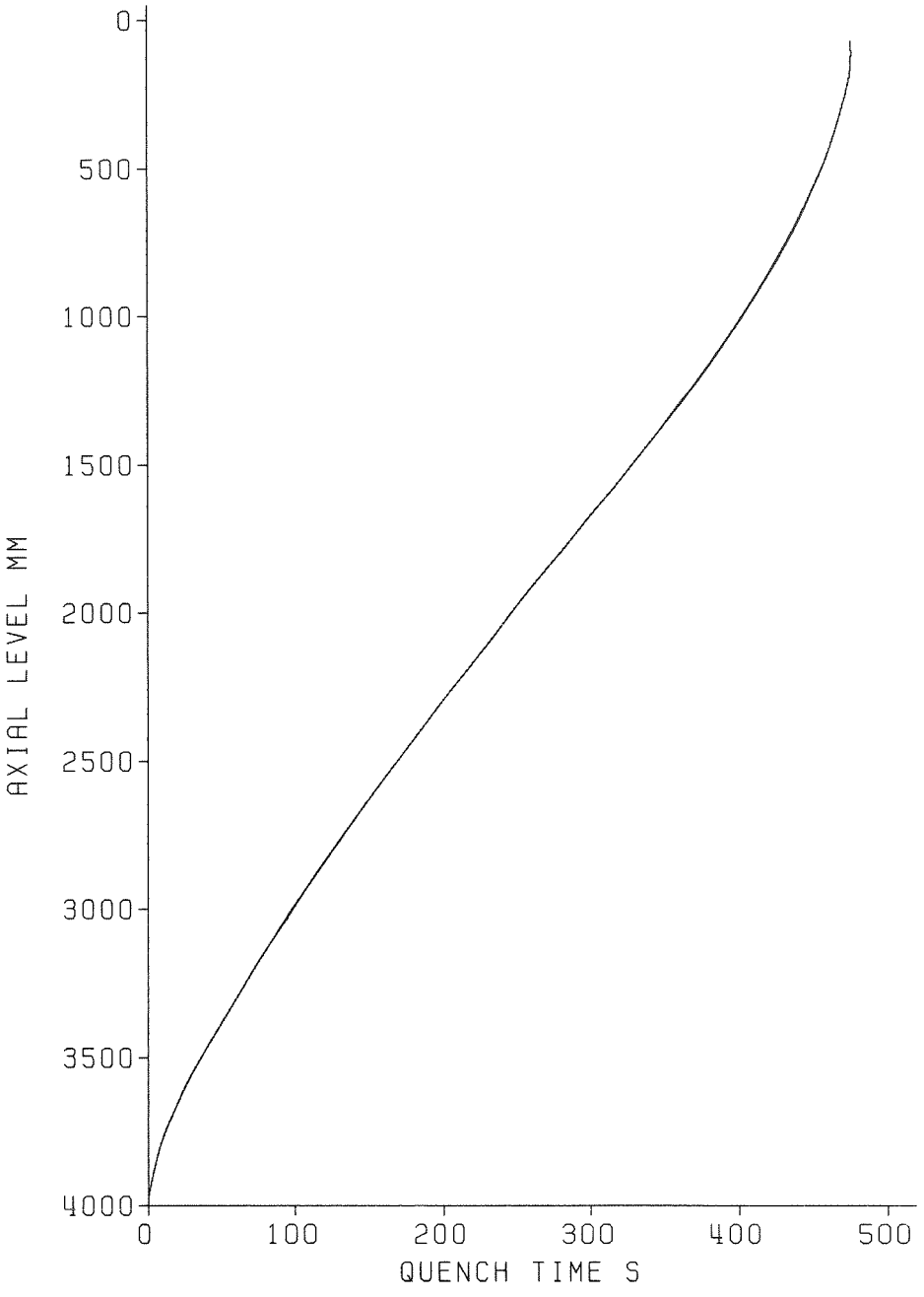

Test No. 216
7 Grid Spacers
Unblocked Bundle

Flooding Rate 3.8 cm/s
System Pressure 4.0 bar

Fig. 40 5x5 rod bundle: Test series I, quench time

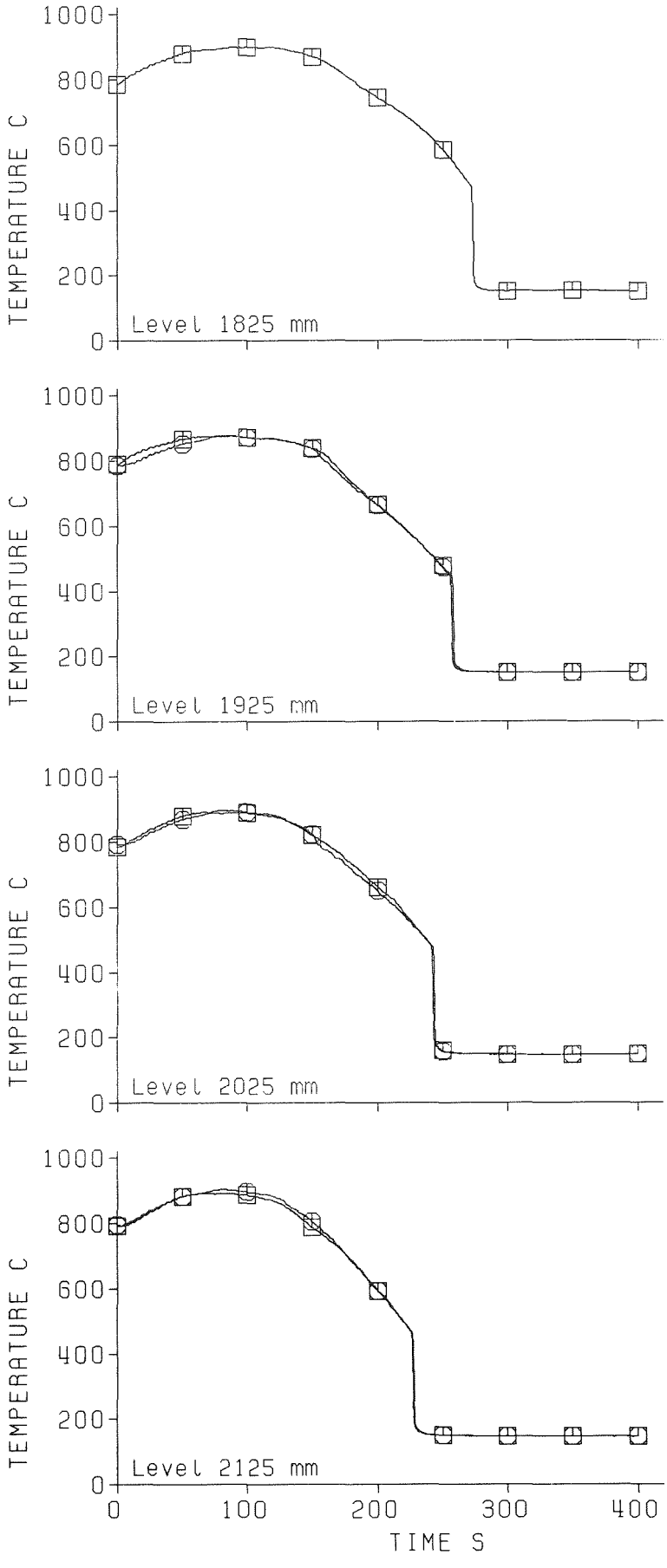

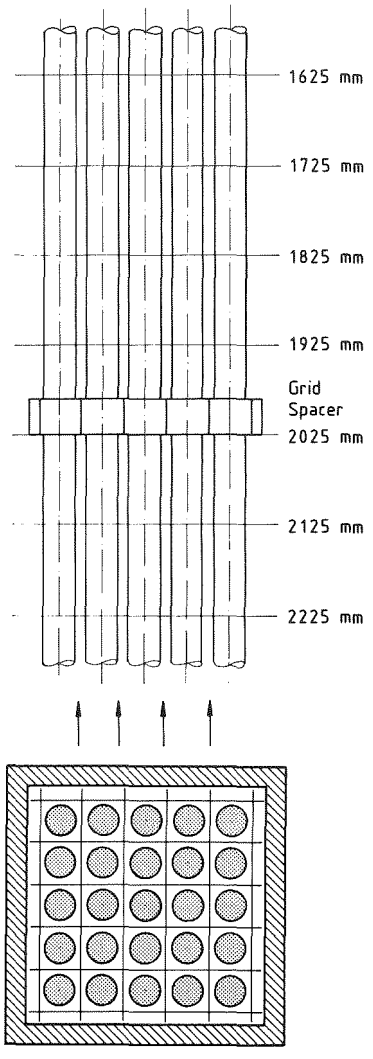

Test No. 216
7 Grid Spacers
Unblocked Bundle

Flooding Rate 3.8 cm/s
Pressure 4.1 bar

□ "Bypass Region"
◷ "Blocked Region"

Fig. 41 5x5 rod bundle: Test series I, cladding temperatures

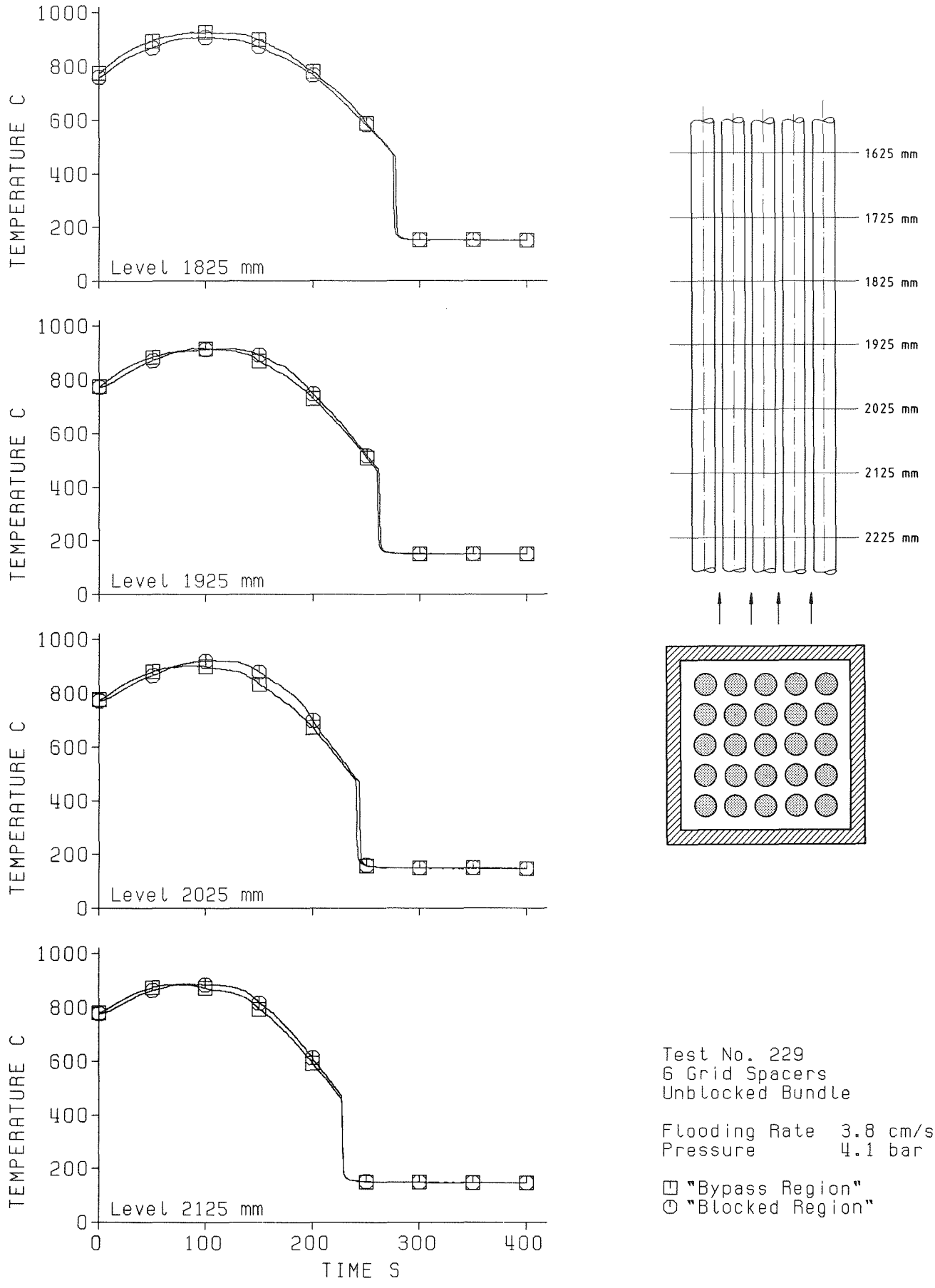

Fig. 42 5x5 rod bundle: Test series II, cladding temperatures

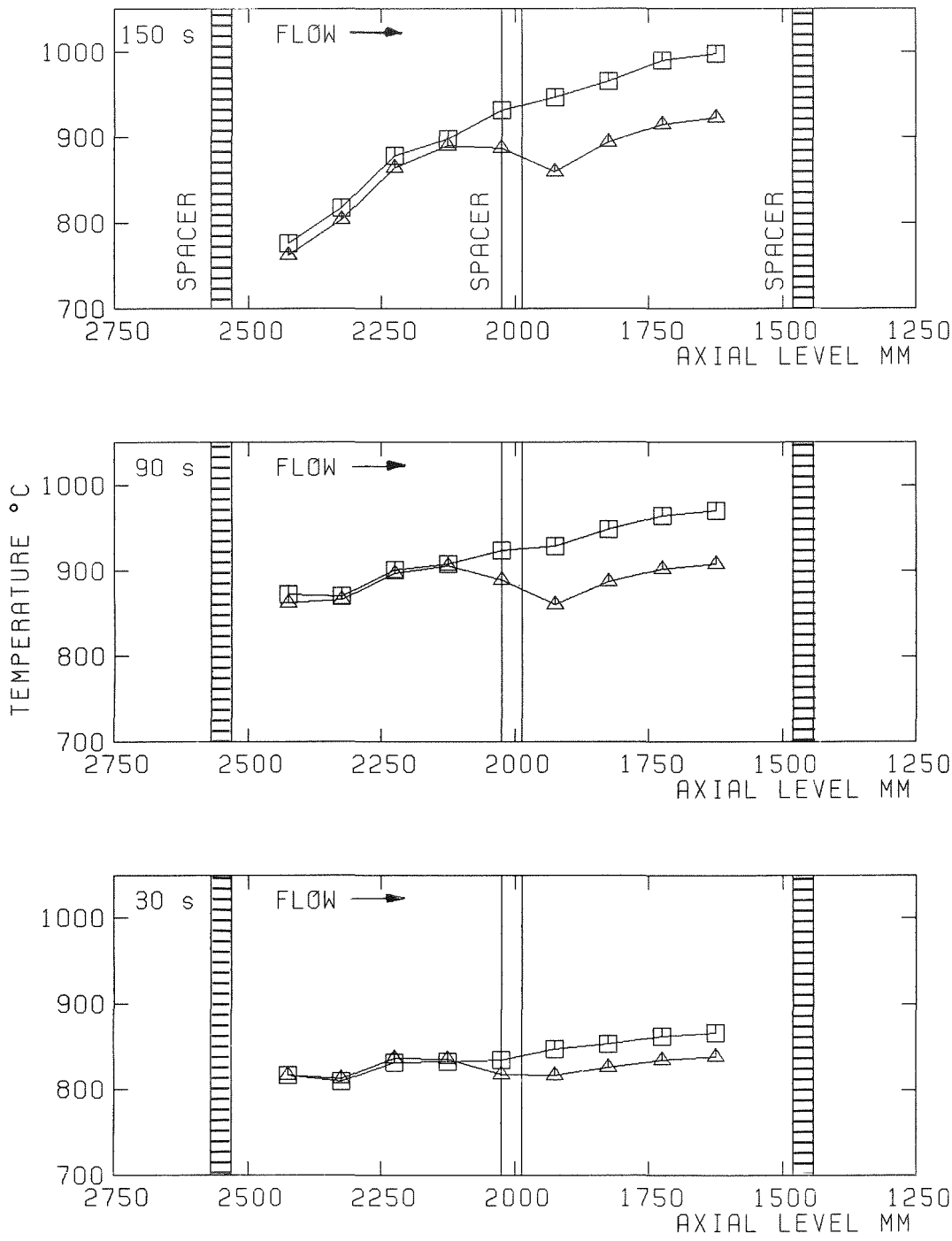

Flooding Rate 3.8 cm/s
System Pressure 2.1 bar

△ Test Series I
Test No. 223
(7 Grid Spacers)

□ Test Series II
Test No. 234
(6 Grid Spacers, without Spacer at Bundle Midplane)

Fig. 43 5x5 rod bundle: Influence of a grid spacer on the axial temperature profile

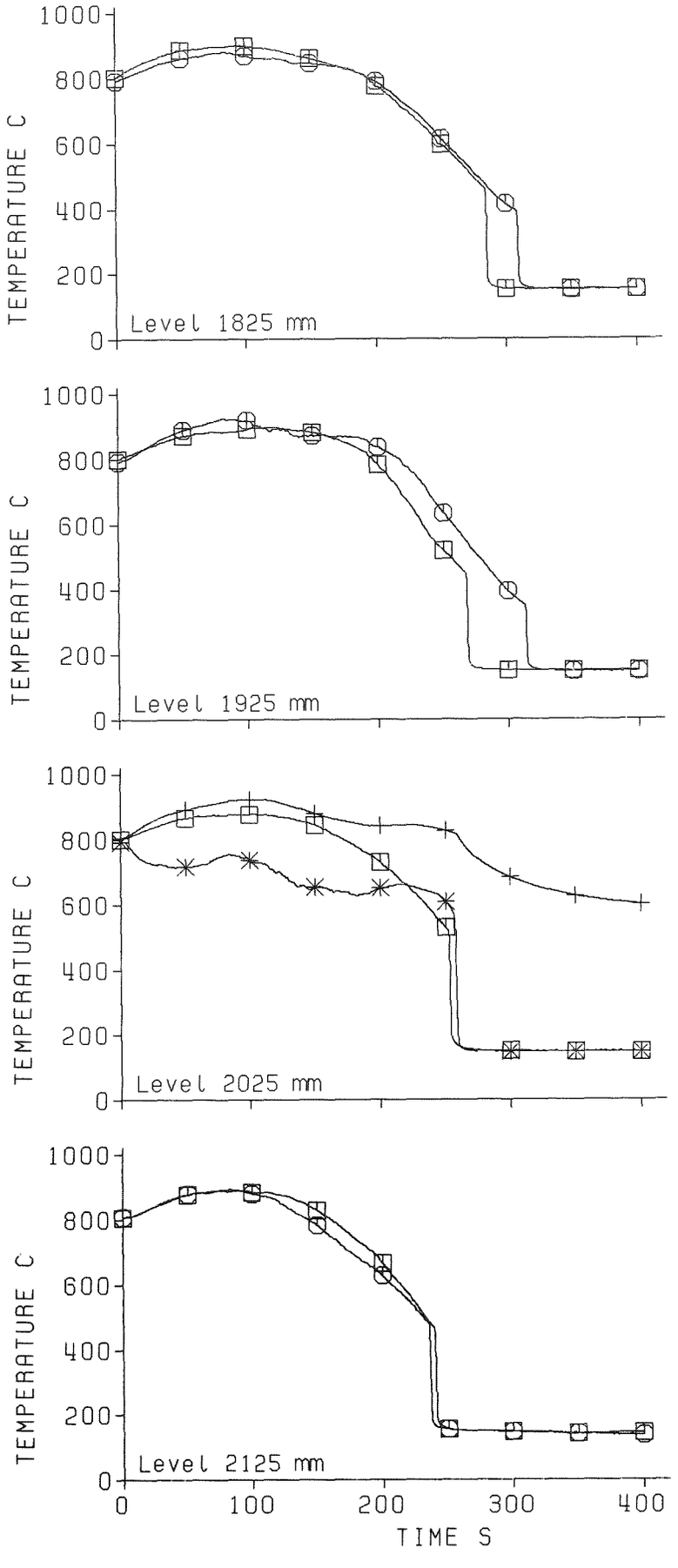

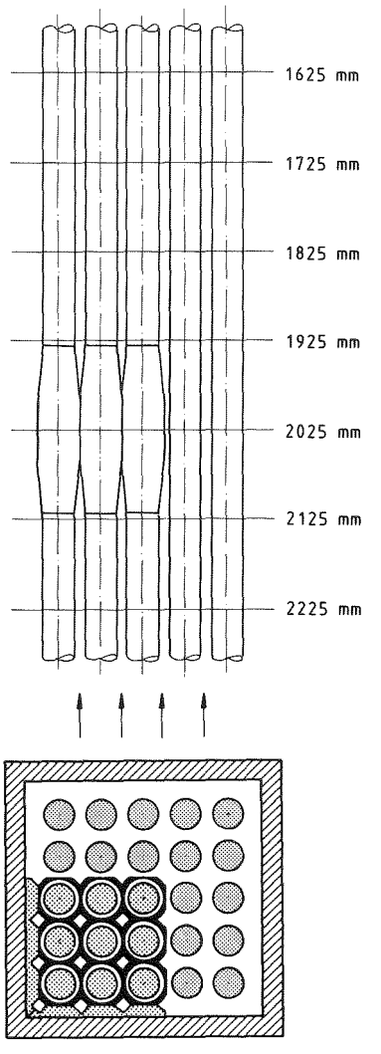

Test No. 239
6 Grid Spacers
Blocked Bundle (3x3 Rods)
Blockage at Level 2025 mm
Blockage Ratio 90%

Flooding Rate 3.8 cm/s
Pressure 4.1 bar

□ Bypass Region
⊙ Blocked Region
✳ Sleeve
+ Underneath Sleeve

Fig. 44 5x5 rod bundle: Test series III, cladding temperatures

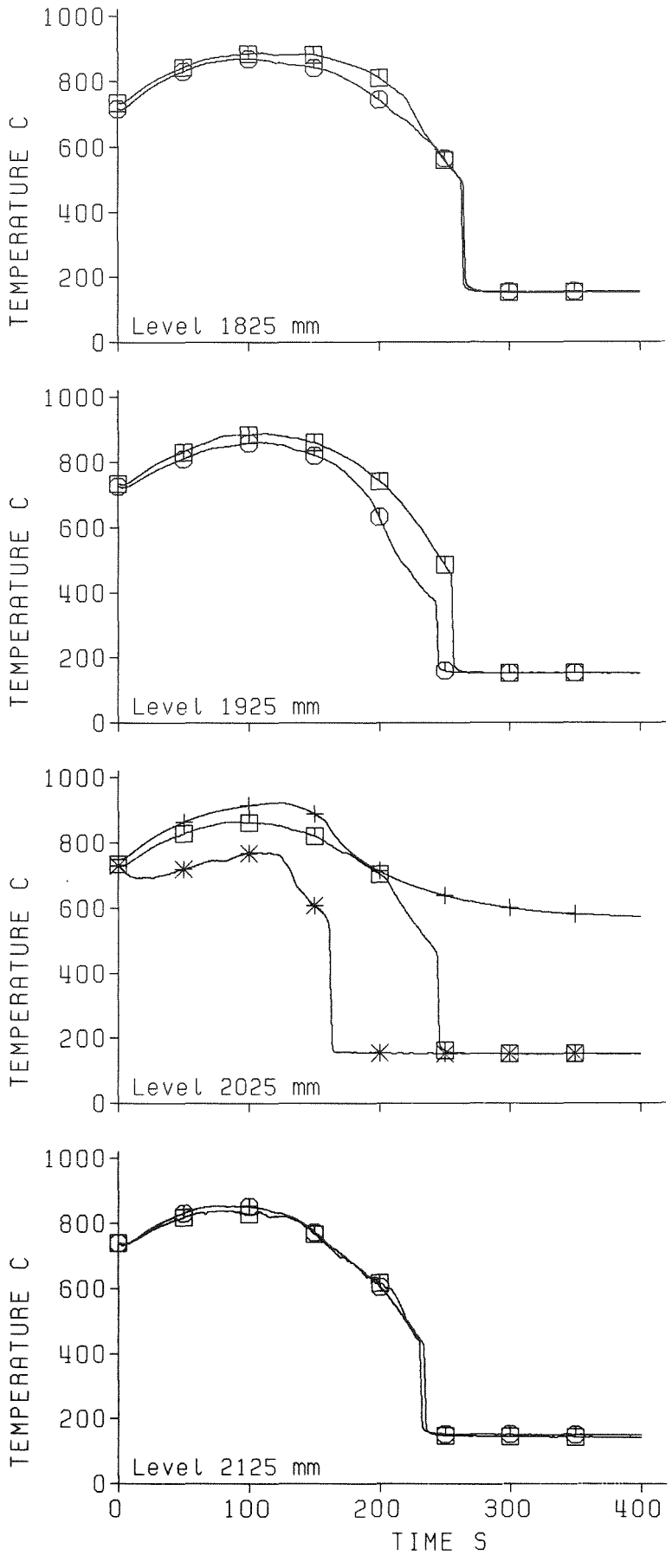

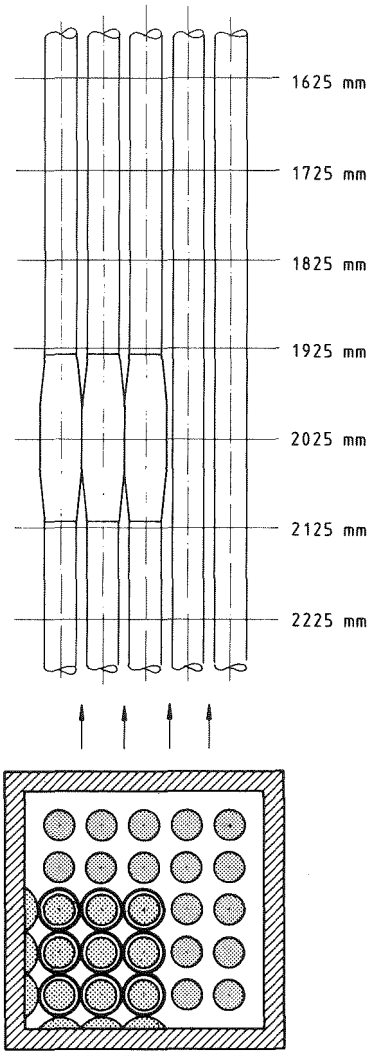

Test No. 263
6 Grid Spacers
Blocked Bundle (3x3 Rods)
Blockage at Level 2025 mm
Blockage Ratio 62%

Flooding Rate 3.8 cm/s
Pressure 4.0 bar

□ Bypass Region
○ Blocked Region
✳ Sleeve
\+ Underneath Sleeve

Fig. 45 5x5 rod bundle: Test series IV, cladding temperatures

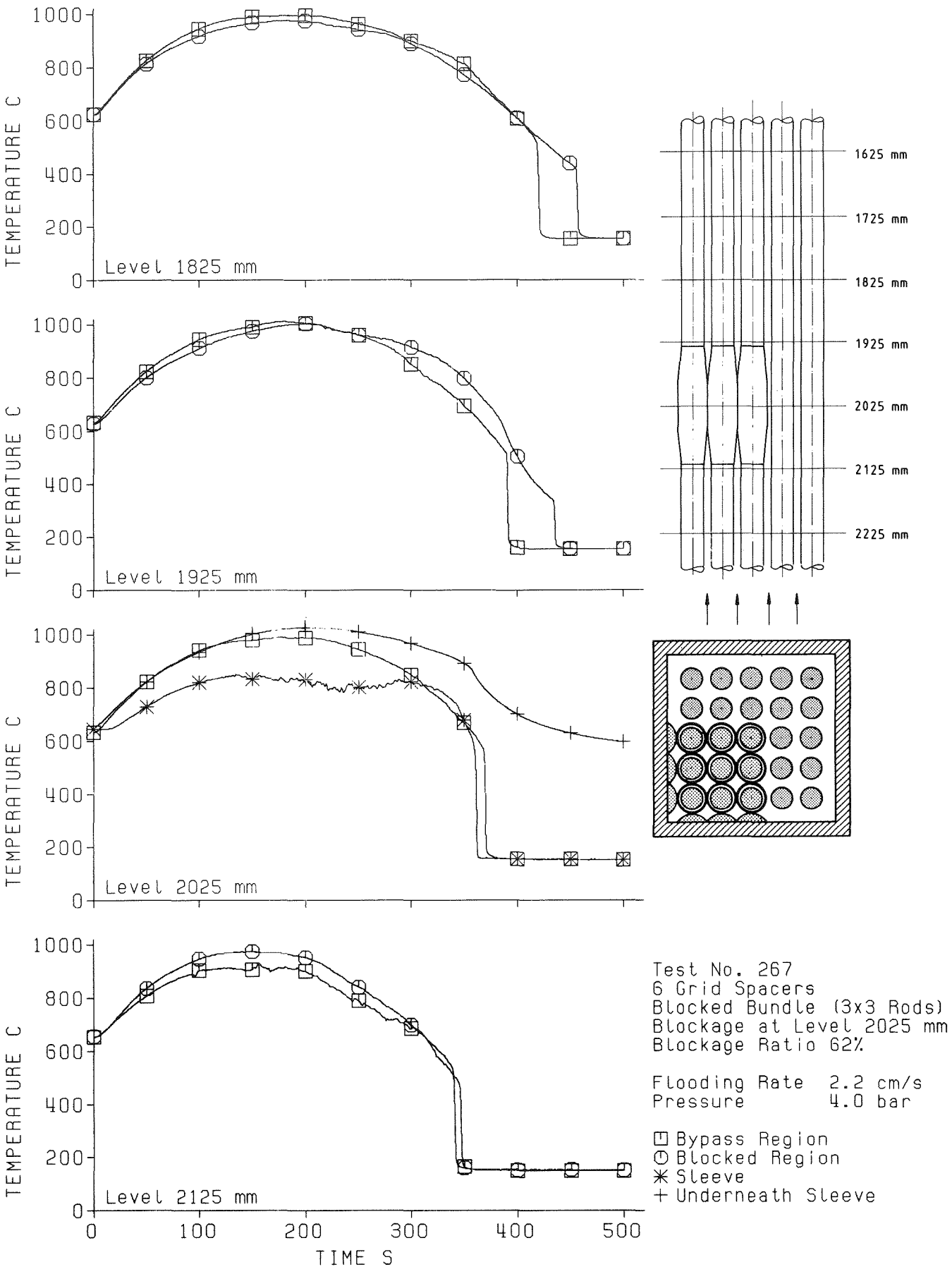

Fig. 46 5x5 rod bundle: Test series IV, cladding temperatures

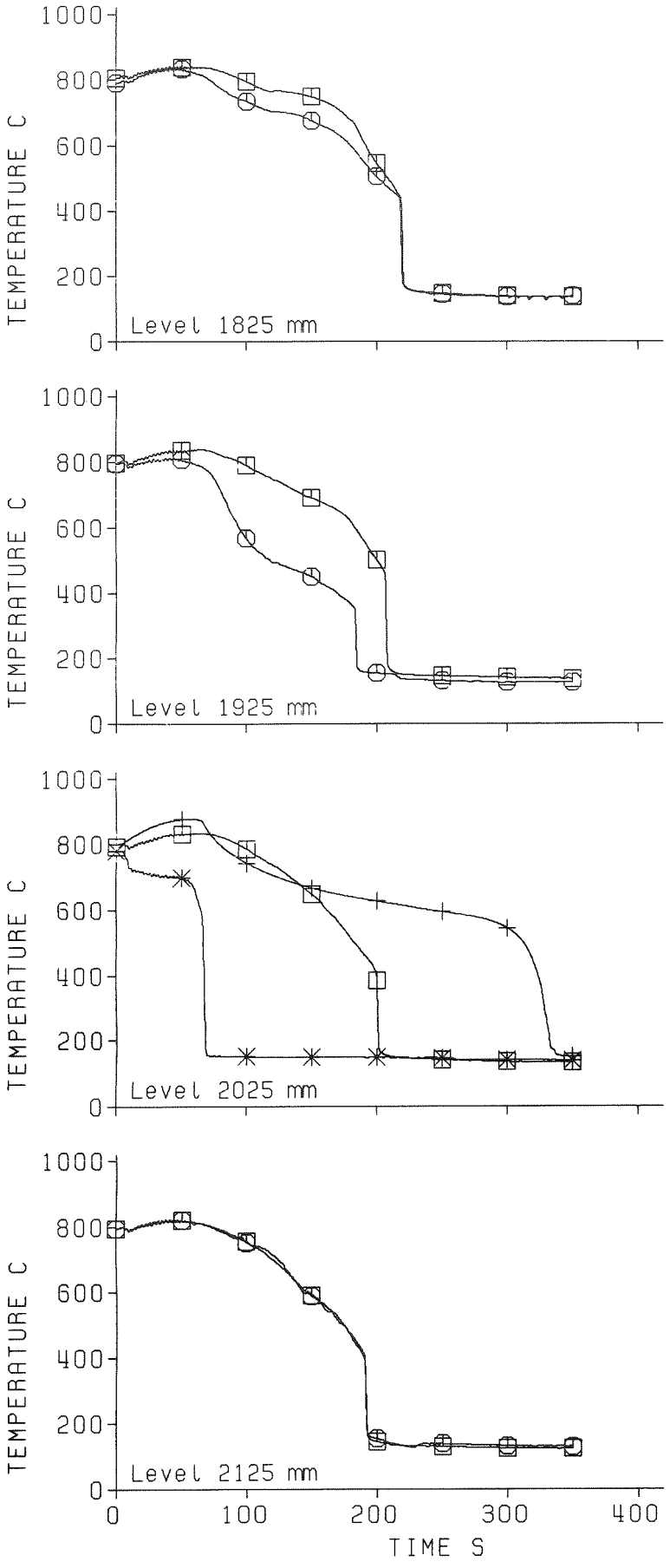

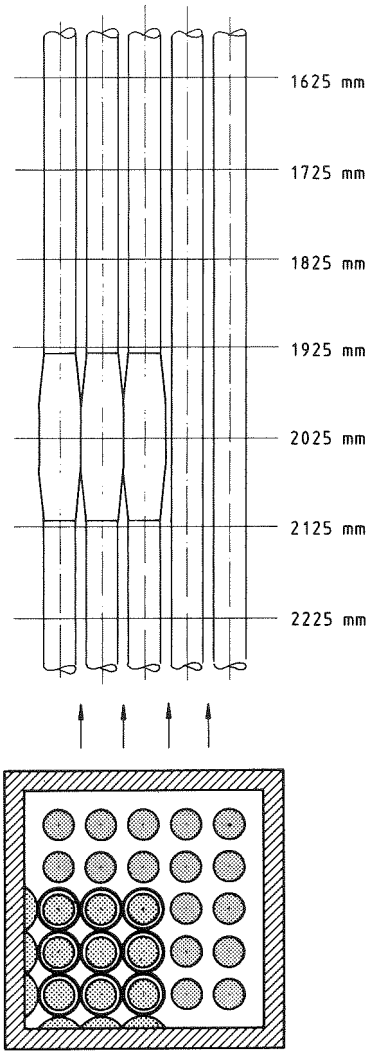

Test No. 264
6 Grid Spacers
Blocked Bundle (3x3 Rods)
Blockage at Level 2025 mm
Blockage Ratio 62%

Flooding Rate 5.8 cm/s
Pressure 4.0 bar

□ Bypass Region
◯ Blocked Region
✳ Sleeve
+ Underneath Sleeve

Fig. 47 5x5 rod bundle: Test series IV, cladding temperatures

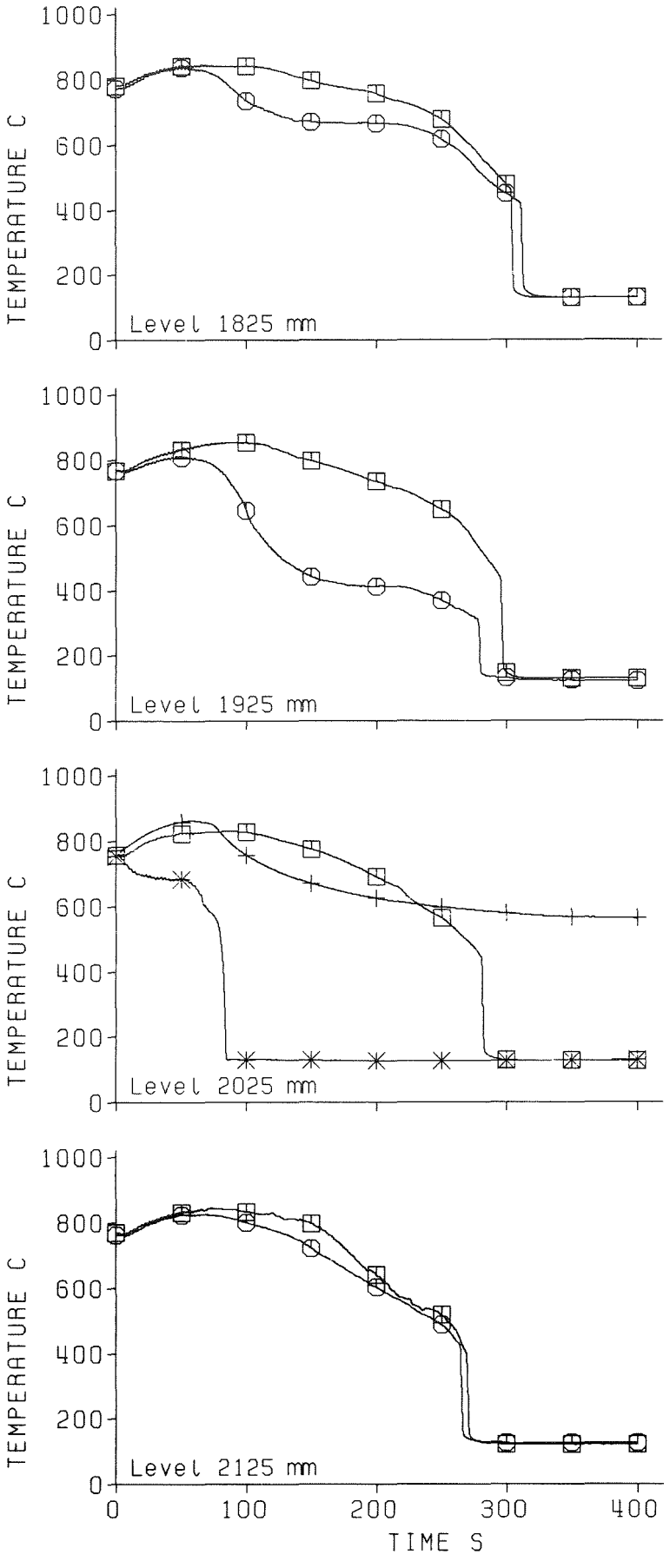

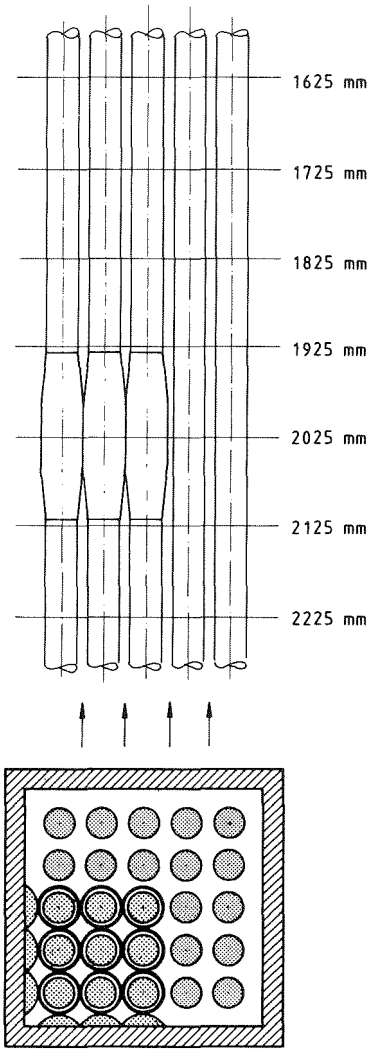

Test No. 261
6 Grid Spacers
Blocked Bundle (3x3 Rods)
Blockage at Level 2025 mm
Blockage Ratio 62%

Flooding Rate 5.8 cm/s
Pressure 2.0 bar

⊡ Bypass Region
⊙ Blocked Region
✳ Sleeve
\+ Underneath Sleeve

Fig. 48 5x5 rod bundle: Test series IV, cladding temperatures

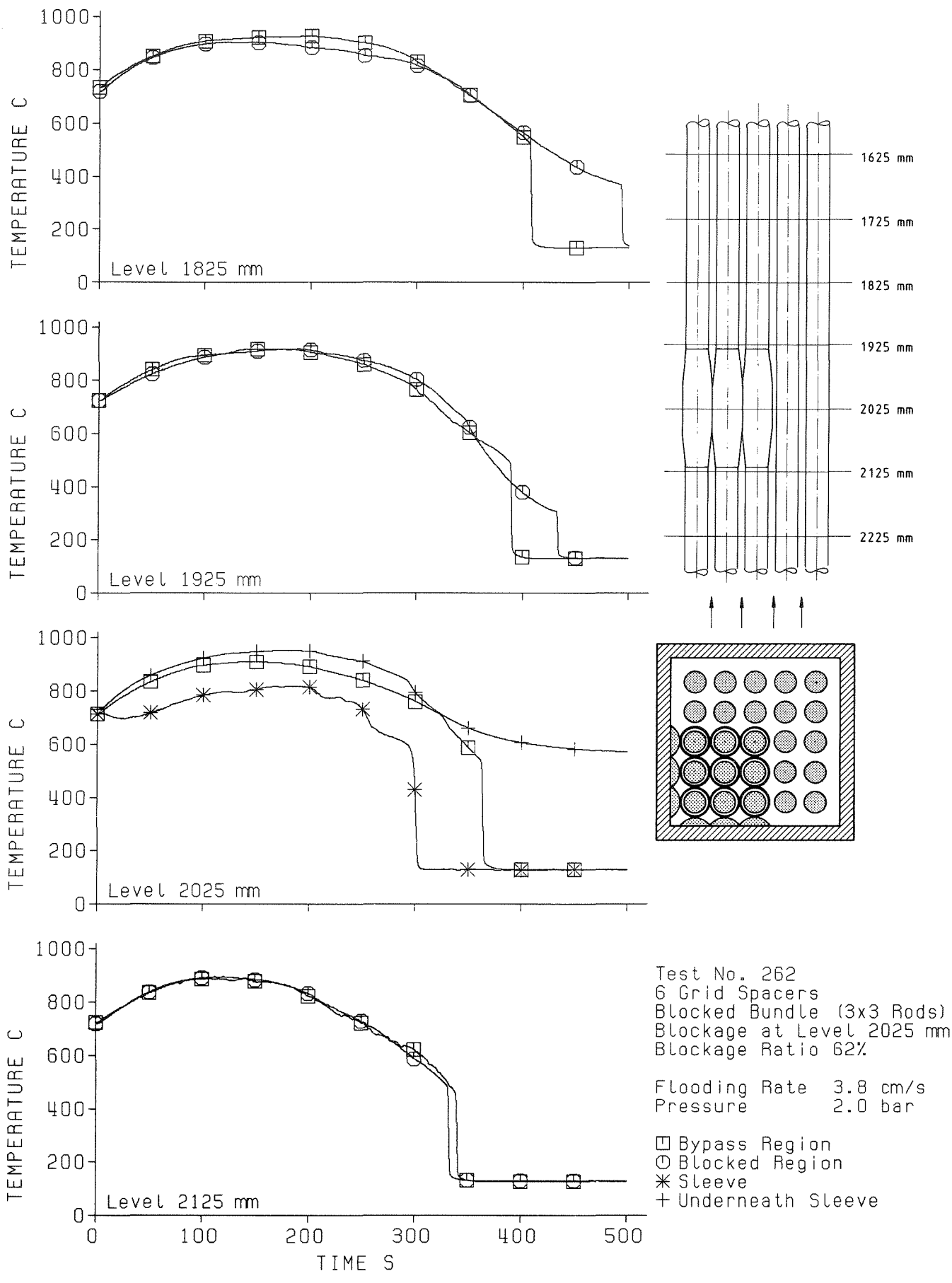

Fig. 49 5x5 rod bundle: Test series IV, cladding temperatures

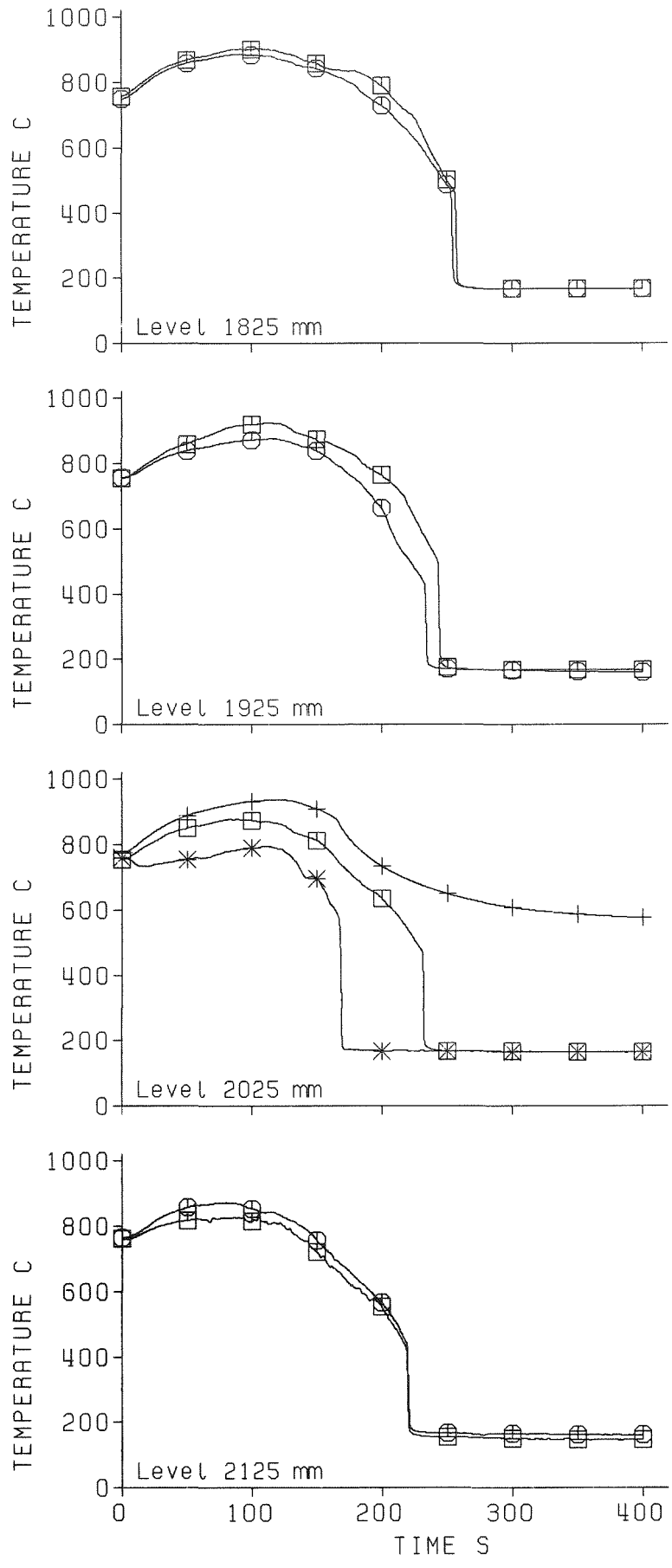

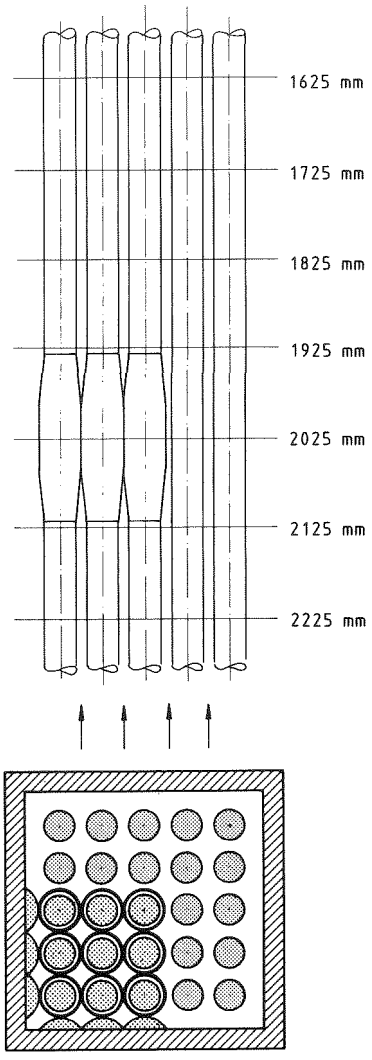

Test No. 268
6 Grid Spacers
Blocked Bundle (3x3 Rods)
Blockage at Level 2025 mm
Blockage Ratio 62%

Flooding Rate 3.8 cm/s
Pressure 6.0 bar

□ Bypass Region
⊙ Blocked Region
✳ Sleeve
+ Underneath Sleeve

Fig. 50 5x5 rod bundle: Test series IV, cladding temperatures

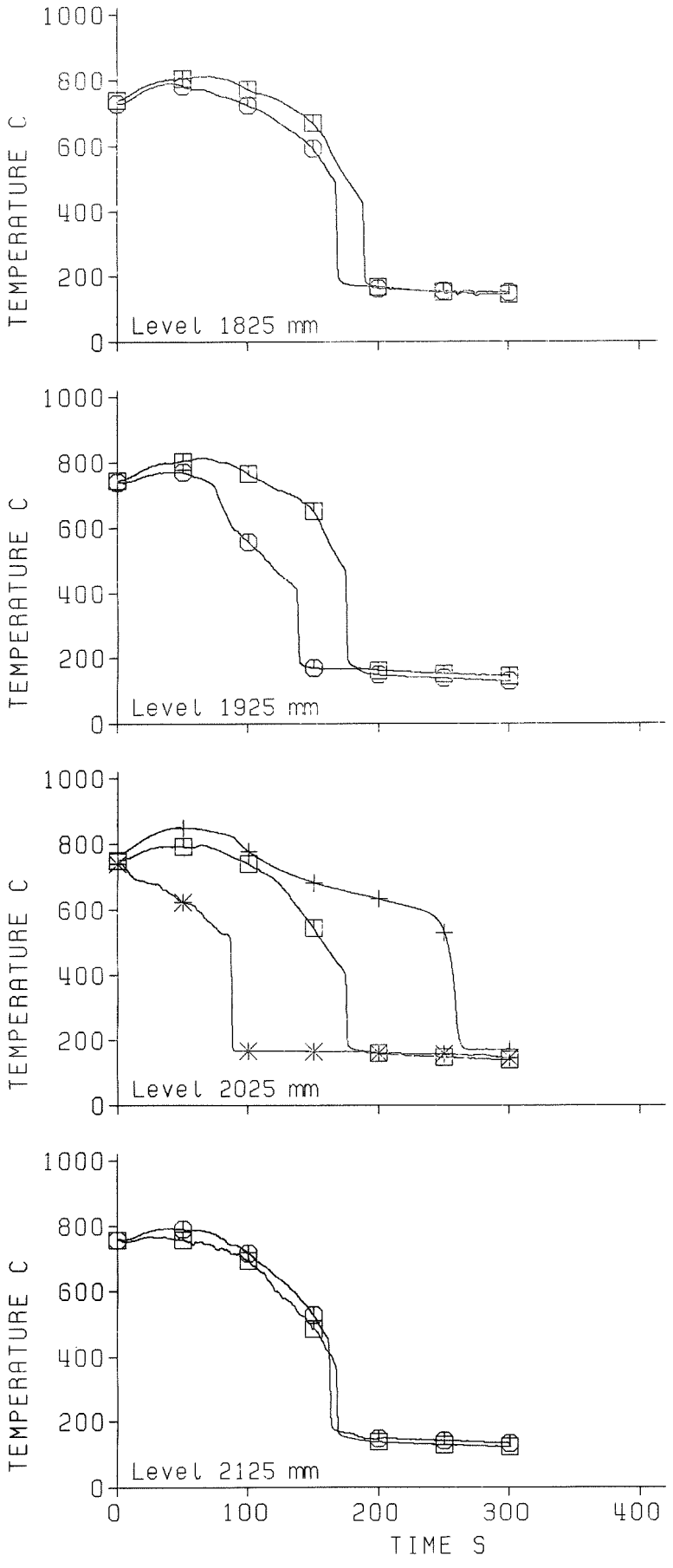

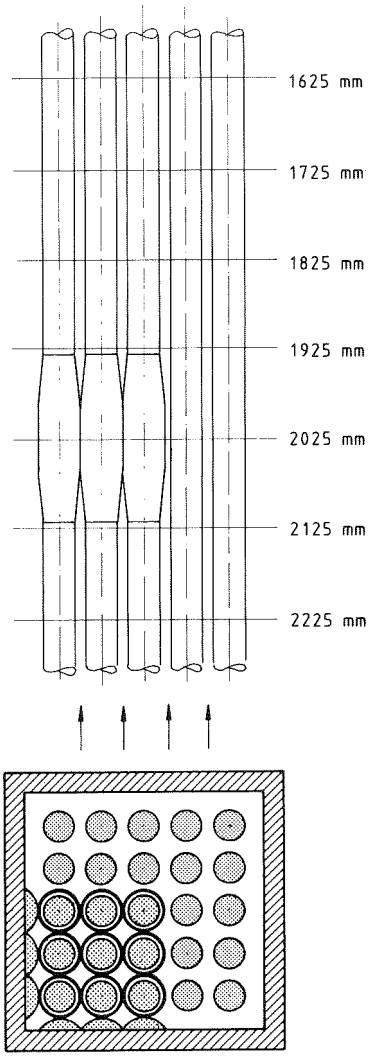

Test No. 269
6 Grid Spacers
Blocked Bundle (3x3 Rods)
Blockage at Level 2025 mm
Blockage Ratio 62%

Flooding Rate 5.8 cm/s
Pressure 6.0 bar

⊡ Bypass Region
⊙ Blocked Region
✳ Sleeve
+ Underneath Sleeve

Fig. 51 5x5 rod bundle: Test series IV, cladding temperatures

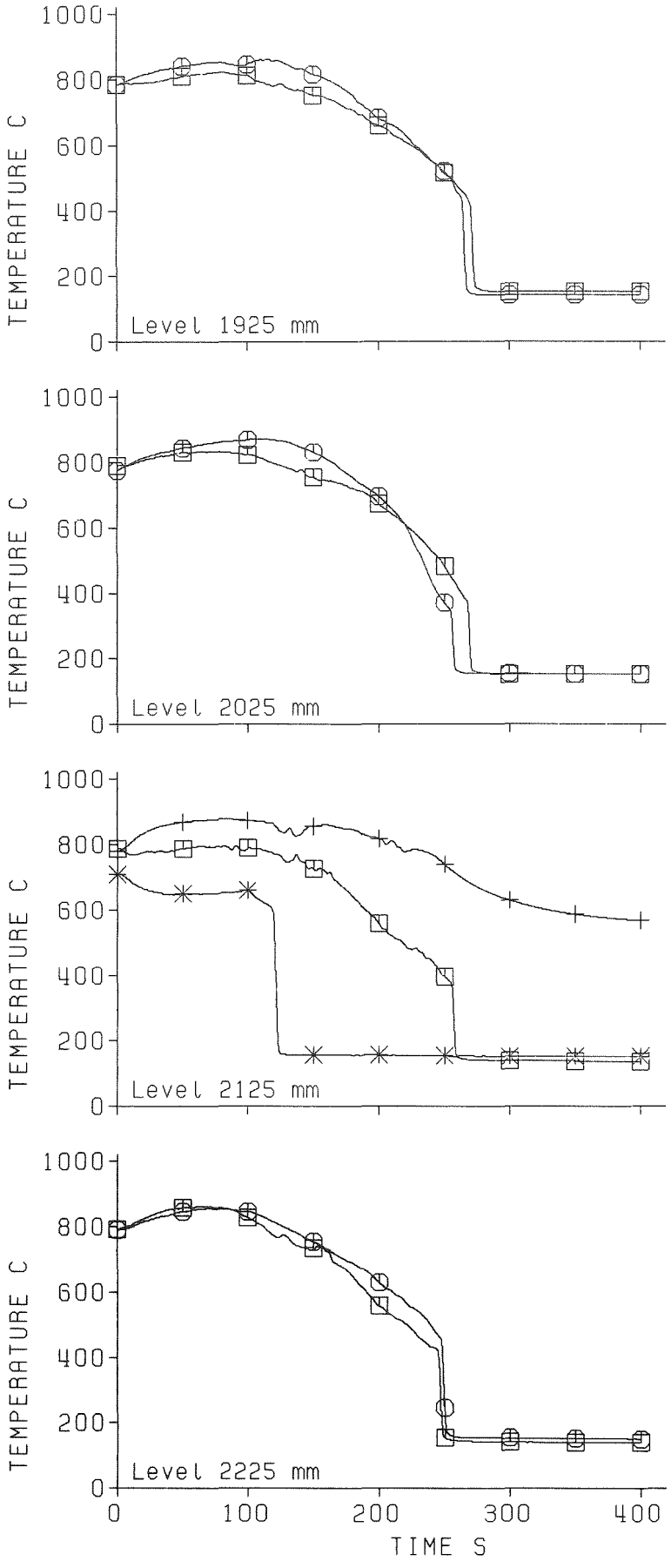

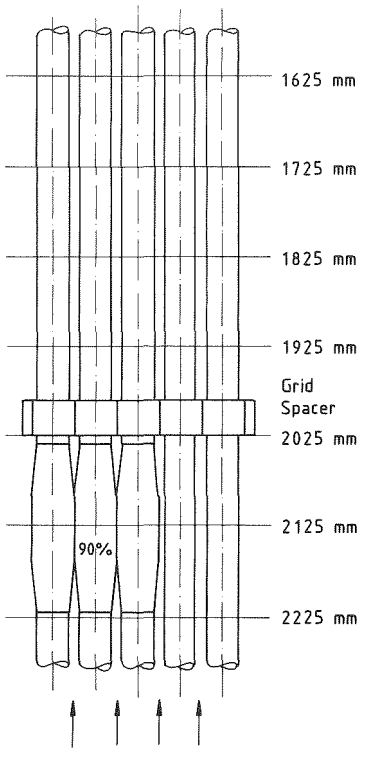

Test No. 282
7 Grid Spacers
Blocked Bundle (3x3 Rods)
Blockage at Level 2125 mm
Blockage Ratio 90%

Flooding Rate 3.8 cm/s
Pressure 4.0 bar

⊡ Bypass Region
⏲ Blocked Region
✳ Sleeve
+ Underneath Sleeve

Fig. 52 5x5 rod bundle: Test series V, cladding temperatures

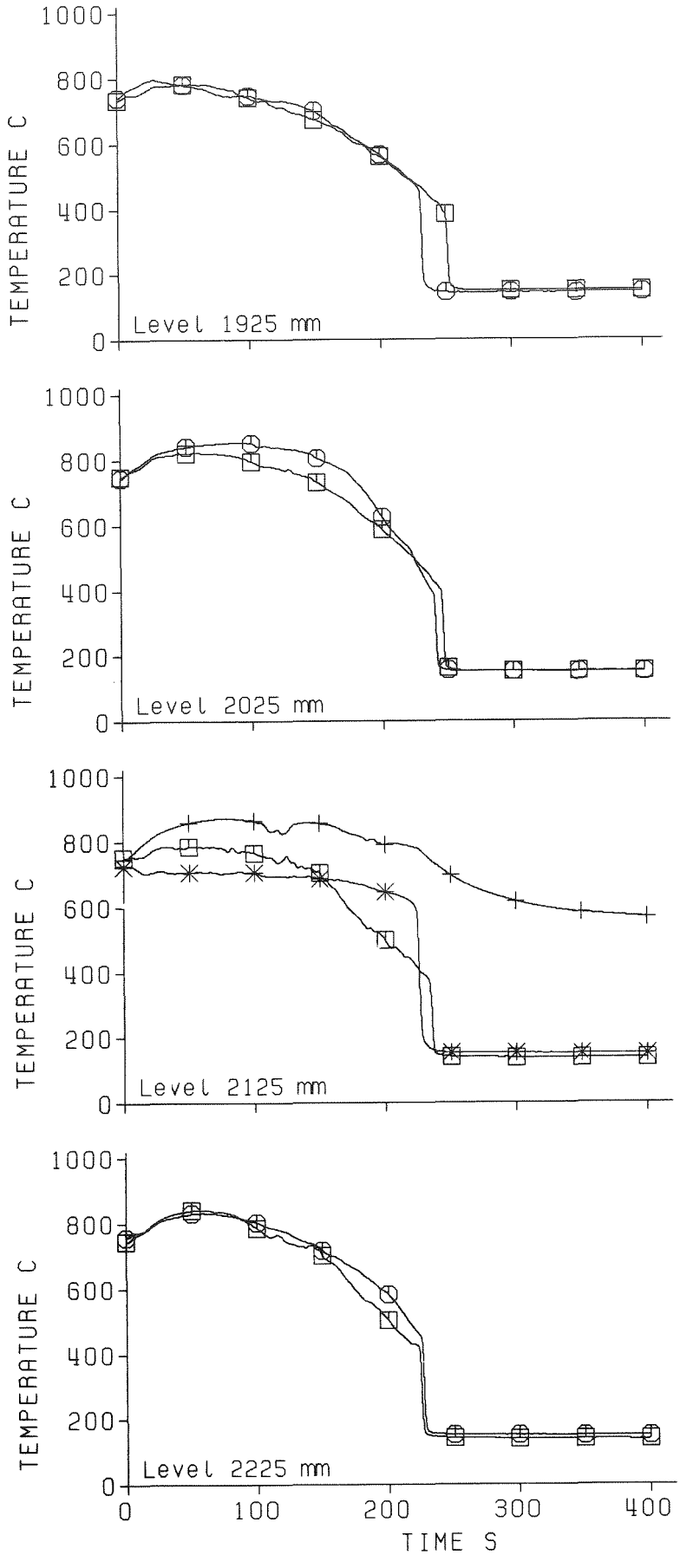

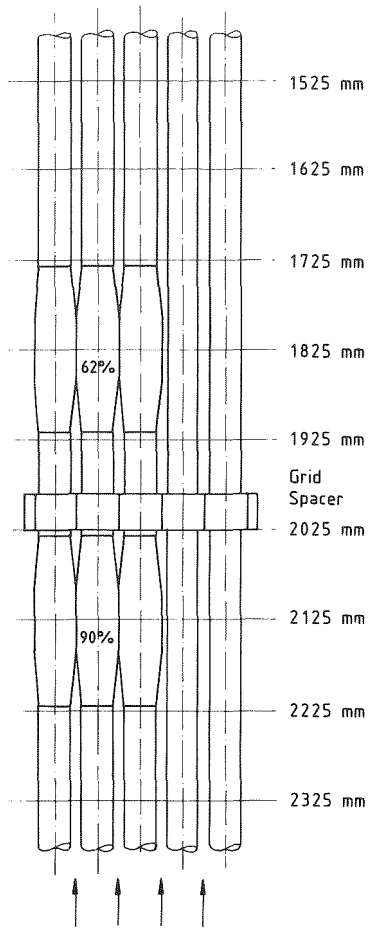

Test No. 276
7 Grid Spacers
Blocked Bundle (3x3 Rods)
Blockage at Level 2125 mm
Blockage Ratio 90%
Blockage at Level 1825 mm
Blockage Ratio 62%

Flooding Rate 3.8 cm/s
Pressure 4.0 bar

□ Bypass Region
◯ Blocked Region
✳ Sleeve
+ Underneath Sleeve

Fig. 53 5x5 rod bundle: Test series VI, cladding temperatures

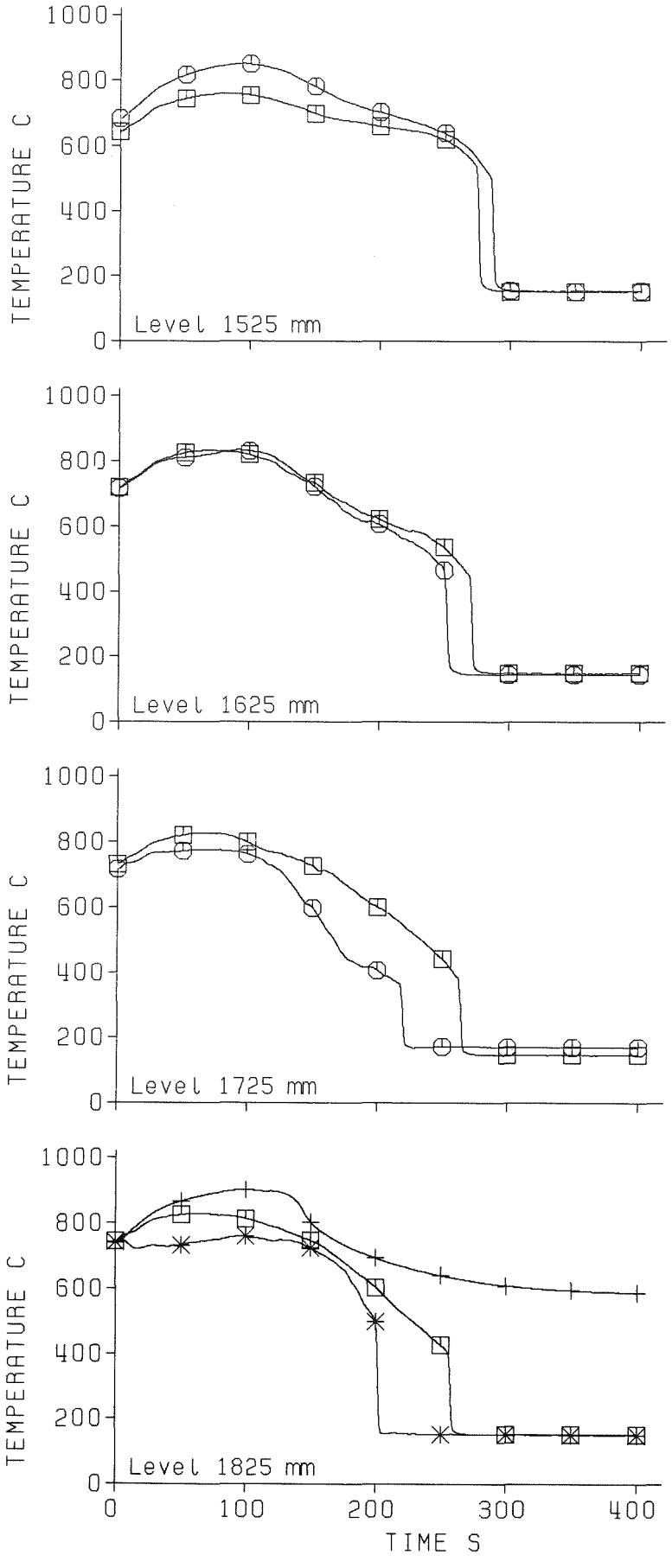

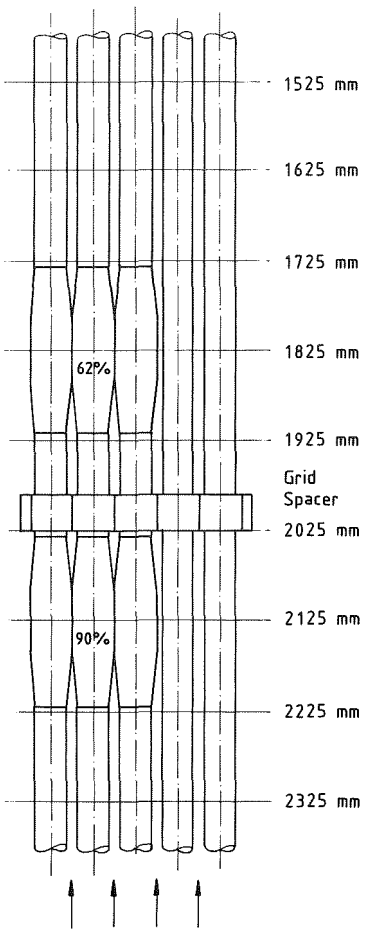

Test No. 276
7 Grid Spacers
Blocked Bundle (3x3 Rods)
Blockage at Level 2125 mm
Blockage Ratio 90%
Blockage at Level 1825 mm
Blockage Ratio 62%

Flooding Rate 3.8 cm/s
Pressure 4.0 bar

⊟ Bypass Region
⊖ Blocked Region
✳ Sleeve
+ Underneath Sleeve

Fig. 54 5x5 rod bundle: Test series VI, cladding temperatures

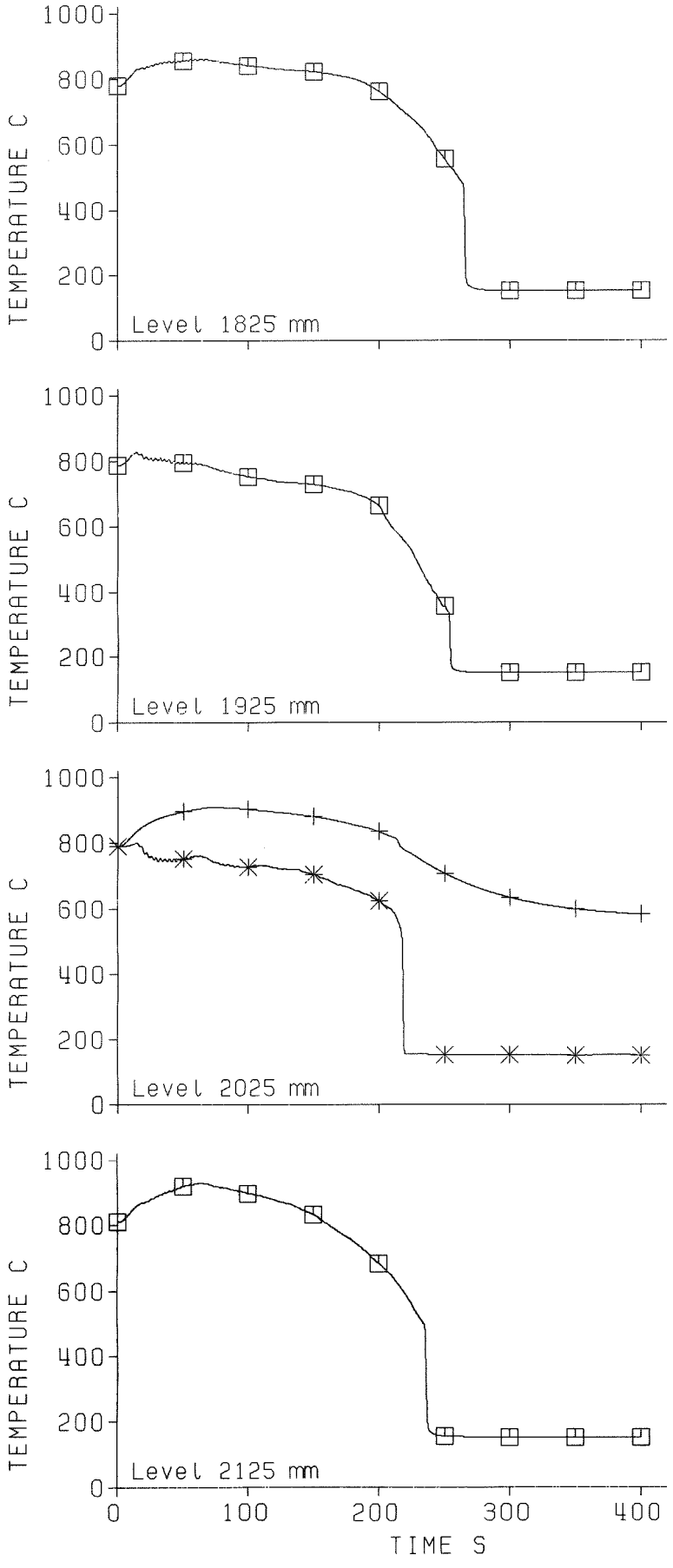

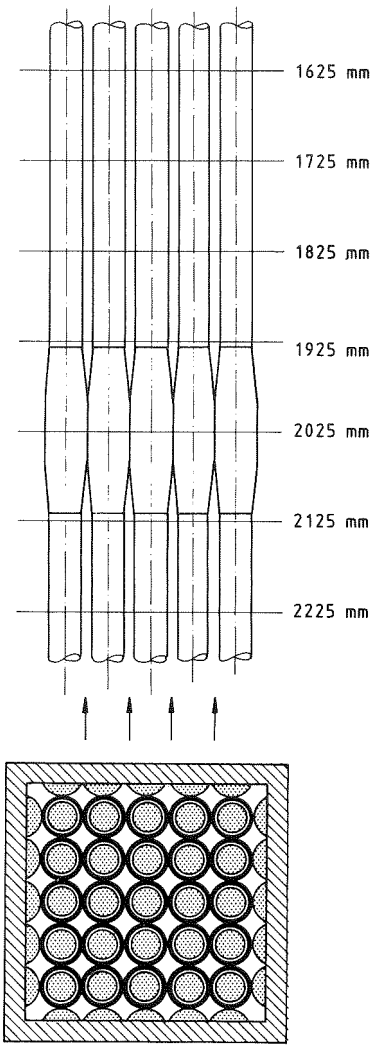

Test No. 324
6 Grid Spacers
Blocked Bundle (5x5 Rods)
Blockage at Level 2025 mm
Blockage Ratio 62%

Flooding Rate 3.8 cm/s
Pressure 4.0 bar

□ cladding
✳ Sleeve
+ Underneath Sleeve

Fig. 55 5x5 rod bundle: Test series VII, cladding temperatures

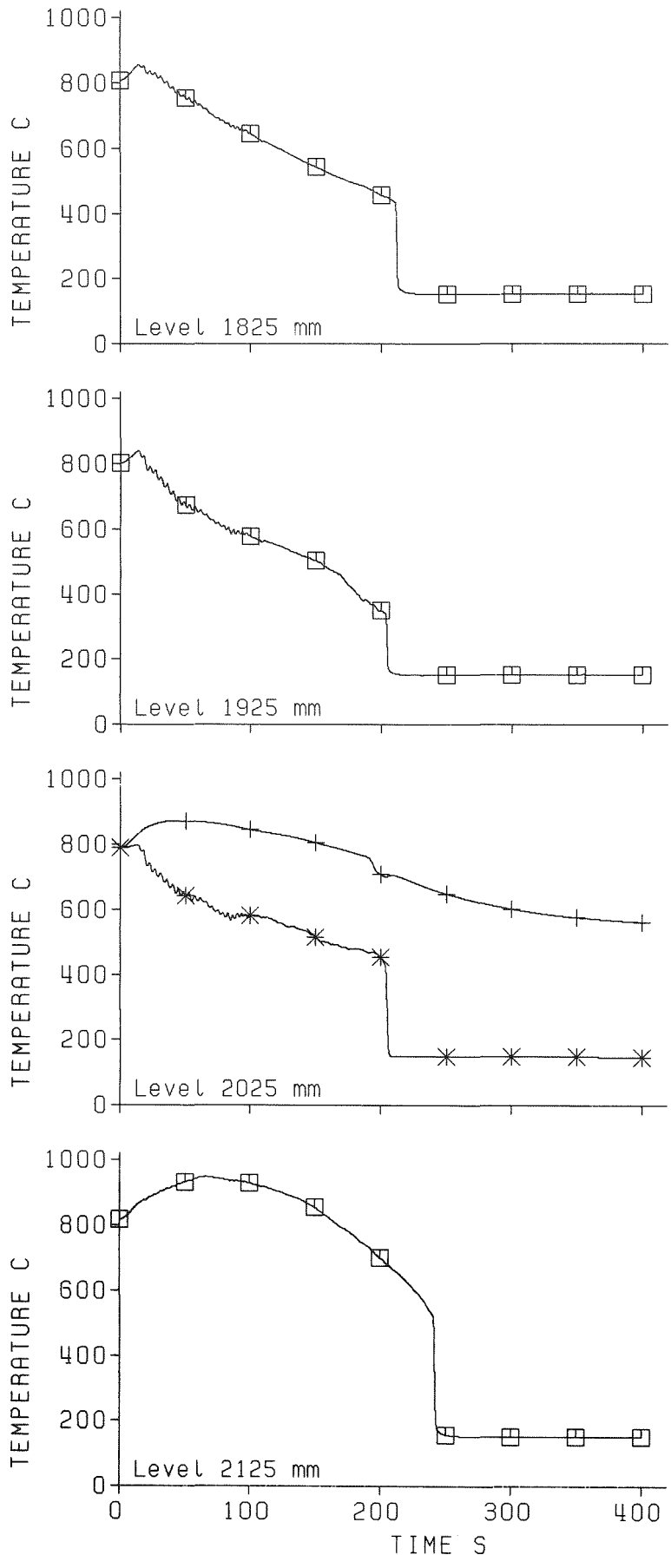

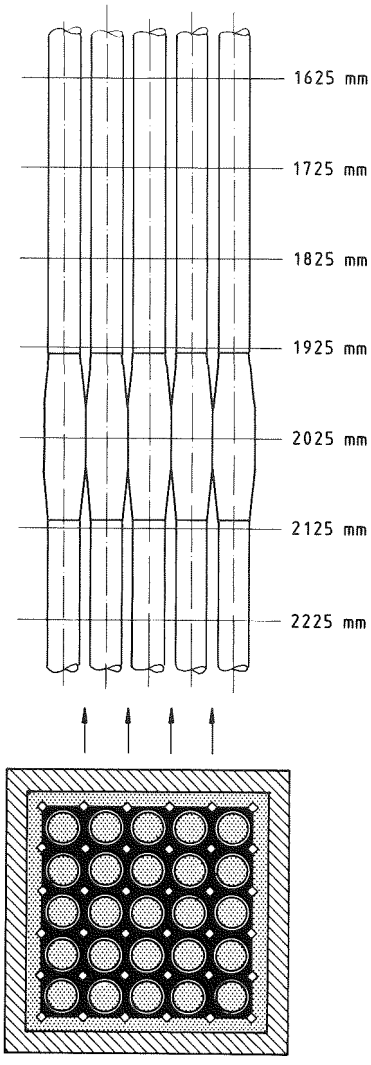

Test No. 337
6 Grid Spacers
Blocked Bundle (5x5 Rods)
Blockage at Level 2025 mm
Blockage Ratio 90%

Flooding Rate 3.8 cm/s
Pressure 4.0 bar

⊡ cladding
✳ Sleeve
+ Underneath Sleeve

Fig. 56 5x5 rod bundle: Test series VIII, cladding temperatures

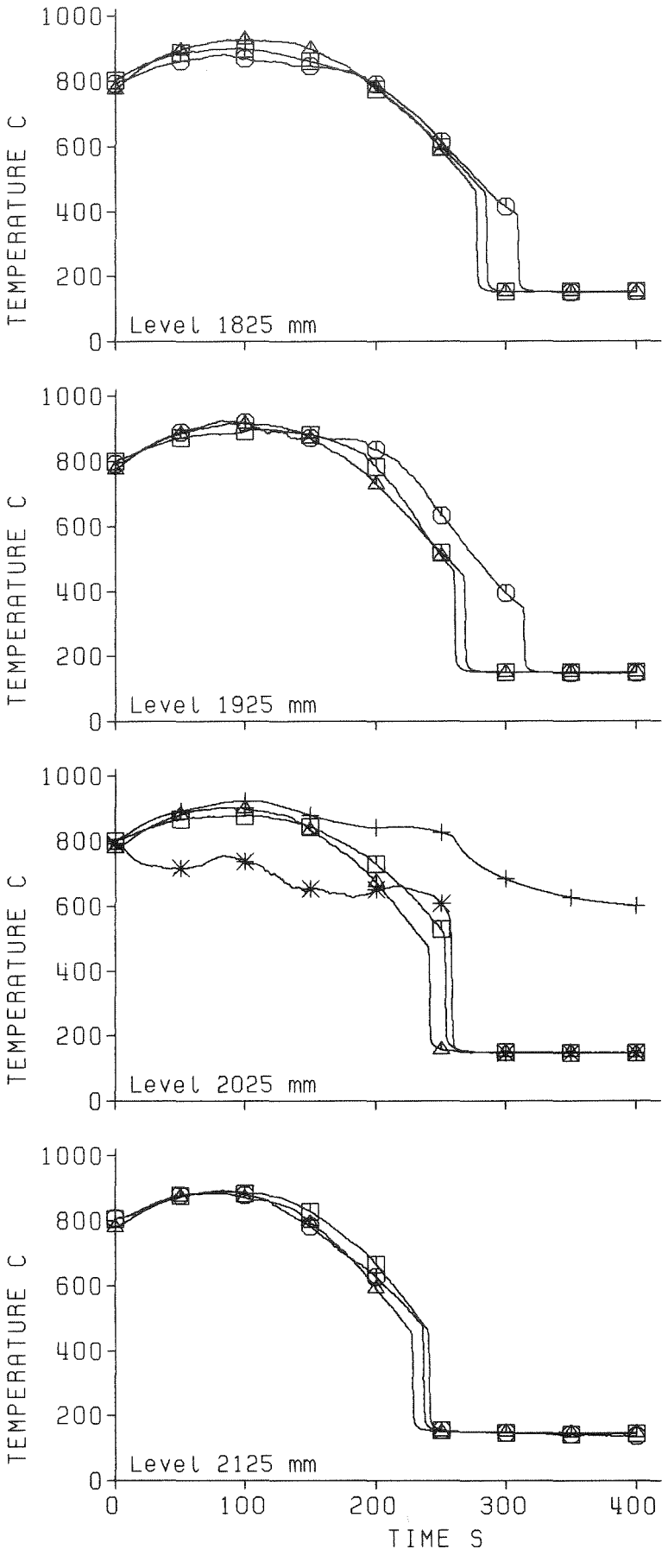

Flooding Rate 3.8 cm/s
System Pressure 4.0 bar

Test Series II

Test No. 229
6 Grid Spacers
Unblocked Bundle

△ Cladding

Test Series III

Test No. 239
6 Grid Spacers
Blocked Bundle (3x3 Rods)
Blockage at Level 2025 mm
Blockage Ratio 90%

⊡ Bypass Region
⊙ Blocked Region
✳ Sleeve
+ Underneath Sleeve

Fig. 57 5x5 rod bundle: Test series II + III, cladding temperatures

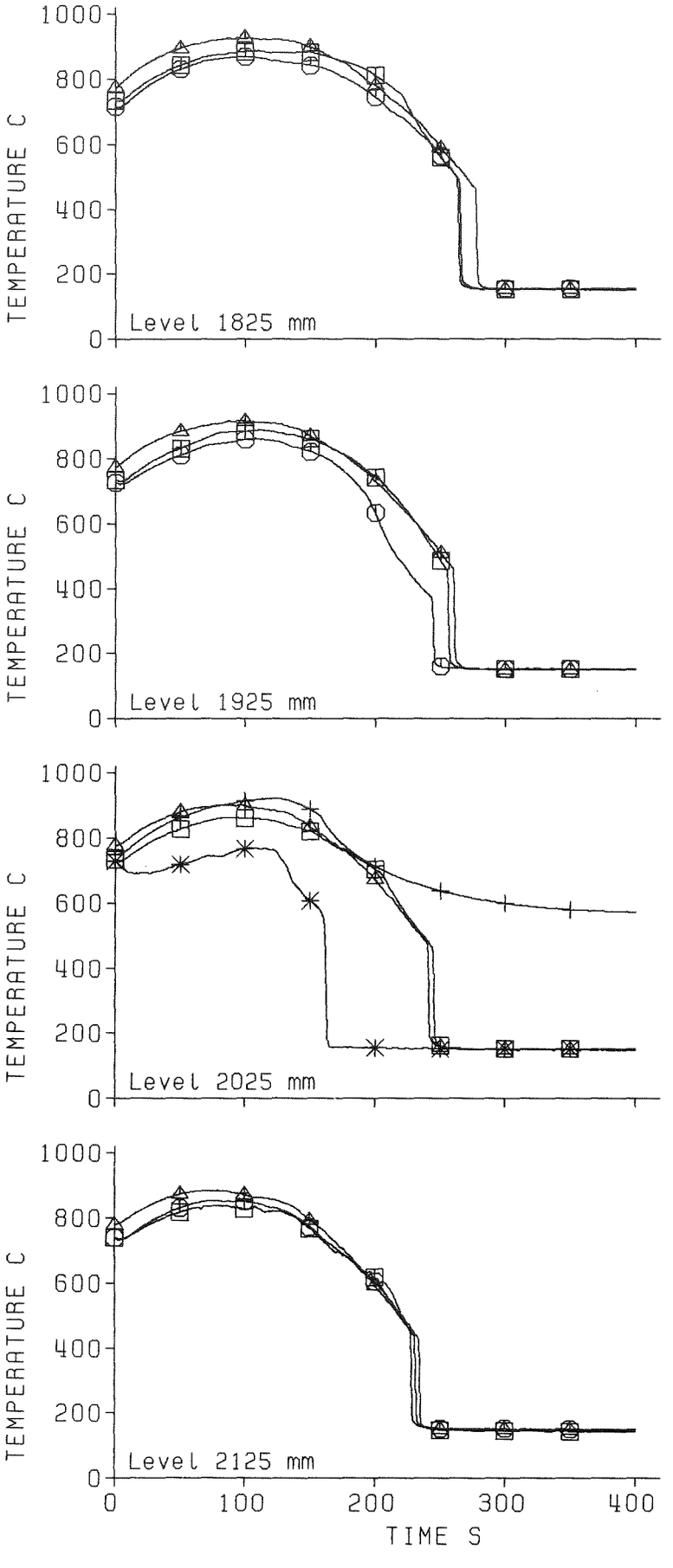

Flooding Rate 3.8 cm/s
System Pressure 4.0 bar

Test Series II

Test No. 229
6 Grid Spacers
Unblocked Bundle

△ Cladding

Test Series IV

Test No. 263
6 Grid Spacers
Blocked Bundle (3x3 Rods)
Blockage at Level 2025 mm
Blockage Ratio 62%

⊡ Bypass Region
⊙ Blocked Region
✳ Sleeve
+ Underneath Sleeve

Fig. 58 5x5 rod bundle: Test series II + IV, cladding temperatures

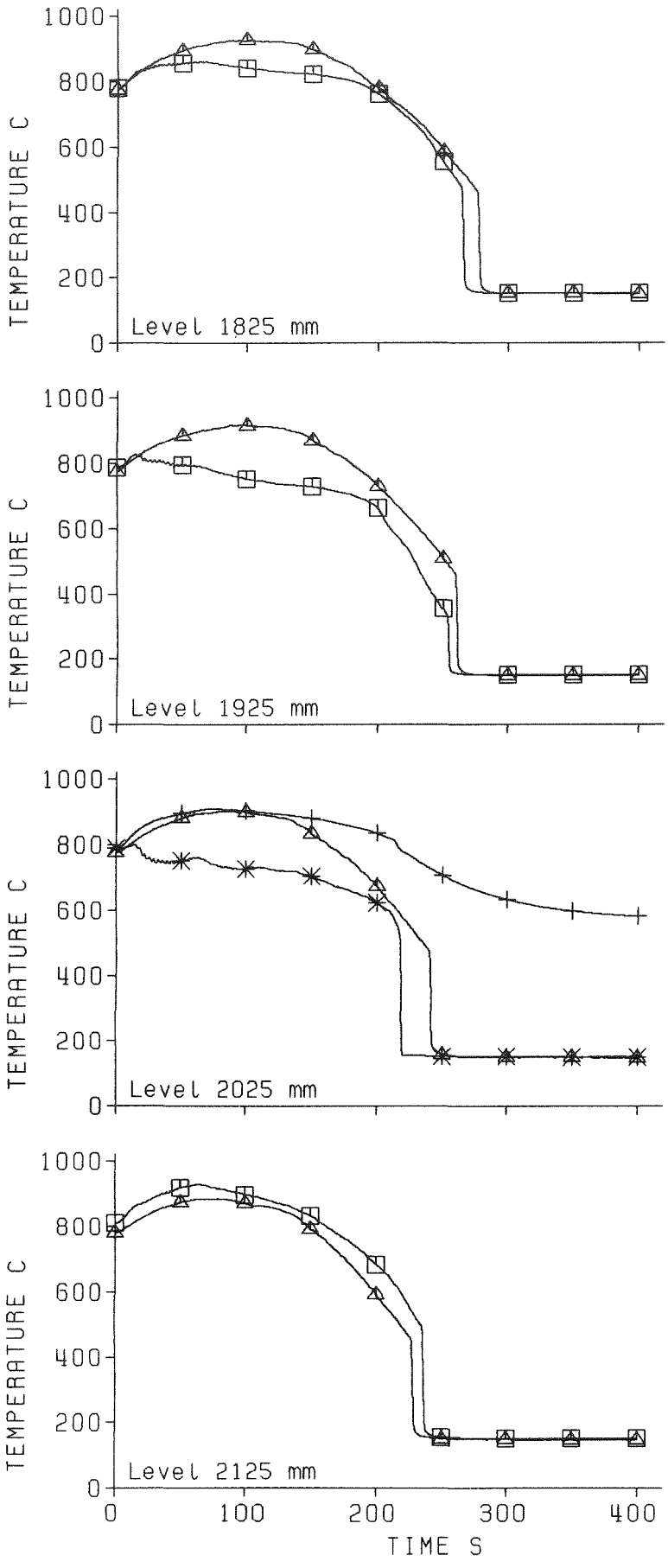

Flooding Rate 3.8 cm/s
System Pressure 4.0 bar

Test Series II

Test No. 229
6 Grid Spacers
Unblocked Bundle

△ Cladding

Test Series VII

Test No. 324
6 Grid Spacers
Blocked Bundle (5x5 Rods)
Blockage at Level 2025 mm
Blockage Ratio 62%

□ Cladding
✳ Sleeve
+ Underneath Sleeve

Fig. 59 5x5 rod bundle: Test series II + VII, cladding temperatures

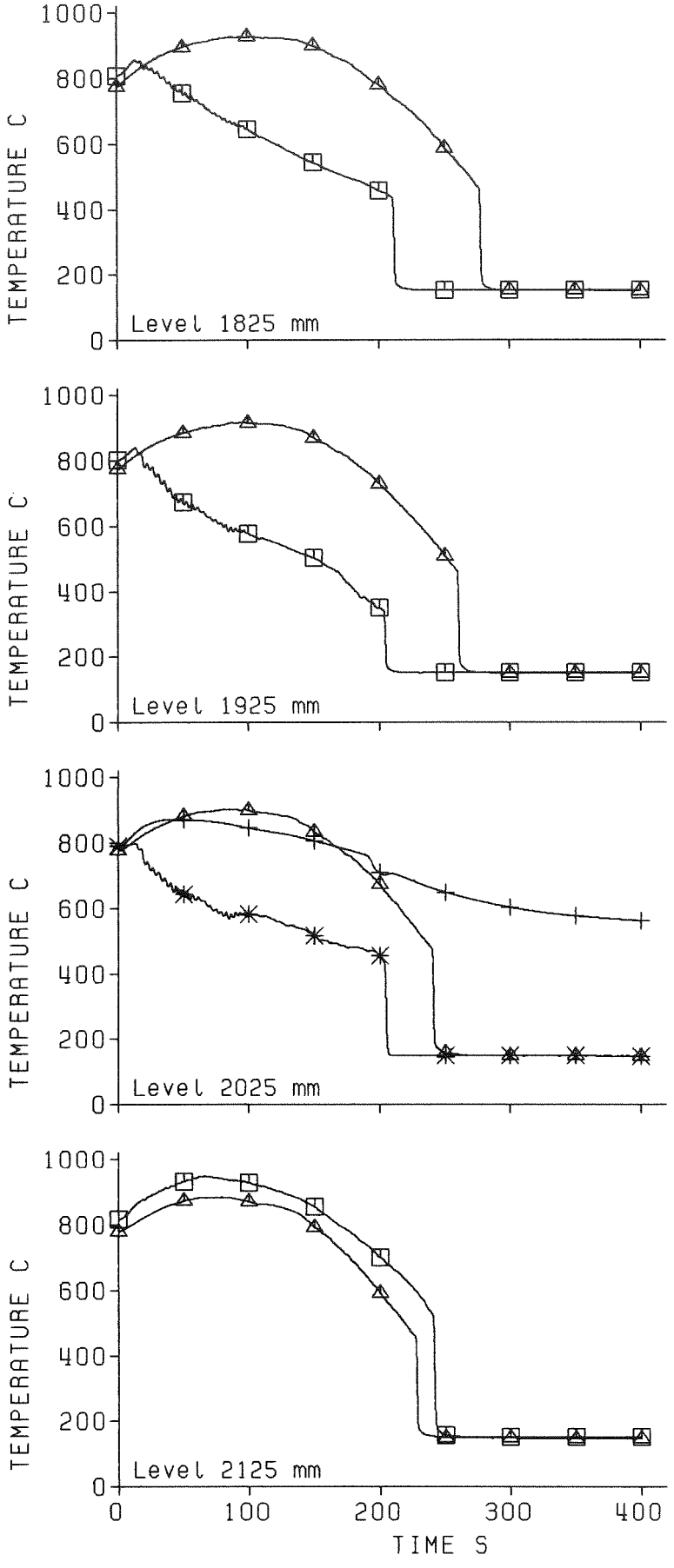

Flooding Rate 3.8 cm/s
System Pressure 4.0 bar

Test Series II

Test No. 229
6 Grid Spacers
Unblocked Bundle

△ Cladding

Test Series VIII

Test No. 337
6 Grid Spacers
Blocked Bundle (5x5 Rods)
Blockage at Level 2025 mm
Blockage Ratio 90%

□ Cladding
✳ Sleeve
+ Underneath Sleeve

Fig. 60 5x5 rod bundle: Test series II + VIII, cladding temperatures

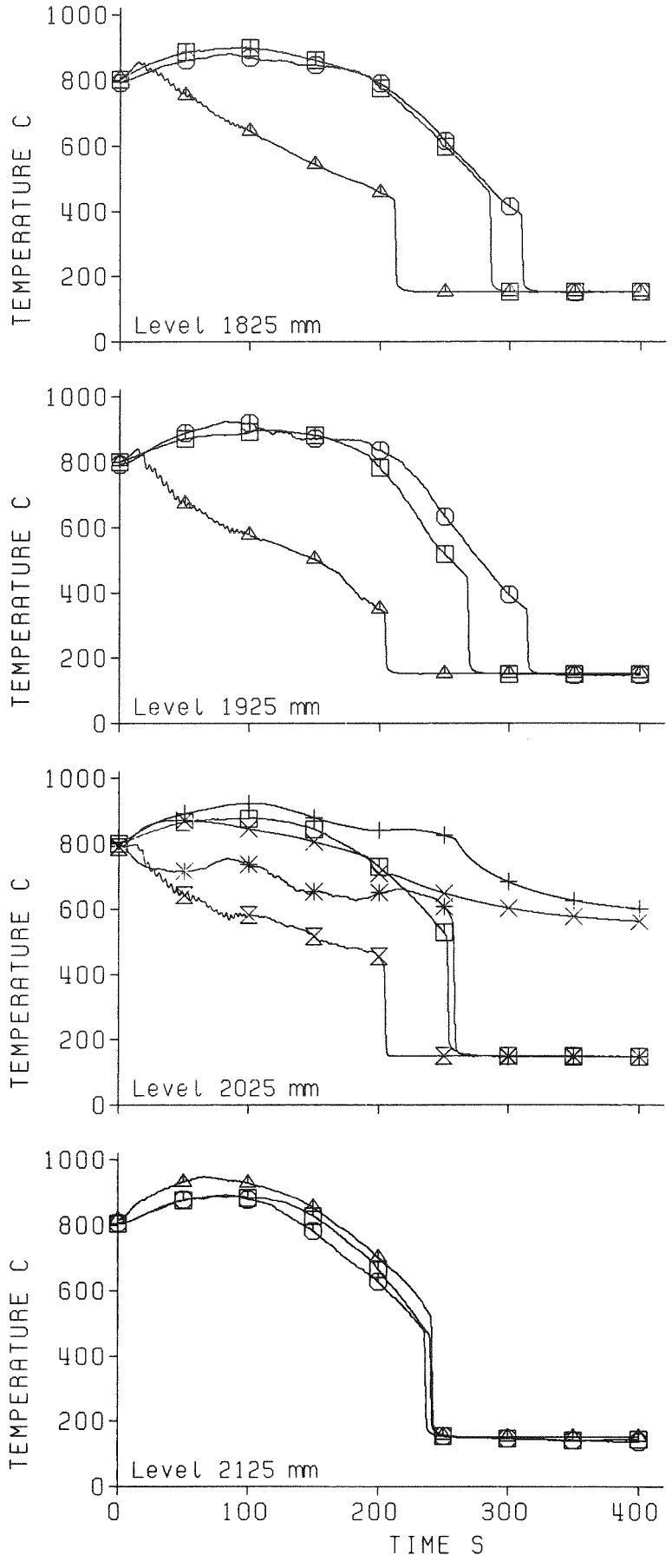

Flooding Rate 3.8 cm/s
System Pressure 4.0 bar

Test Series III

Test No. 239
6 Grid Spacers
Blocked Bundle (3x3 Rods)
Blockage at Level 2025 mm
Blockage Ratio 90%

⊡ Bypass Region
⊙ Blocked Region
✳ Sleeve
+ Underneath Sleeve

Test Series VIII

Test No. 337
6 Grid Spacers
Blocked Bundle (5x5 Rods)
Blockage at Level 2025 mm
Blockage Ratio 90%

△ Cladding
⧖ Sleeve
× Underneath Sleeve

Fig. 61 5x5 rod bundle: Test series III + VIII, cladding temperatures

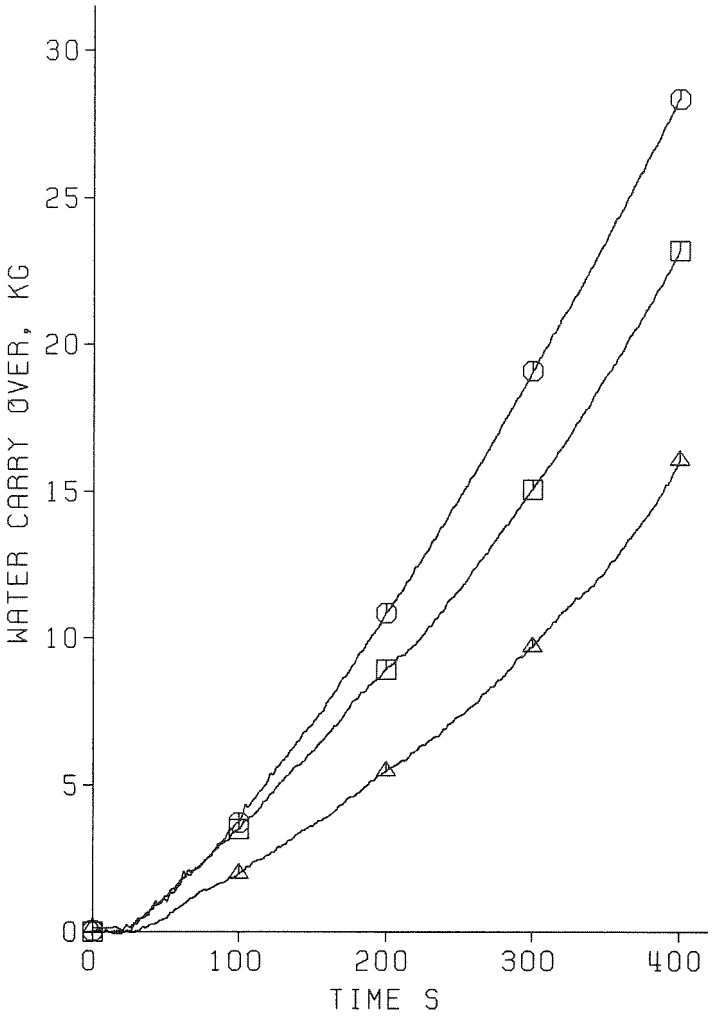

Flooding Rate 3.8 cm/s

Test Series IV

6 Grid Spacers
Blocked Bundle (3x3 Rods)
Blockage at Level 2025 mm
Blockage Ratio 62%

○ Test No. 262
System Pressure 2.0 bar

□ Test No. 263
System Pressure 4.0 bar

△ Test No. 268
System Pressure 6.0 bar

Fig.62 5x5 rod bundle: Water carry over, influence of system pressure

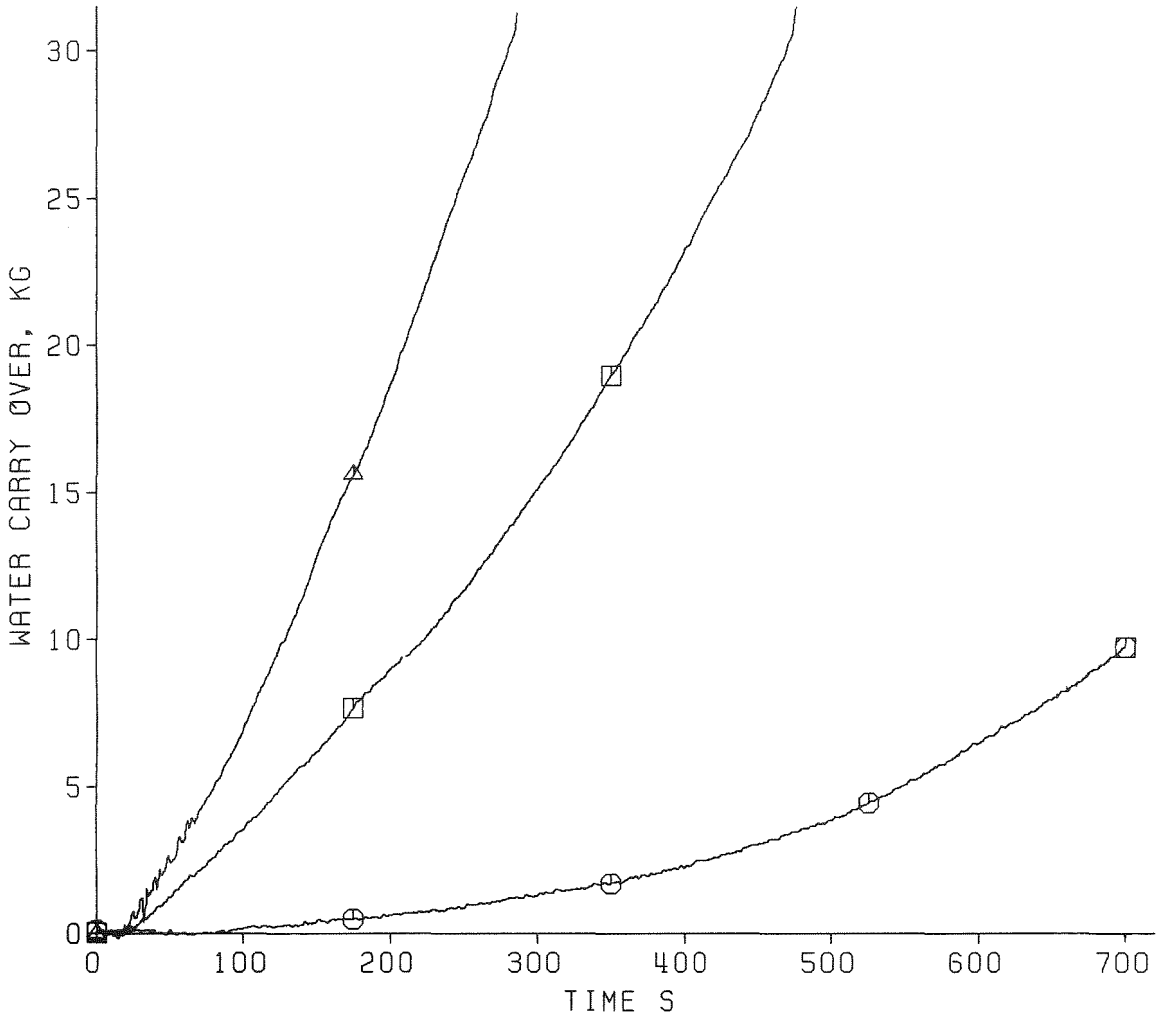

System Pressure 4.0 bar

Test Series IV

6 Grid Spacers
Blocked Bundle (3x3 Rods)
Blockage at Level 2025 mm
Blockage Ratio 62%

○ Test No. 267
Flooding Rate 2.2 cm/s

□ Test No. 263
Flooding Rate 3.8 cm/s

△ Test No. 264
Flooding Rate 5.8 cm/s

Fig. 63 5x5 rod bundle: Water carry over, influence of flooding rate

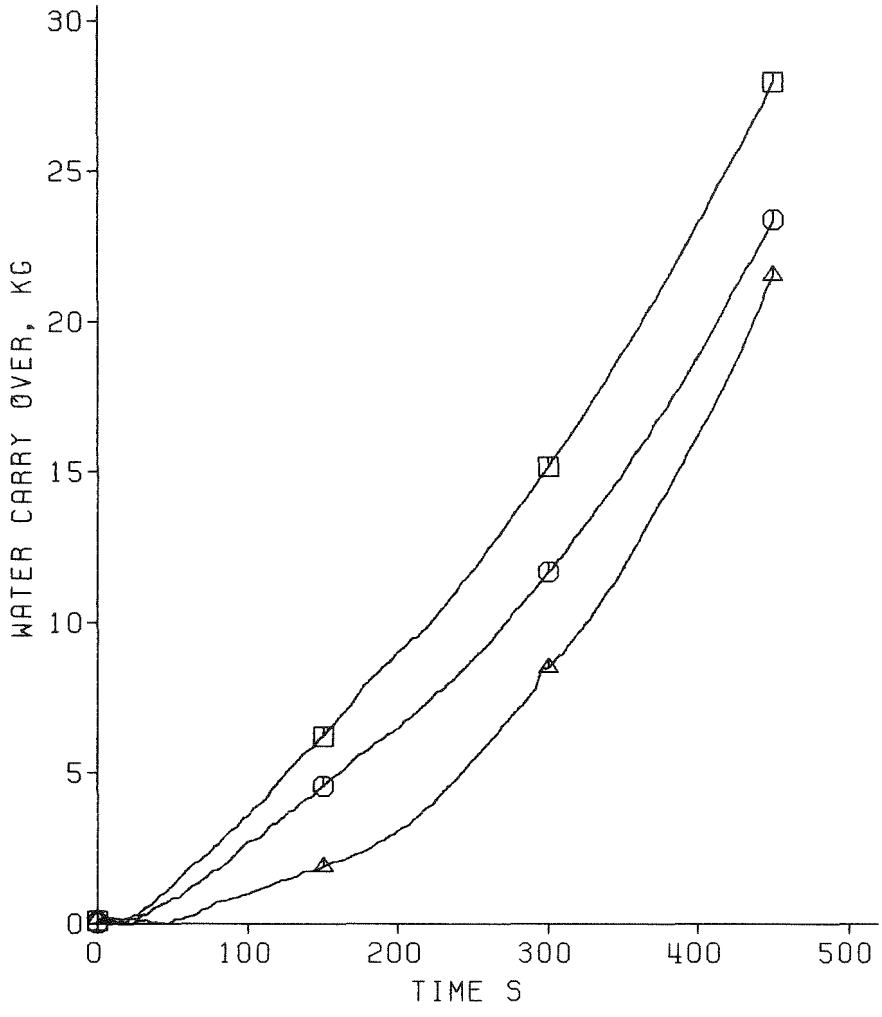

Flooding Parameters: V = 3.8 cm/s, P = 4.1 bar

□ Test Series IV, Test No. 263
○ Test Series V, Test No. 282
△ Test Series VI, Test No. 276

Fig. 64 5x5 rod bundle: Water carry over, influence of flow blockage

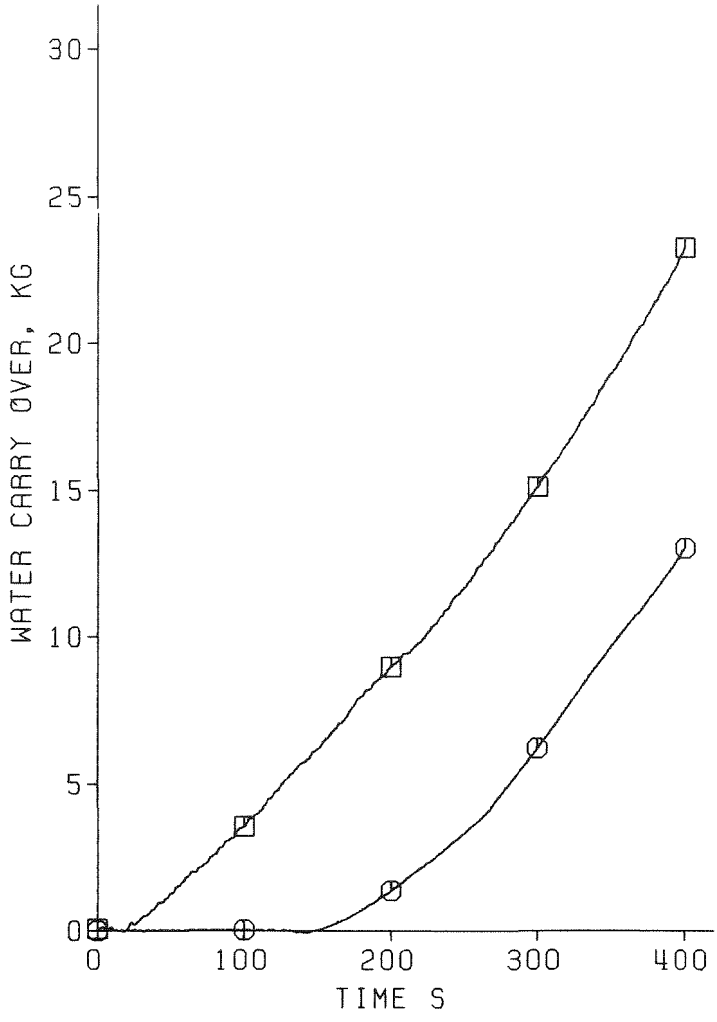

Flooding Rate 3.8 cm/s
System Pressure 4.0 bar

Test Series IV

Test No. 263
6 Grid Spacers
Blocked Bundle (3x3 Rods)
Blockage at Level 2025 mm
Blockage Ratio 62%

Test Series VIII

Test No. 337
6 Grid Spacers
Blocked Bundle (5x5 Rods)
Blockage at Level 2025 mm
Blockage Ratio 90%

Fig. 65 5x5 rod bundle: Water carry over, influence of flow blockage

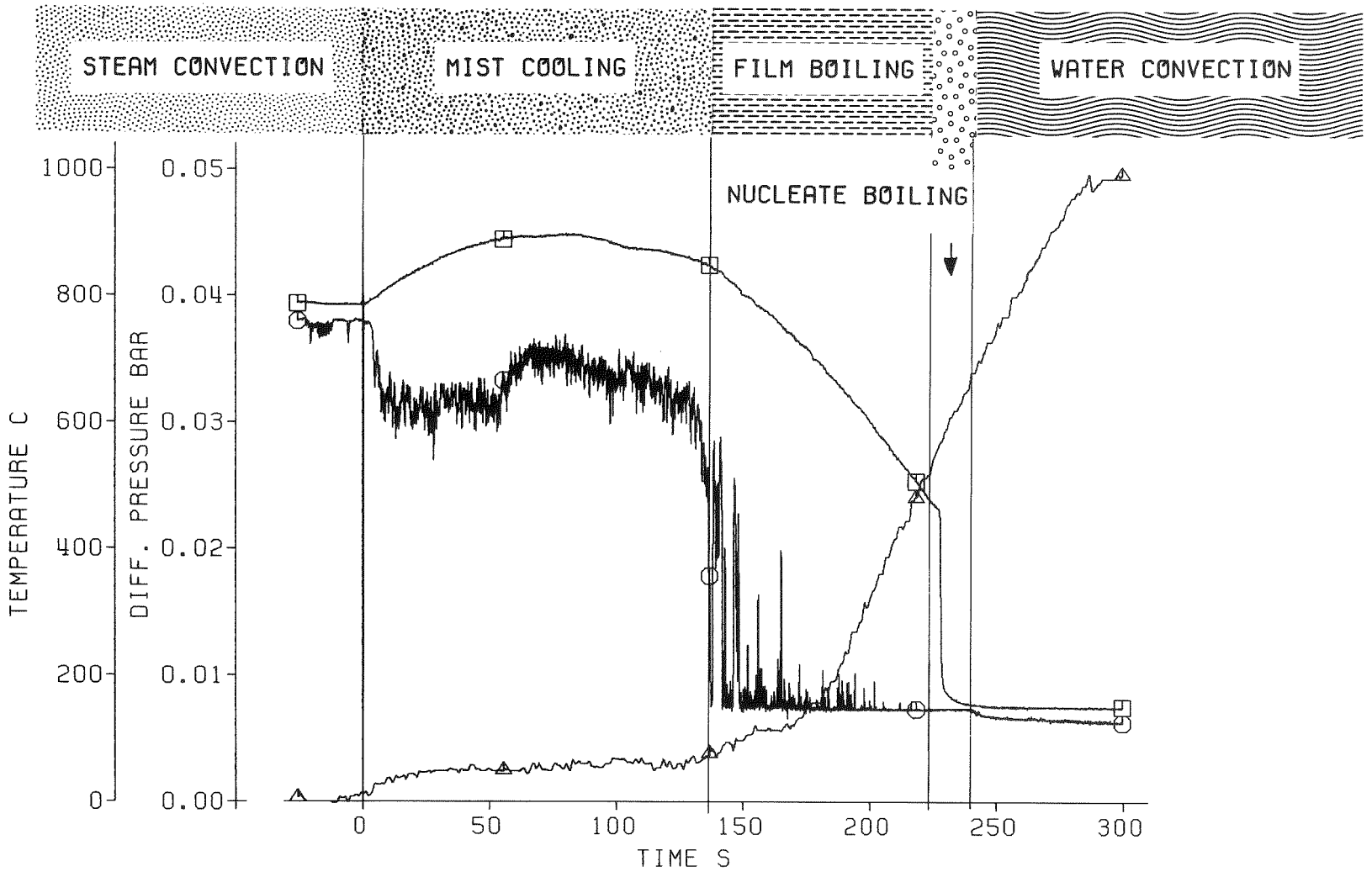

FEBA Test No. 229
Flooding Velocity 3.8 cm/s
System Pressure 4.1 bar
Feedwater Temperature 40 C

TC Measuring Position:
2125 mm

□ Clad Temperature
○ Fluid Temperature
△ Differential Pressure Measured Between Axial Level 2380 and 1835 mm

Fig. 66 Heat transfer regimes observed during reflooding

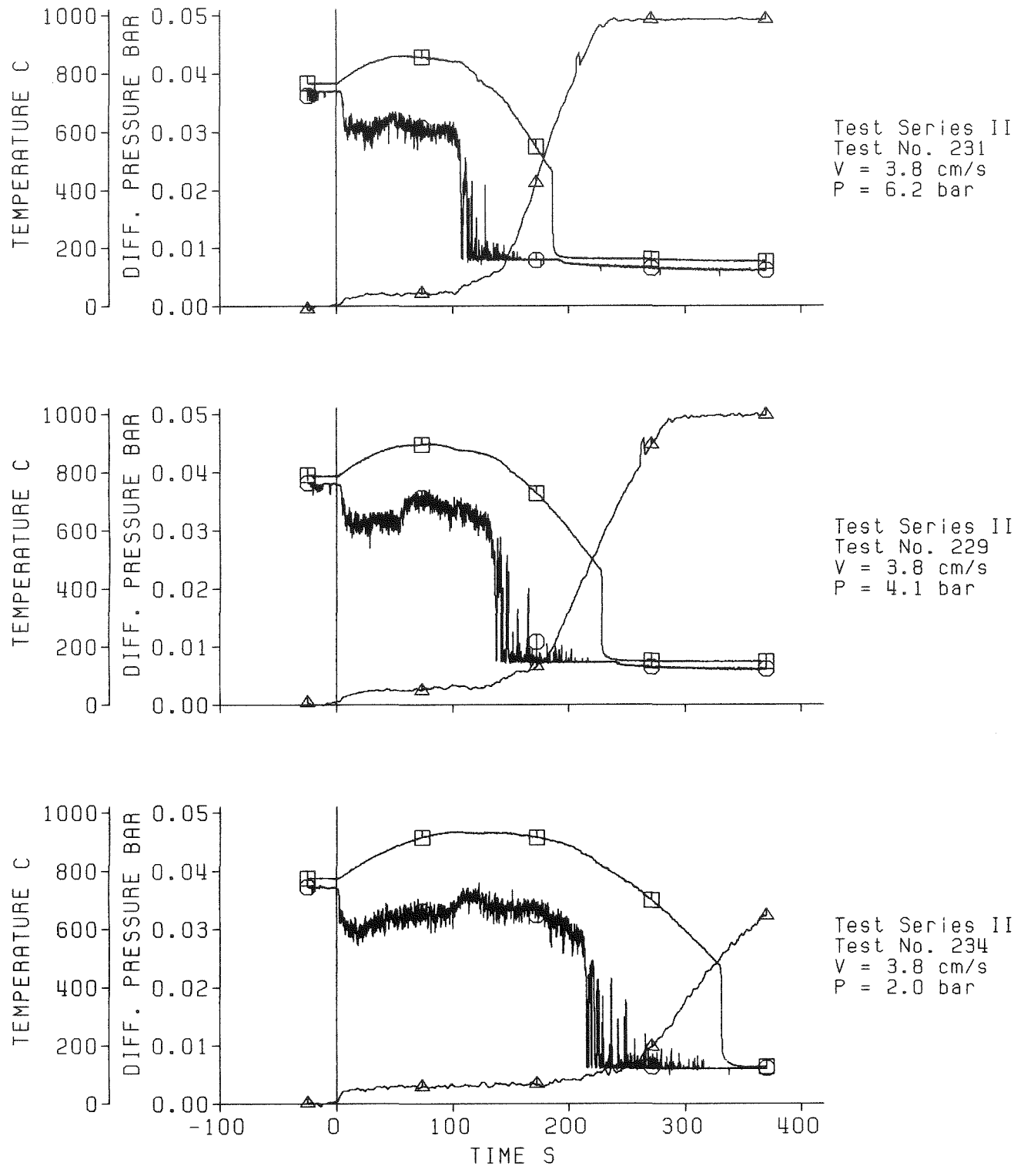

TC Measuring Position:
2125 mm

□ Cladding Temperature
◯ Fluid Temperature
△ Differential Pressure Measured Between Axial Level 2380 and 1835 mm

Fig. 67 5x5 rod bundle: Influence of flooding parameters on cladding and fluid temperatures and differential pressure

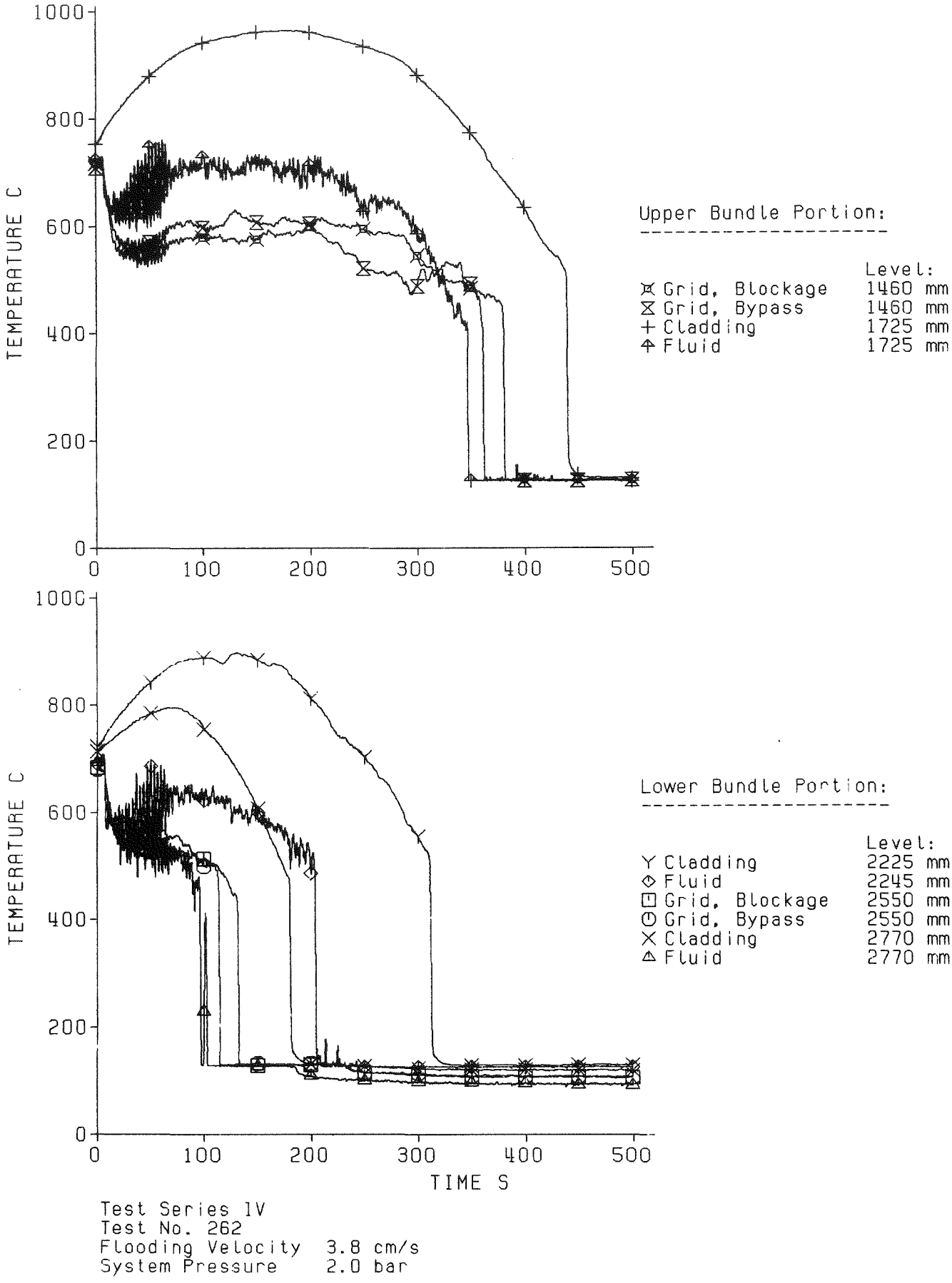

Fig. 68 5x5 rod bundle: Cladding, fluid and grid spacer temperatures measured in the lower and upper bundle portion

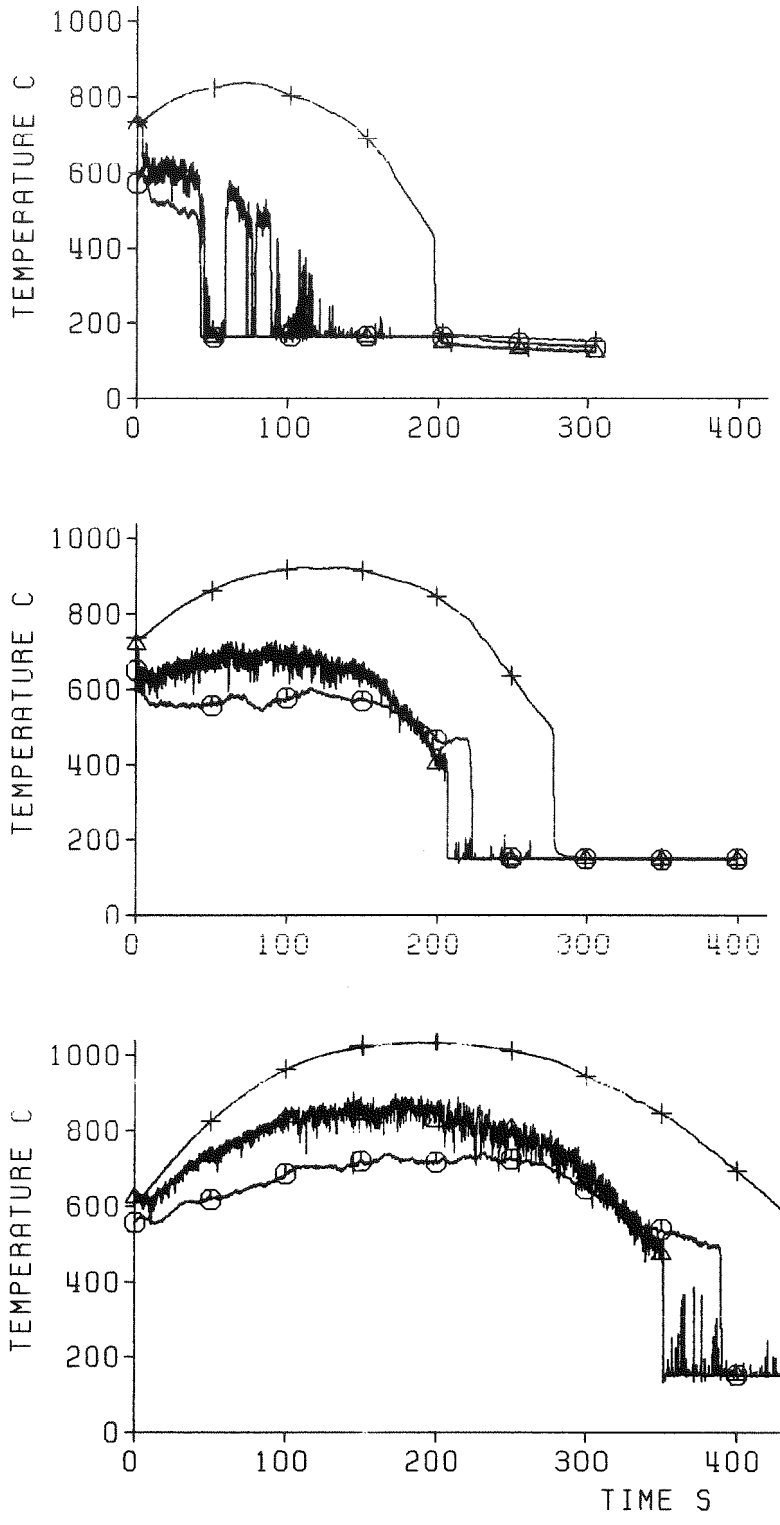

Test Series IV
Test No. 269
V = 5.8 cm/s
P = 6.0 bar

Test Series IV
Test No. 263
V = 3.8 cm/s
P = 4.0 bar

Test Series IV
Test No. 267
V = 2.2 cm/s
P = 4.0 bar

+ Cladding Temperature
△ Fluid Temperature
⏲ Grid Spacer Temperature, Blockage

TC Measuring Position:
1725 mm
1725 mm
1460 mm

Fig. 69 5x5 rod bundle: Influence of flooding rate on cladding, fluid and grid spacer temperatures in the upper bundle portion

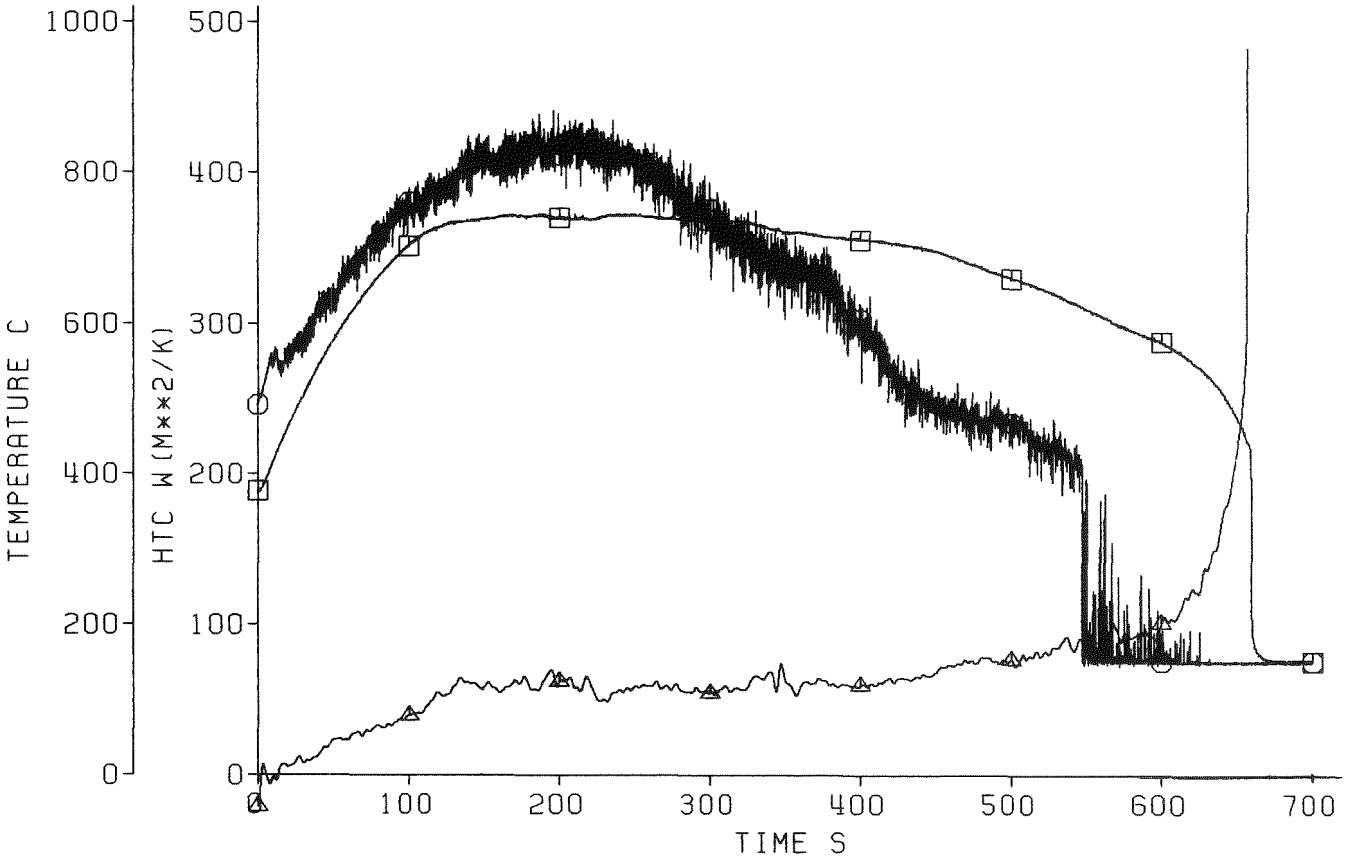

FEBA Test No. 284
Flooding Velocity 2.2 cm/s
System Pressure 4.1 bar
Feedwater Temperature 40 C

Axial Level: 590 mm

□ Clad Temperature
○ Fluid Temperature
△ Heat Transfer

Heat Transfer Related to Saturation Temperature

Fig. 70 5x5 rod bundle: Cladding and fluid temperatures and heat transfer coefficient

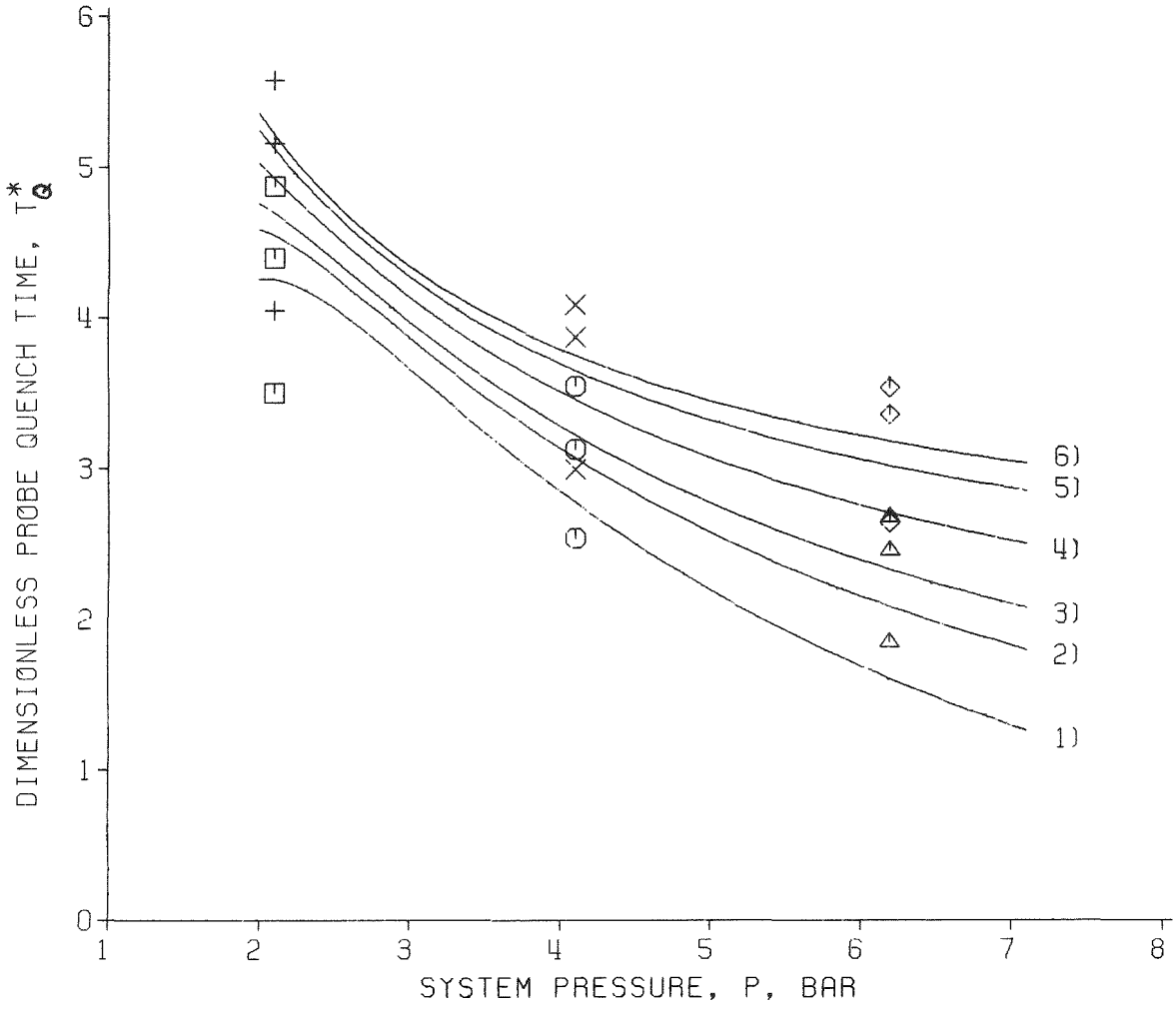

Legend
======

Measured Data	Calculated Data	Pressure P (bar)	Flooding Rate V (cm/s)	Re No.
□	1)	2.1	3.8	2,126
○	2)	4.1	3.8	2,500
△	3)	6.2	3.8	2,749
+	4)	2.1	5.8	3,245
×	5)	4.1	5.8	3,817
◇	6)	6.2	5.8	4,196

Fig. 71 Probe quench time correlation

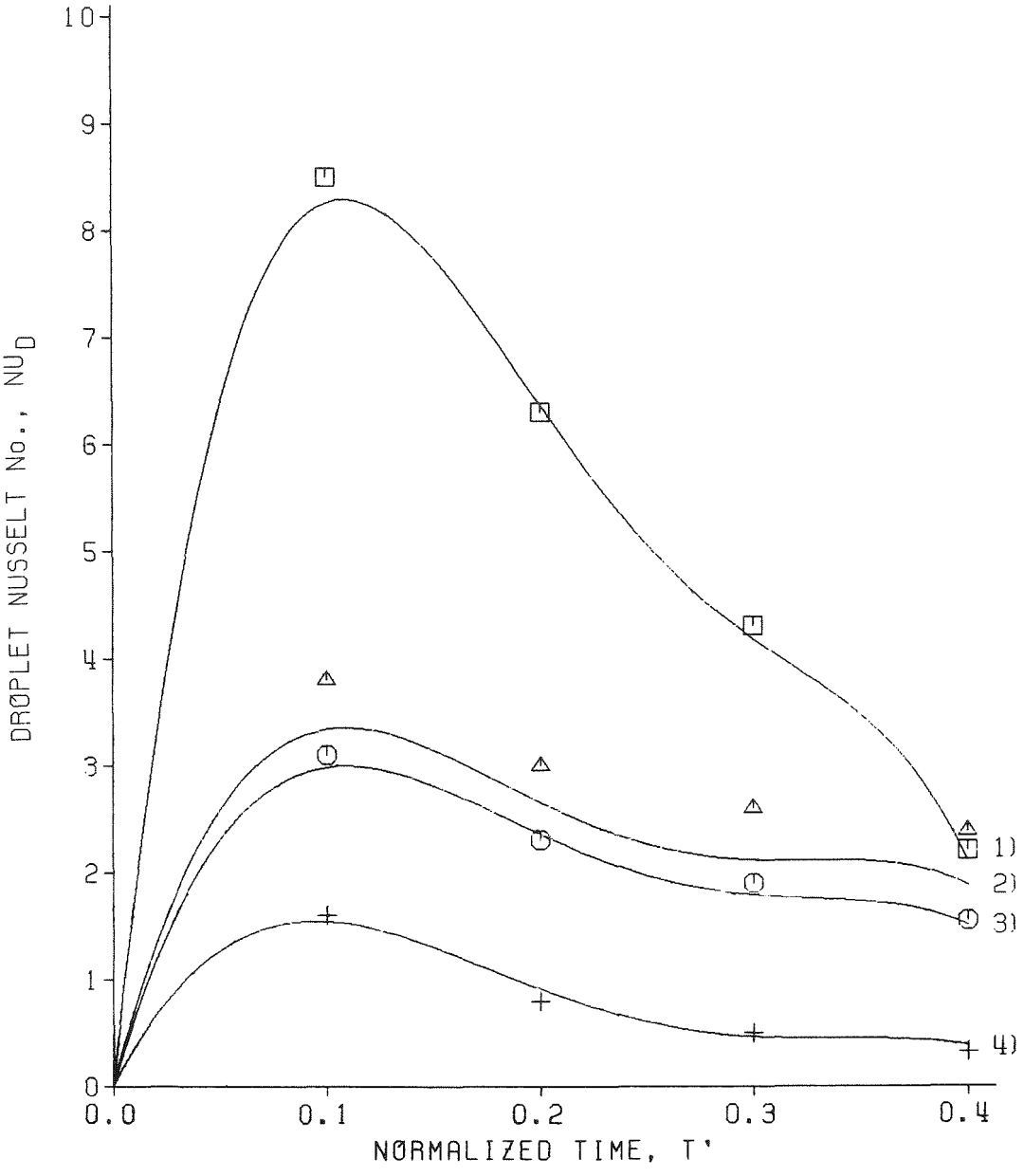

Legend
======

Measured Data	Calculated Data	Pressure P (bar)	Flooding Rate V (cm/s)	Re No.	Re_ℓ No.	Distance Spacer ℓ (mm)
□	1)	4.1	3.8	2,500	61,000	100
○	2)	4.1	3.8	2,500	121,000	200
△	3)	4.1	3.8	2,500	182,000	300
+	4)	4.1	3.8	2,500	242,000	400

Fig. 72 Droplet heat transfer

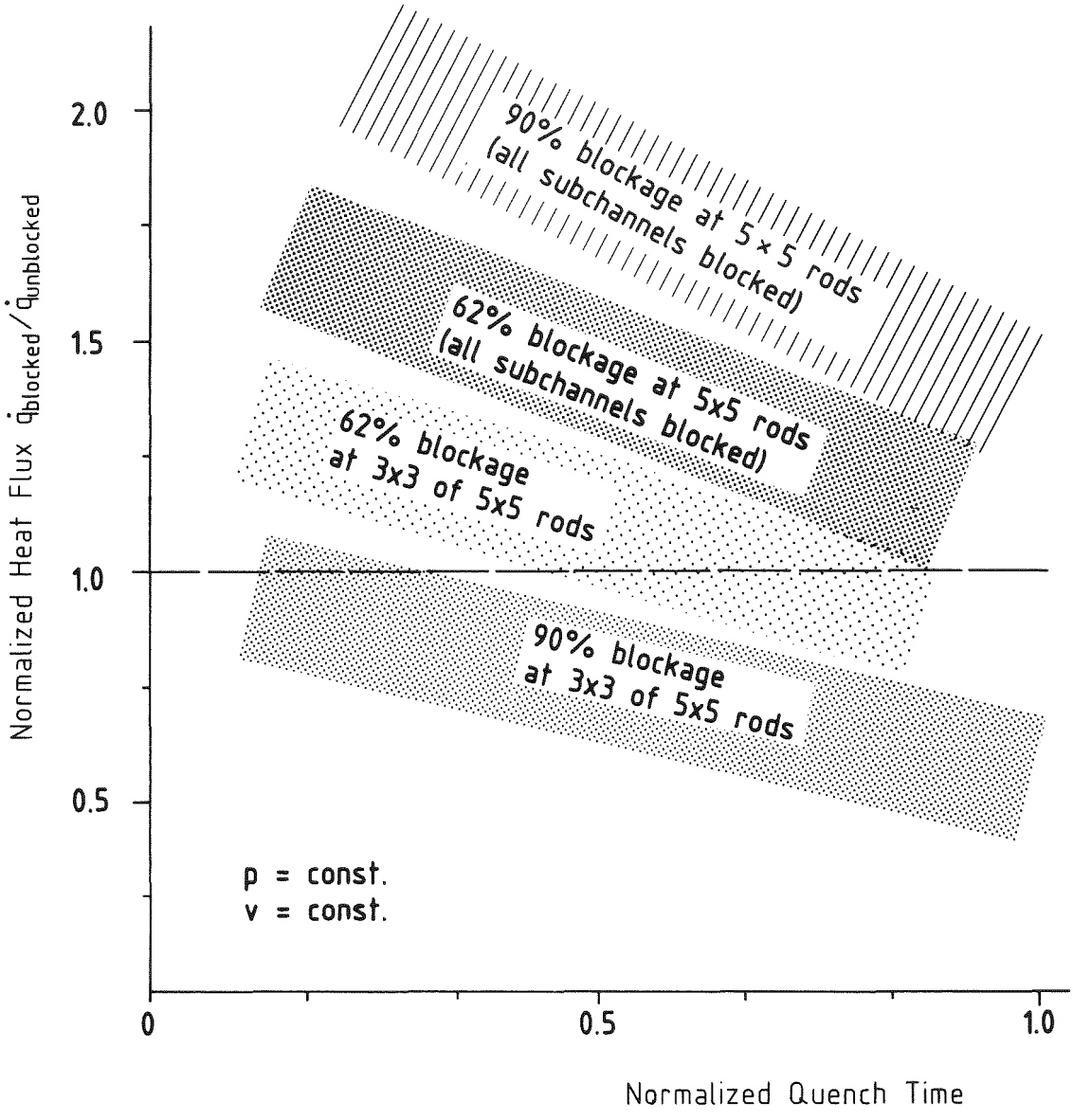

Fig. 73 5x5 rod bundle: Normalized heat flux (blocked/unblocked) downstream of the blockages during mist cooling